Nuclear Pore Behaviour in Interphase and "Open" Mitosis of *Ustilago maydis*

Dissertation

zur
Erlangung des Doktorgrades
der Naturwissenschaften
(Dr. rer. nat)

dem Fachbereich Biologie
der Philipps-Universität Marburg
vorgelegt von

Ulrike Theisen
aus München

Exeter, UK, 2008

Vom Fachbereich Biologie der Philipps-Universität Marburg als Dissertation angenommen am:

Erstgutachter: Prof. Uwe Maier
Zweitgutachter: Prof. Gero Steinberg

Tag der mündlichen Prüfung:

Die Untersuchungen zur vorliegenden Arbeit wurden von November 2004 bis September 2008 am Max-Planck-Institut für terrestrische Mikrobiologie, Marburg, in der Abteilung Organismische Interaktionen und an der Universität Exeter, UK, unter Betreuung von Herrn Prof. Dr. Gero Steinberg durchgeführt.

Teile dieser Arbeit wurden veröffentlich in:

Theisen, U., Straube, A., and Steinberg, G. (2008). Dynamic Rearrangement of Nucleoporins during Fungal "Open" Mitosis. Mol Biol Cell *19*, 1230-1240.

Erklärung

Ich versichere, dass ich meine Dissertation mit dem Titel „Nuclear Pore Behaviour in Interphase and the “Open“ Mitosis of *Ustilago maydis*“ selbstständig und ohne unerlaubte Hilfe angefertigt habe, und mich dabei keiner anderen als der von mir ausdrücklich bezeichneten Quellen und Hilfen bedient habe.

Diese Dissertation wurde in der jetzigen oder einer ähnlichen Form noch bei keiner anderen Hochschule eingereicht und hat noch keinen sonstigen Prüfungszwecken gedient.

Exeter, 03.10.2008
(Ort, Datum)

Ulrike Theisen

Zusammenfassung

Die vorliegende Arbeit befasst sich mit dem dynamischen Verhalten von Kernporen in Interphase und „offener" Mitose des maispathogenen Pilzes *Ustilago maydis*.

Um einen Marker für Kernporen zu etablieren, werden in einer bioinformatischen Analyse Proteine identifiziert, die als Nucleoporine an der Kernpore lokalisieren könnten. Fünf davon werden mit GFP versehen, und ihre Lokalisation wird in Interphasezellkernen und in Mitose lichtmikroskopisch untersucht. Eines dieser Proteine, Nup107, wird weitergehend charakterisiert. Versuche mit Mutanten zeige, dass Nup107 *U. maydis* essentiell ist. Verringerung von Nup107 in den Zellen führt zu einer Akkumulation von Kernporen in einem Punkt der Kernhülle.

Die erste Beobachtung zeigt, dass sich Kernporen in der Kernhülle bewegen. Dieses Verhalten wurde in Studien in Bäckerhefe beobachtet, aber weder der Mechnismus noch die biologische Bedeutung wurden näher untersucht, da Diffusion als Ursache angenommen wurde. Die Ergebnisse an *U. maydis* Interphasezellkernen dagegen zeigen gerichtete Bewegung in zwei Bewegungsmustern. Beide sind energie-abhängig. Der erste, schnellere Bewegungstyp ist abhängig vom Mikrotubuli-Zytoskelett. Die MINUS gerichtete Bewegung benötigt Dynein. Der zweite, langsamere Bewegungstyp hängt mit Transkription zusammen, aber lässt sich nicht unmittelbar mit Bewegung von Chromatin korrelieren. FRAP Experimente belegen, dass Typ 1 Bewegung Kernporen gleichmäßig auf der Kernoberfläche verteilt. Die Verteilung der Kernporen beeinflusst die Effizienz der Expression eines Reporter-Proteins von einem induzierbaren Promoter.

Die Beobachtung fünf GFP-markierter Nucleoporine, die in unterschiedlichen Bereichen der Kernpore lokalisieren, in Mitose zeigt, dass Kernporen in Prophase großenteils noch vollständig sind. Die Kernporen besitzen die Tendenz, an der Spitze der in Prophase verlängerten Kernhülle zu akkumulieren, jedoch kann diese Bewegung nach vorne nicht unmittelbar mit der Wanderung der Chromosomen in die Knospe in Zusammenhang gebracht werden. Am Ende der Prophase zerfallen die Kernporen in Untereinheiten, die während der Mitose unterschiedlich lokalisieren. Die Nup107-160 Untereinheit assoziiert mit Chromatin in Metaphase. Vollständiger Abbau der Kernhülle ist weder für das Zerfallen der Kernporen noch für die Assoziation mit DNA nötig. Im Gegensatz zu Vertebraten-Modellsystemen ko-lokalisiert Nup107-160 in *U. maydis* nicht mit Kinetochoren. In Anaphase verändert Nup107-160 seine Position zu den Außenseiten der Chromatinmassen hin. In Telophase werden die Kernporen in einer bestimmten Abfolge von Nucleoporinuntereinheiten wiederaufgebaut, und Kernimport beginnt, wenn alle untersuchten

Nucleoporine an der Kernhülle verankert sind. Das Zytoskelett scheint im Prozess des Wiederaufbaus der Kernhülle involviert zu sein, auch wenn die genaue Aufgabe noch unklar bleibt.

Die vorliegende Arbeit eröffnet eine neue Sicht auf die Rolle der Kernporen im Informationstransfer von der DNA zur Proteinexpression. Daneben legt die Beobachtung des Zerfalls und Wiederaufbaus der Kernporen in Mitose einen älteren Ursprung der offenen Mitose als bisher angenommen nahe.

Summary

This work presents findings on dynamic nuclear pore behaviour in interphase nuclei and in the “open” mitosis in *Ustilago maydis*.

Proteins likely to function in the nuclear pore complexes (NPCs) are identified in the *U. maydis* genome by bioinformatic search. Of these, five nucleoporins are tagged with GFP and observed microscopically for their localization in interphase and mitosis. One of the stably incorporated nucleoporins, Nup107, is analyzed in more detail. Nup107 appears to be essential in *U. maydis*, with depletion of the protein causing NPC clustering at the nuclear envelope.

The initial observation reveals that NPCs in *U. maydis* are motile. The movement of NPCs in interphase nuclei has been reported in budding yeast, but a detailed analysis of the underlying mechanism and of the biological significance of the phenomenon is missing. In contrast to the studies in budding yeast, which assumed diffusion as cause for NPC motility, this work in *U. maydis* finds directed motility of NPCs. The directed motility is energy-dependent and proceeds in two motility types. Type 1 depends on the microtubule cytoskeleton. Dynein is the driving force behind MINUS end directed movement. NPC type 2 motility is abolished when active transcription is inhibited, but cannot be directly correlated with chromatin movement. FRAP experiments demonstrate that type 1 motility is necessary to equally distribute NPCs across the nuclear envelope. Equal distribution is required to ensure efficient protein expression of a reporter from an inducible promoter.

Following the GFP-tagged nucleoporins from different parts of the NPC structure into mitosis, it appears that NPCs are still assembled in prophase. A tendency of NPCs to accumulate at the tip of the elongated prophase is observed, but the function of NPCs in chromosome migration appears doubtful. At the end of prophase, NPCs disassemble into subcomplexes and disperse in different locations, with the Nup107-160 subcomplex associating with chromatin in metaphase. Complete nuclear envelope (NE) removal is not necessary for NPC disassembly and association of Nup107 with DNA. In contrast to findings in vertebrates, the Nup107-160 subcomplex does not associate with kinetochores in metaphase. In anaphase, the Nup107-160 subcomplex shifts its position to the leading outside edges of the chromatin. Nucleoporins accumulate at the NEs in telophase in a step-wise manner, and nuclear import starts after all nucleoporins investigated are assembled at the nuclei. Inhibitor studies to investigate the role of the cytoskeleton cannot fully explain the involvement of actin and microtubules in NE reassembly.

The results from these observations on NPC motility in interphase nuclei open a new view on basic principles of ensuring efficient protein expression. The findings on NPC disassembly in mitosis place *U. maydis* close to the vertebrate situation, suggesting a more ancient origin for the “open” mitosis.

Glossary

aa	amino acid
α	anti- *(antibodies)*
Amp	Ampicillin
ATP	Adenosintriphosphate
a.u.	arbitrary unit
Ben	Benomyl
ble^R	phleomycin-resistance-cassette
bp	base pair(s)
cbx-locus *ip*	genomic locus of the iron-sulfur-subunit of the Succinate-dehydrogenase from *U. maydis*
cbx^R	carboxin-resistance-cassette
CCCP	Carbonyl cyanide 3-chlorophenylhydrazone
CFP	cyan fluorescent protein
CM	complete medium
CM-A	complete medium containing 1% arabinose
CM-G	complete medium containing 1% glucose
C-terminal	carboxy-terminal
DAPI	4',6'-diamidino-2-phenylindole
ddH_2O	double distilled water
DIC	Differential Interference Contrast
DMSO	Dimethylsulfoxide
DNA	Desoxyribonucleic acid
dNTP	Desoxynucleotides
Dyn1	Dynein 1 from *U. maydis*
Dyn2	temperature-sensitive allele of Dynein 2 from *U. maydis*
EDTA	Ethylendiamintetraacetic acid
eGFP	enhanced green fluorescent protein
EGTA	Ethylene glycol-bi(2-aminoethylether)-*N,N,N',N'*-tetraacetic acid
ER	endoplasmic reticulum
f.c.	final concentration
GFP	green fluorescent protein
GTP	Guanosintriphosphate
h	hour
H4	Histone 4 from *U. maydis*
hyg^R	hygromycin-resistance-cassette
kb	kilo bases
kD	kilo Dalton
LatA	Latrunculin A
mCherry	monomeric Cherry fluorescent protein
MeOH	Methanol
min	minute
ml	milliliter
µl	microliter

µm	micrometer
µM	micromolar
MPA	Mycophenolic acid
mRFP	monomeric red fluorescent protein
mRNA	messenger ribonucleic acid
ms	millisecond
MT	microtubule
MTOC	microtubule organizing centre
nat^R	nourseothricin-resistance-cassette
NE	nuclear envelope
NEBD	nuclear envelope breakdown
NPC	nuclear pore complex
N-terminal	amino-terminal
Nup	nucleoporin
OD	optical density
ORF	open reading frame
otef-promoter	Promoter of Translation-Elongation-Factor 1 from *U. maydis*, enhanced by 14 tetracycline operator units
p	probability
PCR	Polymerase chain reaction
P*crg*	promoter of the Arabinase gene from *U. maydis*
PEG	Polyethylene glycol
PIPES	Piperazine-N-N'-bis(2-ethanesulfonic acid)
RFP	red fluorescent protein
rpm	rounds per minute
RT	room temperature
s	second
SDS	Sodium dodecyl sulfate
SPB	spindle pole body
TE	Tris-HCl + Na_2EDTA, pH 8.0
Thio	Thiolutin
Tris-HCl	Tris(hydroxymethyl)aminomethane hydrochloride
Tub1	α-Tubulin from *U. maydis*
U	Unit
wt	wildtype
YFP	yellow fluorescent protein

Table of Contents

Zusammenfassung V
Summary VII
Glossary IX
Table of Contents XI
1 Introduction 1
1.1 Architecture of NPCs 1
1.2 NPCs in interphase 3
1.3 NPCs in mitosis 4
1.3.1 Mitosis in fungi 4
1.3.2 Open mitosis in higher eukaryotes 6
1.4 Aim of this study 6
2 Results 8
2.1 Identification of *U. maydis* nucleoporins 8
2.1.1 Bioinformatic search for nucleoporins in *U. maydis* 8
2.1.2 Scaffold nucleoporins Nup107 and Nup133 10
2.2 Nuclear Pore motility in interphase 13
2.2.1 Nuclear Pores are motile in the NE 13
2.2.2 Nuclear pores move in distinct motility types 13
2.2.3 NPC Type 1 motility requires extranuclear forces 15
2.2.4 Chromosome motion cannot be correlated with NPC movements 17
2.2.5 Transcription participates in Type2 NPC motility 18
2.2.6 NPC motility ensures equal NPC distribution and efficient protein expression 20
2.3 Nuclear Pore Behaviour in Mitosis 22
2.3.1 Peripheral nucleoporins 22
2.3.2 NPCs accumulate at the tip of the elongated NE in prophase 24
2.3.3 NPCs disassemble at the end of prophase 26
2.3.4 Scaffold nucleoporins disperse in the cytoplasm and aggregate on the DNA 27
2.3.5 NEBD is not necessary for Nup107 dispersal and association with DNA 29
2.3.6 Nup107 does not associate with kinetochores in metaphase 30
2.3.7 Nup2 disperses into the cytoplasm, but accumulates in metaphase 31
2.3.8 Nup107 rearranges localization in anaphase 32
2.3.9 Nuclear import begins when peripheral components are attached to NPCs 34
2.3.10 The role of the cytoskeleton in the reassembly of the NE 35
3 Discussion 38

3.1 Two types of directed nuclear pore motility exist in interphase nuclei 38
3.1.1 NPC type 1 motility in *U. maydis* relies on extranuclear forces 38
3.1.2 NPC type 2 motility depends on intranuclear processes 39
3.1.3 NPC distribution and protein expression are connected in *U. maydis* 41
3.2 NPC disassembly in mitosis resembles vertebrate models 42
3.2.1 *U. maydis*' nucleoporins exhibit fungal and vertebrate features 42
3.2.2 Mitotic events in *U. maydis* resemble vertebrate model systems 43
3.2.3 The cytoskeleton is involved in re-establishing NEs in telophase 45
3.2.4 Model of nuclear pore behaviour in mitosis 45
3.3 Summary and Outlook 46
4 Material and Methods 48
4.1 Material 48
4.1.1 Chemicals, buffers and solutions 48
4.1.2 Available plasmids 48
4.1.3 Plasmids generated in this study 49
4.1.4 *E. coli* strains 55
4.1.5 *U. maydis* strains 55
4.2 Microbiological methods and growth conditions 56
4.2.1 Cultivation of *E. coli* 56
4.2.2 Cultivation of *U. maydis* 57
4.2.3 Determination of optical density 58
4.3 Molecular Methods 58
4.3.1 Standard PCR reactions 59
4.3.2 Transformation of *U. maydis* 59
4.3.3 DNA isolation from *U. maydis* 60
4.3.4 Protein isolation and Western Blotting 61
4.3.5 Plant infections and teliospore isolation 62
4.3.6 Spore germination and analysis 62
4.4 Bioinformatic analyses 62
4.5 Cell biological methods and imaging 63
4.5.1 Fixation and staining 63
4.5.2 Microcopy, image processing and analysis 63
4.5.3 Inhibitor studies 65
5 Bibliography 67

1 Introduction

In interphase, the nuclear envelope surrounds the chromosomes and separates the nucleoplasm from the cytoplasm. Embedded in the double membranes are nuclear pore complexes (NPCs), large protein assemblies which in interphase function in nuclear traffic, transcriptional regulation, chromatin organisation and DNA repair, among others (reviewed in D'Angelo and Hetzer, 2006; Tran and Wente, 2006; Akhtar and Gasser, 2007).

1.1 Architecture of NPCs

Yeast NPCs are composed of 30 different proteins, termed nucleoporins (Rout *et al.*, 2000). Similar numbers were obtained for vertebrates, although their NPCs are slightly larger (Cronshaw *et al.*, 2002). The basic architecture of the nuclear pores is evolutionarily conserved from fungi to animals (Yang *et al.*, 1998; Devos *et al.*, 2006). Nuclear pores consist of a central channel, eight-fold symmetrical scaffold rings, and filaments extending into the cytoplasm and the nucleoplasm (Figure 1, Kiseleva *et al.*, 2004; Alber *et al.*, 2007). In higher eukaryotes, the nucleoplasmic distal rings are connected and anchored in the lamina, a protein layer underneath the nuclear double membranes (reviewed in Gruenbaum *et al.*, 2005; Schirmer and Gerace, 2005). Proteins involved in building the pore are termed nucleoporins. Nucleoporins are incorporated into NPCs at different amounts, but in multiples of 8, following the eight-fold symmetrical composition of the nuclear pore (Alber *et al.*, 2007). Nucleoporins primarily involved in transport mechanisms often have numerous FG repeats in their aminoacid sequence. These nucleoporins localize predominantly to the cytoplasmic filaments, the nuclear basket or the central channel of the pore (Alber *et al.*, 2007; Patel *et al.*, 2007). Scaffold nucleoporins of the central ring structures are assembled into subcomplexes with their direct interaction partners, and, once incorporated, are not readily exchanged, e.g. Nup107 and Nup133 (Boehmer *et al.*, 2008). Binding times at the NPC underline this find, ranging from several seconds for many transport nucleoporins, e.g. Nup2, to several hours for scaffold nucleoporins, e.g. Nup107-160 subcomplex nucleoporins (Rabut *et al.*, 2004a). Components of the Nup107-160 subcomplex are located centrally in the nuclear pore, where they structure the whole protein assembly and function in mRNA transport in budding yeast and vertebrates (Siniossoglou *et al.*, 1996; Vasu *et al.*, 2001; Berke *et al.*, 2004). Recent evidence emerged that this subcomplex is also involved in DNA repair in budding yeast and transcription (Loeillet *et al.*, 2005; Menon *et al.*, 2005; Therizols *et al.*, 2006). In vertebrates, the Nup107-160 subcomplex localizes to kinetochores in mitosis,

where it participates in attaching microtubules to centromers (Belgareh *et al.*, 2001; Loiodice *et al.*, 2004; Orjalo *et al.*, 2006; Zuccolo *et al.*, 2007). In addition, the Nup107-160 subcomplex appears to play an important role in NPC formation after mitosis in vertebrate cells, disrupting NPC reassembly in cells depleted for these proteins (Harel *et al.*, 2003; Walther *et al.*, 2003; D'Angelo *et al.*, 2006). In contrast, the Nup107 homologue *nup84* is not essential in the yeast *S. cerevisiae* (Siniossoglou *et al.*, 1996) and *A. nidulans* (Osmani *et al.*, 2006). Deletion mutants exhibit NPC clustering and temperature sensitivity, underlining a conserved role in NPC structure assembly.

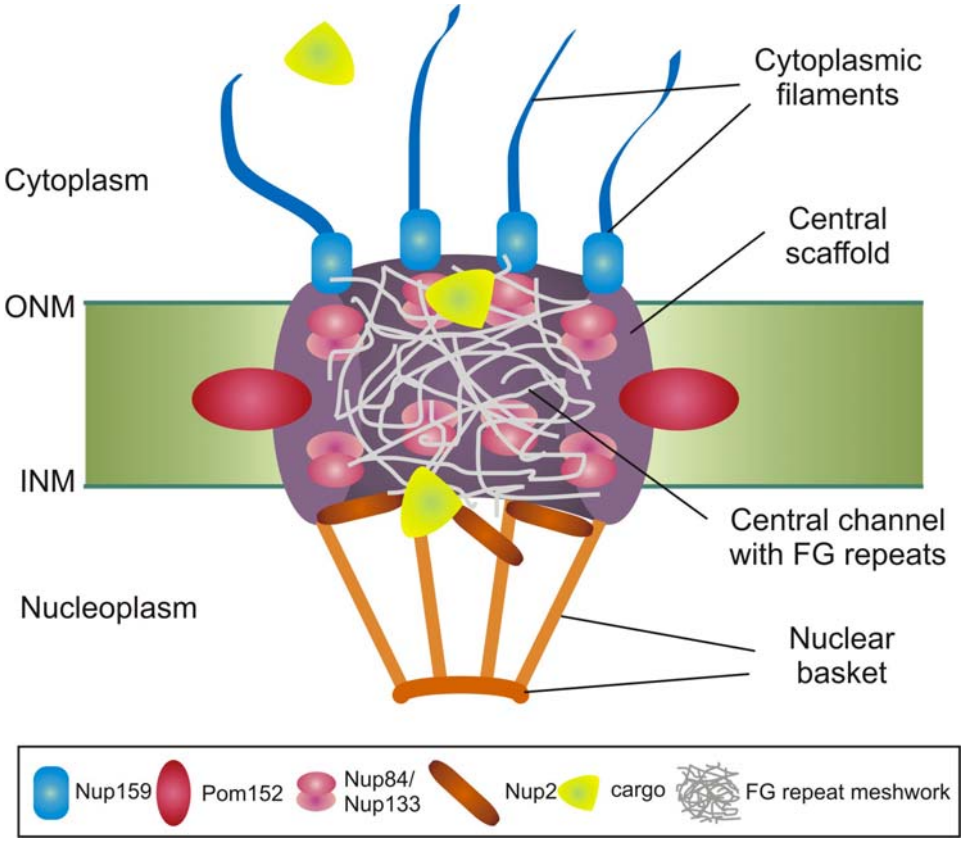

Figure 1. Schematic representation of a budding yeast nuclear pore. Localizations of nucleoporins whose homologues were investigated in this study are indicated. ONM, outer nuclear membrane; INM, inner nuclear membrane.

Peripheral nucleoporins, which in interphase localize to the cytoplasmic filaments and the nuclear basket, disperse in the cytoplasm in vertebrates (reviewed in Margalit *et al.*, 2005). Typically these nucleoporins are involved in transport through the NPC and show a variable number of FG repeats (reviewed in Beck *et al.*, 2007; Stewart, 2007). They have been characterized as “naturally unfolded” proteins (Denning *et al.*, 2003; Patel *et al.*, 2007). The unstructured appearance, together with the finding that many FG repeat nucleoporins are functionally redundant, may lead to poor evolutionary conservation (Strawn *et al.*, 2004; Denning and Rexach, 2007). Nup214/CAN, the homolog of yeast Nup159, possesses a large number of FG repeats and is located on the cytoplasmic face of an NPC (Kraemer *et al.*,

1995; Walther *et al.*, 2002), where it participates in nuclear export (Gorsch *et al.*, 1995; Hutten and Kehlenbach, 2006). Similarly, Nup50, the homolog of yeast Nup2, is an FG repeat containing nucleoporin, located in the nuclear basket, where it is involved in NPC transport processes (Booth *et al.*, 1999; Guan *et al.*, 2000). In addition, recent reports have demonstrated an important role for this nucleoporin in the transcription of reporter genes in *S. cerevisiae* (Ishii *et al.*, 2002; Schmid *et al.*, 2006).

Transmembrane-domain anchored nucleoporins are shown to disperse in the ER (Ellenberg *et al.*, 1997; Yang *et al.*, 1997). Pom152 is a transmembrane nucleoporin found only in fungi, but it might perform similar functions as the vertebrate transmembrane nucleoporins Pom121 and gp210 (Mans *et al.*, 2004). The function of Pom152 is not well understood, but it may be implicated in NPC anchoring or insertion (Madrid *et al.*, 2006).

1.2 NPCs in interphase

One of the fundamental differences in the composition of the nuclear envelope between fungi and higher eukaryotes is the absence of a proteinaceous lamina in fungi (Mans *et al.*, 2004). The lamina is thought to anchor NPCs in vertebrate model systems, while NPCs in budding yeast appear to be motile in the NE (Bucci and Wente, 1997; Daigle *et al.*, 2001). First evidence for NPC movement in budding yeast, and initial estimates of velocities were obtained in heterokaryon fusion nuclei using GFP-labelled nucleoporins (Belgareh and Doye, 1997; Bucci and Wente, 1997). Their results pointed in the direction of diffusion of NPCs in the NE, which recently gained support from FRAP results (Bystricky *et al.*, 2005).

Although NPCs are not spatially restricted by a lamina, they are connected to DNA through promoter or telomere interactions (Galy *et al.*, 2000; Ishii *et al.*, 2002). A link between NPC-promoter association, transcriptional processes and mRNA export in budding yeast has now been established (reviewed in Akhtar and Gasser, 2007; Schneider and Grosschedl, 2007; Dillon, 2008). Several genes, among them galactose-induced ones (Cabal *et al.*, 2006; Drubin *et al.*, 2006), leave their central location in the nuclear interior and become temporarily associated with Nup2 (Ishii *et al.*, 2002; Schmid *et al.*, 2006; Taddei *et al.*, 2006). Others require binding to Nup145 for efficient transcriptional regulation (Feuerbach *et al.*, 2002). The Nup84-120 subcomplex has also been implicated in supporting transcription (Menon *et al.*, 2005). These interactions between NPCs and chromatin, mediated by transcriptional processes, could provide a tether for NPCs to moving chromosomes.

Chromatin is motile in interphase nuclei and in meiotic prophase of *Saccharomyces cerevisiae* (Heun *et al.*, 2001; Scherthan *et al.*, 2007). It is currently not clear whether short-range, sliding motions of chromosomes in interphase and NPC tethering are necessary to facilitate transcription or nuclear export of transcript (Casolari *et al.*, 2004; Taddei *et al.*,

2006; Kurshakova *et al.*, 2007). This short-range interphase motion of chromosomes appears independent of microtubules, but requires energy (Heun *et al.*, 2001). Long-range motility of chromosomes occurs during meiotic prophase of budding yeast and fission yeast (Scherthan *et al.*, 2007; Conrad *et al.*, 2008). In meiosis of these organisms, chromosomes, led by the telomers, slide along the nuclear periphery to form a “bouquet” structure, where recombination takes place (Chikashige *et al.*, 1994; Trelles-Sticken *et al.*, 1999). Velocities of telomeres can be as fast as ~ 1 µm/s (Conrad *et al.*, 2008; Koszul *et al.*, 2008). The actin cytoskeleton is needed in *S. cerevisiae* for rapid motility (Trelles-Sticken *et al.*, 2005; Scherthan *et al.*, 2007; Koszul *et al.*, 2008), whereas microtubules and Dynein are necessary in *Schizosaccharomyces pombe* (reviewed in Yamamoto *et al.*, 1999; Chikashige *et al.*, 2007). Forces generated by Dynein in *S. pombe* are transferred directly onto chromosomes by SUN- and KASH-domain containing proteins (Miki *et al.*, 2004). These proteins have been discovered in many organisms so far (reviewed in Tzur *et al.*, 2006; Wilhelmsen *et al.*, 2006). Although the mechanism of rapid chromosome motility is now well described, recent studies have raised doubt whether the movements of chromosomes are an important factor in recombination itself, leaving open the question of the biological significance of the phenomenon (Conrad *et al.*, 2008; Koszul *et al.*, 2008).

1.3 NPCs in mitosis

At the onset of mitosis, one of the major tasks for the dividing eukaryotic cell is the regulated rearrangement of the nuclear envelope (NE) to allow entry and exit of factors regulating mitosis itself and cytokinesis (reviewed in Rabut *et al.*, 2004b; Margalit *et al.*, 2005).

1.3.1 Mitosis in fungi

The model systems *S. cerevisiae* and *S. pombe* possess a “closed mitosis”, in which the mitotic spindle is assembled inside the intact nuclei (Byers, 1981; Ding *et al.*, 1993). During closed mitosis, the NE remains mostly unchanged. NPCs are functional, but import properties are changed to allow passage of factors needed for mitosis to progress (Winey *et al.*, 1997; Makhnevych *et al.*, 2003). GFP-fusion of nucleoporins did not reveal any changes of localization for the majority of nucleoporins during mitosis (Tran and Wente, 2006). However, intermediate stages between fully closed or open mitosis, in which the NE is entirely disassembled, exist among groups of fungi (reviewed in De Souza and Osmani, 2007). In the ascomycete *Aspergillus nidulans,* entry into closed mitosis begins with partial disassembly of NPCs (De Souza *et al.*, 2003; De Souza *et al.*, 2004), thus challenging the term "closed" mitosis. Several peripheral components disperse in the cytoplasm, one

nucleoporin (Nup2) associates with DNA (Osmani *et al.*, 2006). However, the centrally located scaffold component Nup84-120 subcomplex remains part of the incomplete NPC (Osmani *et al.*, 2006).

Early reports looking at mitotic cells using electron microscopy identified open mitosis in zygomycetes (Heath, 1980). This group of fungi is thought to be one of the most ancient (Fitzpatrick *et al.*, 2006). Recently, open mitosis was described in the basidiomycete *Ustilago maydis* (Figure 2A, Straube *et al.*, 2005). At the onset of mitosis in haploid sporidia, a Dynein-based mechanism removes the mitotic nuclear envelope. In prophase, MTs are nucleated by the spindle pole bodies at the bud-neck, thereby establishing a polarized cytoskeleton in which the PLUS ends are at the cell poles and the MINUS ends in the neck region (Figure 2C, Steinberg *et al.*, 2001; Straube *et al.*, 2003). Movement of the SPBs into the bud stretches the nuclear envelope. The NE subsequently ruptures at the tip and remains in the mother cell (Figure 2B), while the chromosomes leave the old envelope and migrate into the daughter cell, where the spindle forms. This process is partly regulated by the Septation Initiation Network/Mitotic Exit Network (Straube *et al.*, 2005). Anaphase itself proceeds in two steps distinguished by different velocities of spindle elongation. The first phase is relatively slow, presumably driven by spindle internal pushing forces (anaphase A). The second phase proceeds much faster and relies on Dynein at the cell cortex (anaphase B, Fink *et al.*, 2006).

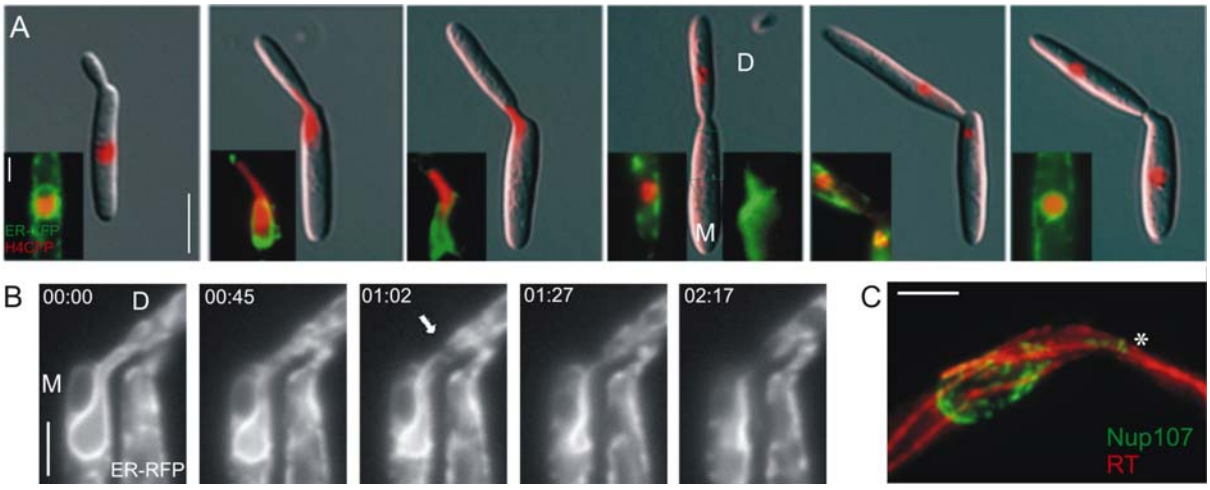

Figure 2. Open mitosis in *U. maydis*. **(A)** DIC images and fluorescent images of Histone 4-YFP illustrate the position of the DNA inside cells during the different mitotic stages. D, daughter cell; M, mother cell. Bar: 5 µm. Inset shows overlays of Histon4-YFP with ER-CFP to visualize NE removal at the end of prophase. Bar: 2 µm. **(B)** The NE is stretched in prophase and reaches into the daughter cell. Arrow marks the opening that appears at the tip of the elongated NE. The NE is subsequently collected in a membrane stack and deposited at the side of the mother cell. Bar: 3 µm. Time in min:s. **(C)** Maximum projection of a Z-stack showing microtubules passing the NE in prophase. Planes of live cells were taken at intervals of 0.4 µm in Z with a Piezo device. Asterisk indicates the bud neck, where MTs are nucleated from the SPBs. Bar: 2 µm.

1.3.2 Open mitosis in higher eukaryotes

Higher eukaryotes possess an “open” mitosis, in which the NE is removed from the chromosomes and NPCs disassemble into subcomplexes at the onset of mitosis (reviewed in Margalit *et al.*, 2005; Prunuske and Ullman, 2006), but partially open forms have also been reported in embryonal syncytia of *Drosophila melanogaster* and *Caenorhabditis elegans* (Stafstrom and Staehelin, 1984; Paddy *et al.*, 1996; Lee *et al.*, 2000). Well-studied examples of nuclear envelope breakdown (NEBD) include starfish, *Homo sapiens* and *Xenopus laevis*. These organisms remove the NE either by fragmentation, tearing of the NE or vesiculation (Beaudouin *et al.*, 2002; Salina *et al.*, 2002; Lenart *et al.*, 2003). Membrane removal often requires the microtubule cytoskeleton and the MINUS end moving motor protein Dynein (Beaudouin *et al.*, 2002; Salina *et al.*, 2002; Muhlhausser and Kutay, 2007). The removal of the envelope is accompanied by the disassembly of the nucleoporins, which either disperse in the endoplasmic reticulum (ER) or are released into the cytoplasm (Ellenberg *et al.*, 1997; Yang *et al.*, 1997). From their respective locations in mitosis, nucleoporin subcomplexes are recruited in a sequential manner to reconstitute the NPCs in the newly forming nuclei (Chaudhary and Courvalin, 1993; D'Angelo *et al.*, 2006). The different steps involved in reassembly of NPCs and NEs are especially well characterised in the *X. laevis* oocyte system and in human cells (reviewed in Margalit *et al.*, 2005; Antonin *et al.*, 2008). Depletion of Nup107 or other members of this subcomplex leads to loss of NPCs in the new nuclei in both organisms (Boehmer *et al.*, 2003; Harel *et al.*, 2003; Walther *et al.*, 2003), as the subcomplex is an important intermediate step in the reassembly process, and many other nucleoporins appear to become attached to this scaffold (D'Angelo *et al.*, 2006). A highly resolved order of attachment of nucleoporins in human cells has been resolved (Bodoor *et al.*, 1999; Dultz *et al.*, 2008). According to these results, Nup2 and Pom121 become attached shortly after Nup107-160, followed by Nup214 and finally gp210.

In contrast to the initial steps of membrane removal, the role of the cytoskeleton in the establishment of new nuclei is less clear. However, actin might be necessary to reassemble functional NEs in *X. laevis* oocytes (Krauss *et al.*, 2003).

1.4 Aim of this study

This work attempts to characterize nuclear pore behaviour both in interphase and mitosis of *U. maydis*.

As interphase movement of NPCs has never been analyzed in detail in other fungi, the observation of interphase nuclei exhibiting NPC movements could provide clues as to the underlying mechanism. In particular extranuclear forces and possible intranuclear processes

should be considered as driving forces for NPC motility. After the mechanism of NPC motility is characterized, the biological significance of the process is investigated.

The second part investigates the nuclear pores in mitosis. Observing five nucleoporins from different parts of the nuclear pore in mitosis should reveal whether NPCs disassemble similar to the open mitosis of vertebrate model systems. The comparison to the vertebrate models should include the kinetochore localization of Nup107-160 subcomplex, and the step-wise reassembly of nucleoporins in telophse. Also, the role of the cytoskeleton in the reassembly of functional NEs should be tested, as little is known about the role of the cytoskeleton in this highly ordered process.

2 Results

2.1 Identification of *U. maydis* nucleoporins

2.1.1 Bioinformatic search for nucleoporins in *U. maydis*

To investigate nuclear pore behaviour in interphase and the open mitosis of *U. maydis*, it was necessary to establish a marker for NPCs. Many nucleoporins are stably attached to NPCs, making a homologously GFP-tagged nucleoporin a good marker (Rabut *et al.*, 2004a). Therefore, homologues of nucleoporins were identified in the *U. maydis* protein databases of MIPS and the Broad Institute. A list of nucleoporins in *S. cerevisiae* and *H. sapiens* was formed from the literature (Rout *et al.*, 2000; Cronshaw *et al.*, 2002). In most cases, putative homologues with significant e-values (>e-03) were found by BLAST search with the respective nucleoporin sequences from budding yeast or their human homologues deposited in the NCBI administered databases (Table 1). However, several nucleoporins are poorly conserved in evolution (Denning and Rexach, 2007). In cases in which the budding yeast and human proteins did not produce significant hits, other fungal sequences were included in the searches. A putative homologue of the nucleoporins Ndc1 and Nup160 could thereby be detected using the *A. nidulans* protein in the searches, and the homologue of Nup88 was found by probing with the *S. pombe* homologue.

The identity of the found *U. maydis* proteins was tested by BLASTing their sequence against the *S. pombe*, *A. nidulans*, *S. cerevisiae* and *H. sapiens* proteins in the PubMed database. In a second analysis, the *U. maydis* protein sequences were checked for specific protein domains using SMART. These results are included in Table 1.

Three putative nucleoporins with transmembrane domains were found, Pom152 (um03963, as identified in the MIPS database), Brl1 (um11655) and Ndc1 (um06416). All of them exhibit significant similarity to other fungal sequences. Of their respective budding yeast counterparts only one, Ndc1, has been demonstrated to possess a vertebrate analogue (Mansfeld *et al.*, 2006; Stavru *et al.*, 2006). Other transmembrane nucleoporins (Pom34, Brr6) present in budding yeast produced no significant hits in the BLAST searches. Similarly, nucleoporins known so far only in vertebrate cells (Nup37, Nup43, Nup358, Pom121, gp210) do not possess homologues in fungi (Mans *et al.*, 2004).

Notably, although Nup53 from budding yeast has a vertebrate homologue in Nup35, no homologue was identified in *U. maydis*. Neither could a homologue of Nup60 be found. A comprehensive search for nucleoporins in *A. nidulans* neither produced a homologue for

these nucleoporins (Osmani *et al.*, 2006). This could indicate that these genes were lost in the evolution of these organisms, maybe due to functional redundancy with other nucleoporins, similar to what has been described in budding yeast (Strawn *et al.*, 2004). The other notably absent nucleoporin in *U. maydis* is Seh1. In budding yeast, Seh1 is a close

Table 1. Nucleoporins in *U. maydis*

U. maydis	***S. cerevisiae***	***H. sapiens***	**Protein domains***
um04509	Nsp1p (25.9)	Nup62 (28.4)	C-terminal Nsp1_C domain
um05489	Nup1p (21.4)	Nup153 (21.3)	Coiled coil domain
um02688	Nup2p (18.2)	Nup50 (14.3)	C-terminal Ran Binding Domain
um02245	Sec13p (45.3)	Sec13R (45.7)	WD repeats
	Seh1 (27.3)	Seh1L (22.9)	
um01308	Nup42p (26.5)	NupL2 (21.9)	N-terminal zinc finger
um01418	Nup49p (23.8)	NupL1 (20.4)	Coiled coil domain
um11701	Nup57p (23.4)	Nup54 (17.6)	
um00333	Nup82p (15.8)	Nup88 (15.7)	C-terminal coiled coil domain
um04795	Nup84p (21.2)	Nup107 (23.6)	Nup84_Nup100 domain
um04624	Nup85p (16.9)	Nup85 (22.6)	N-terminal Nup85 domain
um03813	Nic96p (27.3)	Nup93 (27.3)	NIC domain
um00639	Nup120p (16.5)	Nup160 (19.7)	
um02855	Nup133p (15.9)	Nup133 (18.5)	C-terminal Nup133 domain
um05158	Nup100p (18.3)	Nup98-96 (25.5)	Central nucleoporin 2 domain
	Nup116p (18.8)		
	N/C-Nup145 (19.0)		
um03853	Nup157p (20.2)	Nup155 (24.2)	Nup170 domain
	Nup170p (20.9)		
um01089	Nup159p (16.2)	Nup214 (20.2)	3 coiled coil domains
um06099	Nup188p (13.8)	Nup188 (14.3)	
um02524	Nup192p (15.9)	Nup205 (21.5)	
um01075	Mlp1 (18.9)	TPR (18.5)	C-terminal TPR_Mlp1_2 domain
	Mlp2 (19.6)		
um03950	Yrb2p (24.7)	RanBP3 (21.3)	C-terminal Ran Binding Domain
um03762	Gle2p (34.7)	RAE1 (37.3)	WD repeats
um06416	Ndc1p (14.8)	Ndc1 (16.8)	6 TM domains**, Ndc1_Nup domain
um03963	Pom152p (22.5)	--	3 N-terminal TM domains
um11655	Brl1p (16.5)	--	2 TM-domains

Table 1. Sequences of full-length *U. maydis* proteins were compared to sequences of *S. cerevisiae* and *H. sapiens*. Proteins derived from gene duplications are grouped, but were individually compared to *U. maydis* proteins. % identity of full-length *U. maydis* proteins to their respective homologues is given in parenthesis (Lalign).
*Protein domains were predicted by the SMART server (http://smart.embl-heidelberg.de/).
**Number of TM domains predicted by TMHMM (http://www.cbs.dtu.dk/services/TMHMM-2.0).

homologue of Sec13 (Siniossoglou *et al.*, 1996). It is possible that Sec13, which possesses a clear homologue in *U. maydis*, might compensate the absence of Seh1. Alternatively, the level of conservation of the "missing" nucleoporins might be too low to produce significant hits in these BLAST searches.

Although Table 1 might not comprise all *U. maydis* nucleoporins, it identifies good candidates for GFP-labelling.

2.1.2 Scaffold nucleoporins Nup107 and Nup133

Protein identity levels of the identified putative *U. maydis* nucleoporins (Table 1) and phylogenetic analyses (Figure 3A and 3B) unexpectedly showed a higher degree of conservation between several of the *U. maydis* and their human homologues than to the ascomycete's. Among these are all members of the Nup107-160 complex (Nup107, Nup133, Seh1, Nup160, Nup85 and Nup96; Siniossoglou *et al.*, 1996; Lutzmann *et al.*, 2002) with the exception of Seh1, which does not seem to possess a homologue in *U. maydis* (see above). In addition, protein domain models of the *U. maydis* homologues um04795 and um00639 by SMART strongly support the identity of the proteins as Nup107 and Nup133 (Figure 3A and 5B). The Nup107-160 subcomplex, or its homologous Nup84-120 subcomplex in budding yeast, is thought to be involved in providing a scaffold to other nucleoporins and thereby structuring the nuclear pore, but additional functions in mRNA export and DNA repair have been reported (Siniossoglou *et al.*, 1996; Loeillet *et al.*, 2005; Menon *et al.*, 2005).

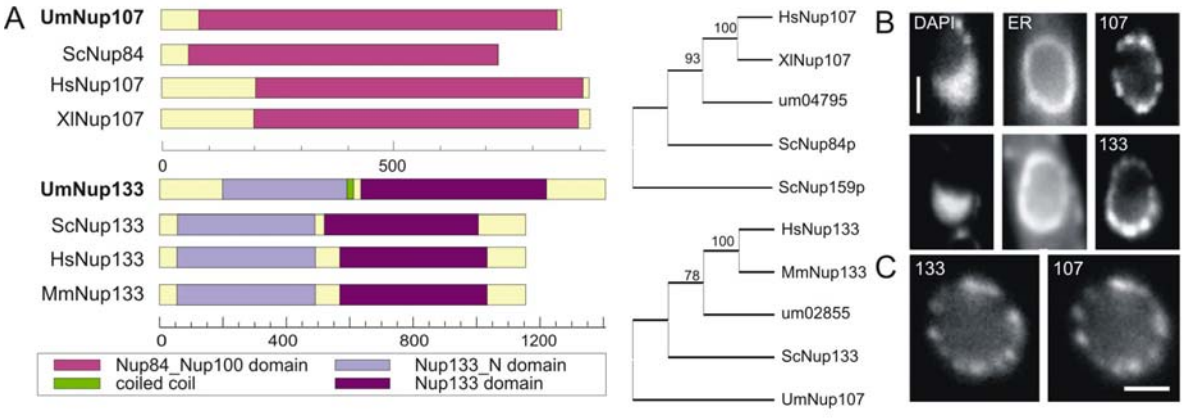

Figure 3. Scaffold nucleoporins in *U. maydis*. **(A)** *U. maydis* homologues of nucleoporins were identified by BLAST search and domain models were predicted by the SMART server (Pfam Nup84_Nup100: P=1.3e^{-44}, Pfam Nup133_N: P=1.5 e-147, Pfam Nup133: P=1.0 e^{-06}). UmNup107 serves as outgroup for the phylogenetic tree for UmNup133, ScNup159 for the tree for UmNup107. Bootstrap values are noted on the tree (minimum evolution). Um, *Ustilago maydis*; Sc, *Saccharomyces cerevisiae*; Hs, *Homo sapiens*; Xl, *Xenopus laevis,* Mm, *Mus musculus.* **(B)** GFP-fusion proteins of *U. maydis* Nup107 and Nup133 localize to the nuclear envelope in a punctuate pattern. The ER is visualized by monomeric RFP retained by the HDEL signal. DNA is stained with DAPI. Cells expressing Nup107-GFP were briefly fixed with 0.5%, cells expressing Nup133-GFP with 1% formaldehyde prior to observation. Bar: 2 µm. **(C)** As expected for proteins functioning in the same stable subcomplex Nup107 and Nup133 co-localize at the interphase NPC. Nup133 was visualized by GFP, while Nup107 was fused to RFP. Live cells were simultaneously imaged using dual-view technology. Bar: 1 µm.

DAPI staining of fixed cells co-expressing the GFP-tagged nucleoporin and mRFP with an ER-retention signal showed both nucleoporins in a punctuate pattern in the NE (Figure 3C). Simultaneous observations of live cells expressing Nup133-GFP and Nup107-RFP revealed co-localization of the proteins at the nuclear rim (Figure 3C).

Further evidence for the identity and significance of um04795 as Nup107 could be gained from a deletion mutant. Deletion of *nup84* in *S. cerevisiae* and *A. nidulans* leads to temperature-sensitivity and NPC clustering (Siniossoglou *et al.*, 1996; Osmani *et al.*, 2006), while depletion of the protein in human cells leads to NPC defects (Harel *et al.*, 2003; Walther *et al.*, 2003).

Two knockout constructs for *nup107* in *U. maydis* did not produce the desired deletion in several transformations of the haploid wildtype strains FB1 and FB2, although cells were propagated at 22°C. However, the constructs efficiently deleted one copy of the gene in the diploid strain FBD11, as verified by Southern analysis (not shown). One of these strains (FBD11ΔN107) was then used to infect plants and harvest the spores, to obtain a haploid deletion strain after germinating spores had undergone meiosis. The spores were germinated at 22°C on CM-G plates without the selective agent. Next, 57 colonies were selected and transferred to CM-G plates containing nourseothricin at 22°C, as the desired haploid knockout strain should be resistant to nourseothricin. Of these, only 36 were able to grow on nourseothricin-containing medium. However, when analyzed by Southern Blot and in a PCR based approach, all resistant strains still retained a wildtype copy of *nup107*. These results strongly suggest that *nup107* is an essential gene in *U. maydis*, similar to *nup107* in vertebrate cells and *S. pombe* (Harel *et al.*, 2003; Walther *et al.*, 2003; Bai *et al.*, 2004).

As it was impossible to study the role of Nup107 by deletion, *nup107* was placed under the control of the regulatable *crg*-promoter (Bottin *et al.*, 1996). Over night growth in arabinose-containing medium (CM-A), in which the promoter is switched on, did not result in any noticeable defects (not shown). Although Western Blot analysis showed a strong reduction of the protein after overnight growth in repressive medium (CM-G), the fluorescent signals at the NE in a strain carrying Nup107 C-terminally fused to GFP were only reduced to ~ 20% of wildtype levels (Figure 4A). The strain did not show any strong growth defect in overnight growth in CM-G (not shown). Minor defects in morphology could be seen in the majority of cells, but more severe defects were rare (Figure 4B), maybe due to the predicted high stability of the protein (Bai *et al.*, 2004; Rabut *et al.*, 2004a) or the incomplete repression of the *crg*-promoter. However, levels of Nup107-GFP in the NE did not exhibit a clear correlation to the severity of the morphological defect, as severely aberrant cells did not always show significantly less signal at the NE (Figure 4B).

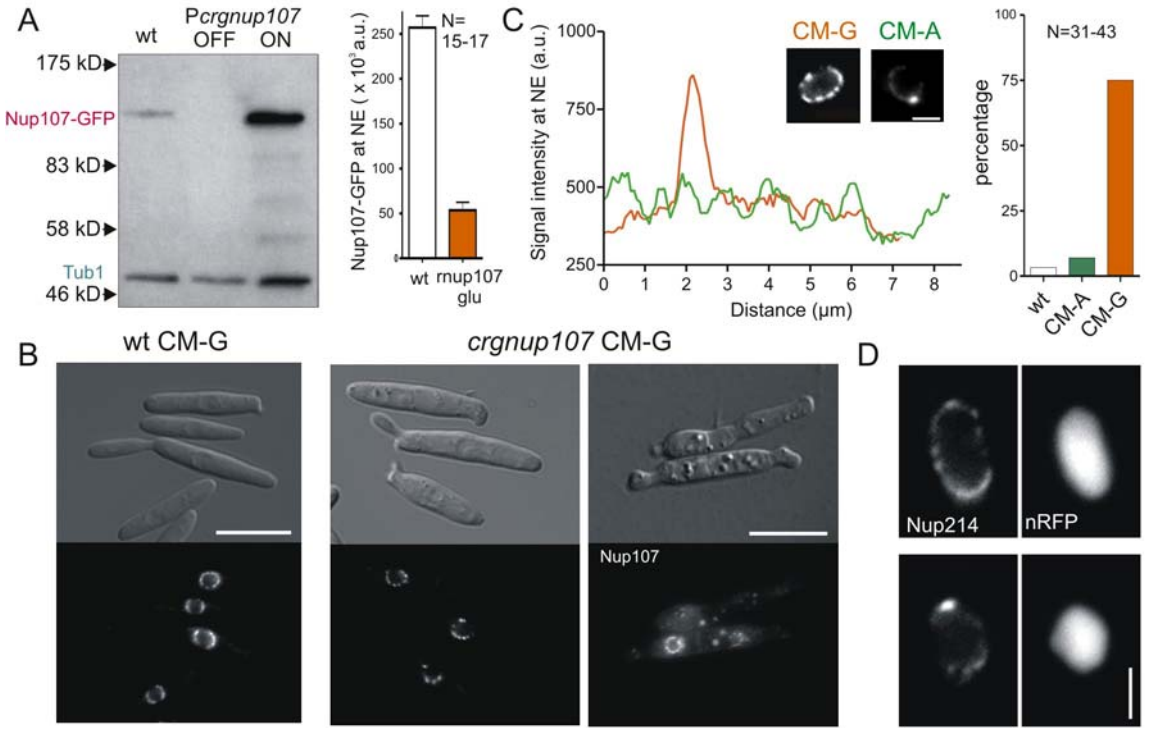

Figure 4. Downregulation of *nup107* results in NPC clustering. **(A)** Left lane of the blot is Nup107-GFP, endogenously integrated, grown in CM-G. The middle lane is P*crg-nup107-gfp* grown over night in CM-G, right lane same strain grown under CM-A. Over night growth in CM-G strongly reduces protein levels in P*crg-nup107-gfp* mutants as illustrated by the Western Blot. Note that the *crg*-promoter gives overexpression in ON conditions (CM-A). However, not all protein is lost from the cells when Nup107-GFP in live cells at the NE is measured. For both analyses, cells were grown in CM-G over night. **(B)** Reduction of Nup107 causes only slight morphological alterations in the majority of cells. Severe defects are rare (~13% of cells, compared to 4% in wildtype strains), but do not directly correlate with Nup107 levels. Cells were grown over night in CM-G. Bar: 10 µm. **(C)** The majority of cells show accumulations of NPCs in one – sometimes two – clusters at the NE when grown over night in CM-G. Linescans along the NE of cells grown in CM-A or CM-G illustrate the accumulation of NPCs identified by Nup214-GFP. Bar: 2 µm. **(D)** Nuclear import is not impaired by NPC clustering compared to growth in CM-A as visualized by the Nls-3xRFP reporter construct. Bar: 3 µm.

Live cell imaging of these Nup107-depleted cells with Nup214-GFP as NPC marker (see below) revealed clustering of the majority of NPCs in one, occasionally two areas at the NE in most of the cells (Figure 4C). This phenotype has been reported for members of the Nup84-120 subcomplex in *S. cerevisiae* (summarized in Fabre and Hurt, 1997), and for deletion of other members of the Nup107-120 complex in *S. pombe* (Bai *et al.*, 2004). Functionality of the NPCs in these cells was assessed by observing the intranuclear accumulation of a reporter protein. This reporter consists of a fused triple mRFP behind a nuclear localization signal (Straube *et al.*, 2005). Once the protein folds inside the nucleus, it cannot diffuse through intact NPCs with their size exclusion limit of 40kD for diffusion (Shulga *et al.*, 2000). P*crg-nup107* cells grown in CM-G over night were able to import and retain the reporter construct, demonstrating that nuclear import is unaffected by depletion of Nup107 and NPCs are still functional (Figure 4D).

These studies of deletion and protein depletion confirm the identity of um04795 as homologue of Nup84 from budding yeast and Nup107 from vertebrates, incorporating phenotypes reported in these organisms.

2.2 Nuclear Pore motility in interphase

2.2.1 Nuclear Pores are motile in the NE

Having established um04795 as nucleoporin Nup107 in *U. maydis*, the fusion to GFP was used in microscopic analysis of interphase NPC behaviour. The protein is stably incorporated into NPCs in 16 or 32 copies in other organisms (Rabut *et al.*, 2004a, Rout *et al.*, 2000), making it a good marker for moving NPCs.

At first glance, many interphase cells appeared to possess aggregations of NPCs. These accumulations could be easily visualized in 3D reconstructions of fixed cells (Figure 5A). As the aggregation often appeared at the poles of nuclei, which might indicate a connection to an underlying structure, the signal intensity of Nup107-RFP was measured in the area of the nucleolus and the region of the NE adjacent to DNA. According to these results, NPC aggregations did not preferentially occur at specific locations at the NE (Figure 5B).

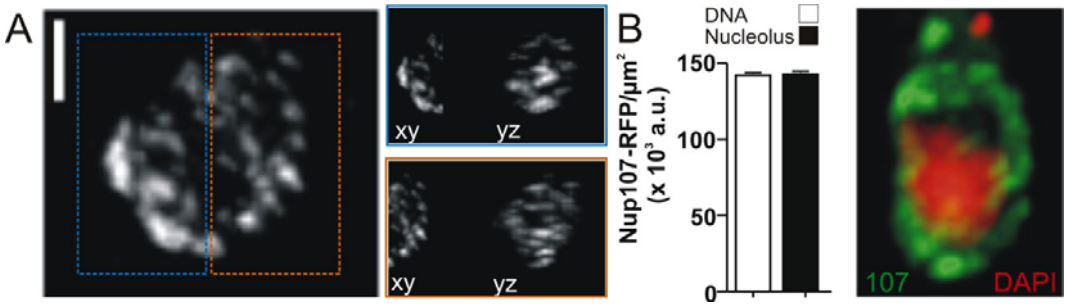

Figure 5. NPCs show a tendency to cluster in interphase nuclei. **(A)** Maximum projection of a Z-stream of an interphase nucleus shows an uneven distribution of NPCs in the left and right half. These halves are represented in the middle and lower panel in xy- and yz-orientation. Cells were briefly fixed with 0.5% formaldehyde. Images were acquired every 0.5 µm in Z. Bar: 1 µm. **(B)** Maximum projection of a Z-stream of a DAPI stained cell shows no asymmetry in NPC aggregations. This finding is reflected in the signal intensities of Nup107-RFP per μm^2 in the area of the NE adjacent to DNA, labelled by Histone 4-GFP, or in the region of the nucleolus (N=18). Images were taken every 0.5 µm in Z. Bar: 1.5 µm.

2.2.2 Nuclear pores move in distinct motility types

The aggregations of NPCs appeared to be only temporary in live cells. NPCs can be observed moving in 2D on the surface of the nucleus when focussing on the top of a nucleus. Overlays of different planes from the film show displacement of NPCs over time (Figure 6A). In these overlays, NPCs are found to be displaced in different directions from their respective start points in short time intervals. If the perceived movement of NPCs were due to a rotation of the whole nucleus, which has been reported in other organisms (De Boni and Mintz, 1986; Levy and Holzbaur, 2008), all NPCs should be displaced in the same direction. Therefore, nuclear rotation is not responsible for the observed NPC displacements.

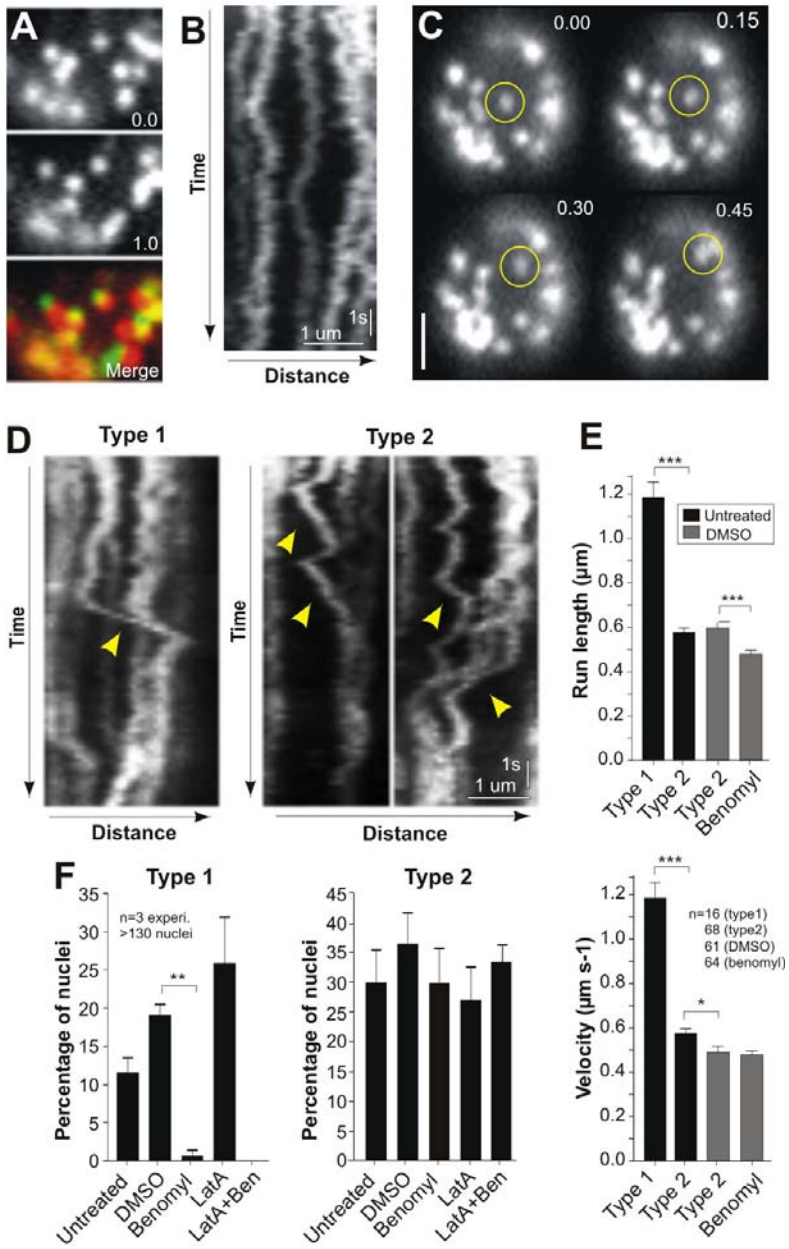

Figure 6. NPCs exhibit two types of directed motility **(A)** Moving NPCs are filmed looking at the top of a nucleus. The overlay of two planes of the film illustrates the shift in position of NPCs, identified by Nup107-GFP. Note that signals are displaced in different directions. Time in s. Bar: 1 µm. **(B)** Kymographs were created from top view films of nuclei along the cell axis to visualize NPC motility. **(C)** Representative images from a stream follow the directed motion of a single NPC (circled). Time in s.ms. Bar: 1 µm. **(D)** Directed NPC motility can be grouped into two classes. Type 1 comprises long range, fast motility, type 2 short range motion. Examples are indicated by arrowheads. Bars: 1 µm and 1.5 s. **(E)** Both run length and velocity of NPCs are strongly reduced in the absence of MTs. Type 2 is almost unaffected by Benomyl treatment. Cells were incubated with 30 µM Benomyl, control cells with DMSO for 30 min. *, p<0.05; ***, p<0.0001 **(F)** Type 1 motility depends on intact MTs, while Type 2 motility does not. Actin does not influence NPC motility. Cells were treated with 30 µM Benomyl, 10 µM Latrunculin A, or both, for 30 min. **, p<0.001.

In order to trace and measure movements, kymographs were constructd. In kymographs the position of a fluorescent signal along a line is plotted horizontally, while every plane of a stream is plotted vertically to represent time (Figure 6B). According to the kymographs, individual NPCs occasionally moved in a directed manner (Figure 6C and 6D). Two types of directed motility of NPCs in wildtype cells become apparent. The first is characterized by long range, fast movement, on average reaching 1.2 µm, spanning over half of a nucleus (arrowheads in Figure 6D, and Figure 6E). The second type incorporates short-distance, slow movements (arrowheads in Figure 6D, and Figure 6E).

2.2.3 NPC Type 1 motility requires extranuclear forces

Many cellular processes involving directed motility depend on the cytoskeleton. Therefore, the next step was to test the involvement of the components of the cytoskeleton in interphase NPC motility. In interphase, microtubules run from one end of the cell to the other, passing the nucleus (Steinberg *et al.*, 2001, Straube *et al.*, 2003). When MTs pass the nucleus, they could come into contact with NPCs, thereby providing tracks for moving NPCs. Rapidly moving NPCs were found to co-localize with and move along a MT passing the nucleus (not shown).

To test whether the cytoskeleton is involved in moving NPCs, wildtype cells were treated with 30 µM Benomyl (inhibitor of MTs) or 10 µM Latrunculin A (inhibitor of F-actin) for 30 min to specifically disrupt either component of the cytoskeleton (Coué *et al.*, 1987; Fuchs *et al.*, 2005). All experiments involving inhibitors were carried out in triplicates, with control strains to evaluate the inhibitors. From the kymographs, velocities and run lengths of NPCs were determined. In the presence of Benomyl, the percentage of nuclei exhibiting type 1 motility was almost abolished, while type 2 motility appeared largely unaffected, although a slight, but significant reduction in run length could be detected (Figure 6E and 6F). Latrunculin A, however, had no effect on either motility type (Figure 6F). Simultaneous disruption of both components of the cytoskeleton did not have additional effects on either motility type. Therefore, type 1 NPC motility requires MTs, while type 2 is independent of the cytoskeleton.

In addition to the reduction in NPC motility, a significant fraction of Benomyl treated nuclei exhibited NPC clustering at the poles of the nuclei (see below, Figure 11D). These clusters appeared stable over the observation time of 12 s (not shown).

The MT cytoskeleton and its MINUS-end moving motor Dynein have previously been implicated in NE deformations in *U. maydis*. Temporary extensions of the NE have been reported (Wedlich-Söldner *et al.*, 2002a; Straube *et al.*, 2001). These extensions rely on the function of Dynein (Straube *et al.*, 2001). Occasionally, extensions of the NE were observed along MTs (not shown). These extensions were often led by an NPC at the tip. The interior of the extension was still connected with the nuclear interior, as indicated by the presence of the nuclear reporter 3xRFP in the extension (Figure 7A).

The Benomyl experiments and the NE extensions suggested the involvement of molecular motors in NPC motility. The velocity determined for type 1 NPC motility is in the range of values measured *in vivo* for Dynein and Kinesins (Presley *et al.*, 1997; King and Schroer, 2000; Wedlich-Söldner *et al.*, 2002b; Lee *et al.*, 2003; Cai *et al.*, 2007). These motors could therefore provide the force to move NPCs along MTs.

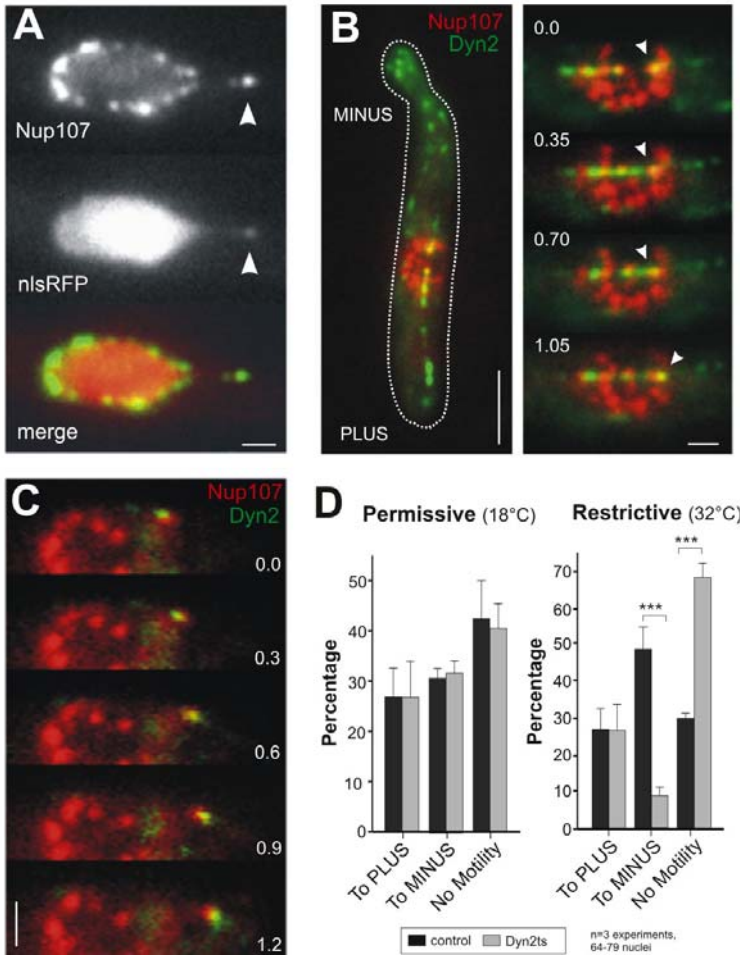

Figure 7. NPC long range motility and NE deformation are partly driven by Dynein. **(A)** Occasionally, a deformation of the NE can be seen. Typically, the extension shows an NPC at the tip. The extension retains its connection to the nuclear interior as indicated by the presence of the nuclear triple RFP fusion. Bar: 1 µm. **(B)** In budded cells, MTs are nucleated at the neck region. The orientation of MTs is indicated. MINUS end moving Dynein (3xGFP-Dyn1) sometimes co-localizes with Nup107-RFP. Dotted white line traces the cell's outline. Time in s.ms. Bars: 3 µm. in overview image, 1 µm in film sequence **(C)** In cases of NE deformation in the MINUS direction, Dynein was sometimes observed co-localizing with the leading NPC. Time in s.ms. Bar: 1 µm. **(D)** Quantitative analysis of temperature sensitive mutants of Dynein exhibit a strong decrease in MINUS end directed NPC motility. Cells were incubated at 32°C for 2 h before analysis. ***, $p<0.0001$

To determine the direction of NPC type 1 motility and NE extensions, budded cells were chosen for analysis. In budded cells, MTs are nucleated from MTOCs in the neck region (Figure 7B, Steinberg *et al.*, 2001; Straube *et al.*, 2003; Fink and Steinberg, 2006). Therefore, MT MINUS ends are located in the neck region and PLUS ends extend towards the cell poles. Co-localization of 3xGFP-Dyn1 with Nup107-RFP could provide cues whether the MINUS end directed motility could be driven by Dynein. In several instances, Dynein could be found co-localizing, or even travelling with an NPC (Figure 7B and 7C). To gather further evidence that MINUS end directed type 1 nuclear pore motility is supported by Dynein, NPCs were observed in a strain carrying the temperature-sensitive allele of Dyn2 (Wedlich-Söldner *et al.*, 2002a). When a control strain expressing Yup1-GFP was shifted to the restrictive temperature of 32°C for 2 h, all MINUS end directed endosome motility was abolished (not shown). Temperature-sensitive Dyn2 mutants expressing Nup107-YFP were subsequently incubated at restrictive temperature for 2 h, and all motile events in nuclei of budded cells counted according to their direction towards PLUS or MINUS ends of the MTs. Compared to control strains and $Dyn2^{ts}$ mutants at permissive temperature, the MINUS end motility of NPCs was significantly reduced in $Dyn2^{ts}$ mutants at restrictive temperature (Figure 7D). Taken together, these results strongly suggest that MINUS end directed rapid

NPC movements depend on Dynein. PLUS end motility is likely to be mediated by an as yet unidentified Kinesin.

2.2.4 Chromosome motion cannot be correlated with NPC movements

In the absence of MTs or actin, type 2 motility persists. To test whether type 2 motility is an active, energy-dependent process, cells were depleted for ATP by adding CCCP (Figure 9A). This treatment abolishes both type 1 and type 2 motility, proving that also type 2 requires energy. As NPCs are (temporarily) linked to chromatin in other organisms (Ishii *et al.*, 2002; Cabal *et al.*, 2006), chromosome motility could play a role in interphase NPC type 2 motility. To address this question, centromers were labelled by Mis12-3xGFP and chromatin movement monitored microscopically (Figure 9B).

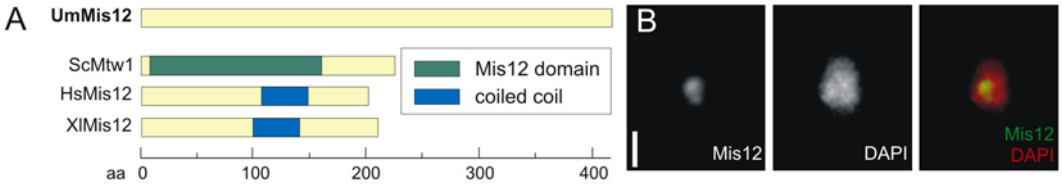

Figure 8. um04180 is a homologue of Mis12. **(A)** Protein models were constructed as predicted by the SMART server. **(B)** In metaphase, chromosomes labelled by DAPI gather in the bud. Mis12-3xGFP localizes to the centre of the accumulation, where the spindle forms. Cells were briefly fixed with 0.4% formaldehyde and 0.1% glutaraldehyde. Bar: 1 µm.

Mis12, and its budding yeast homologue Mtw1, is part of the MIND complex which forms kinetochores (Goshima *et al.*, 2003). Mis12 in human cells has been demonstrated to bind to interphase centromeres (Hemmerich *et al.*, 2008). In human cells, Mis12 binds to centromers in interphase and in mitosis, although residence times at the centromers are strongly increased in mitosis (Hemmerich *et al.*, 2008) The *U. maydis* homologue um04180 has 18.8% identity to Mtw1 from *S. cerevisiae*, 12.5% identity to *S. pombe* Mis12 and 11.0% identity to *H. sapiens* Mis12. SMART did not detect any annotated protein domains, but the 3xGFP labelled protein localizes in the center of the spindle in metaphase (Figure 8A and 8B). Using this marker, rapid centromere movements could be detected, sometimes reaching across most of the nucleus (Figure 9B and 9C). Most of these movements occurred in the interior of the nucleus, but sliding along the NE was also observed (not shown). This is similar to what has been found in budding yeast interphase nuclei (Heun *et al.*, 2001; Cabal *et al.*, 2006).

In budding yeast and fission yeast the cytoskeleton can drive rapid chromatin movement (Yamamoto *et al.*, 1999; Koszul *et al.*, 2008). To investigate this possibility in *U. maydis*, Mis12-3xGFP expressing cells were treated with Benomyl and Latrunculin A. Disruption of the cytoskeleton did not significantly alter centromere motility as described by velocity

measured in kymographs (Figure 9D). Comparable values for centromere movement have been obtained in budding yeast interphase nuclei and meiotic prophase (Heun *et al.*, 2001; Scherthan *et al.*, 2007; Koszul *et al.*, 2008). These velocities are significantly faster than the velocity determined for type 2 NPC motility under Benomyl exposure, making it unlikely that chromatin motion is largely responsible for NPC type 2 motility. In most NPC type 2 events, observed under Benomyl to remove interfering type 1 motility, Mis12-3xGFP was not found co-localizing with the moving NPC (Figure 9E). However, these co-localization results could be misleading, as centromeres might not interact with NPCs. Histone 4-GFP was used to identify total DNA in co-localization with NPCs. Although Histone 4 and Nup107-RFP signals now are adjacent to each other, NPCs were found moving independently of Histone 4-GFP signals (Figure 9F). While these results do not rule out that short-lived contacts between chromatin and NPCs contribute to NPC displacement, it seems unlikely that NPC and chromatin motility are directly coupled.

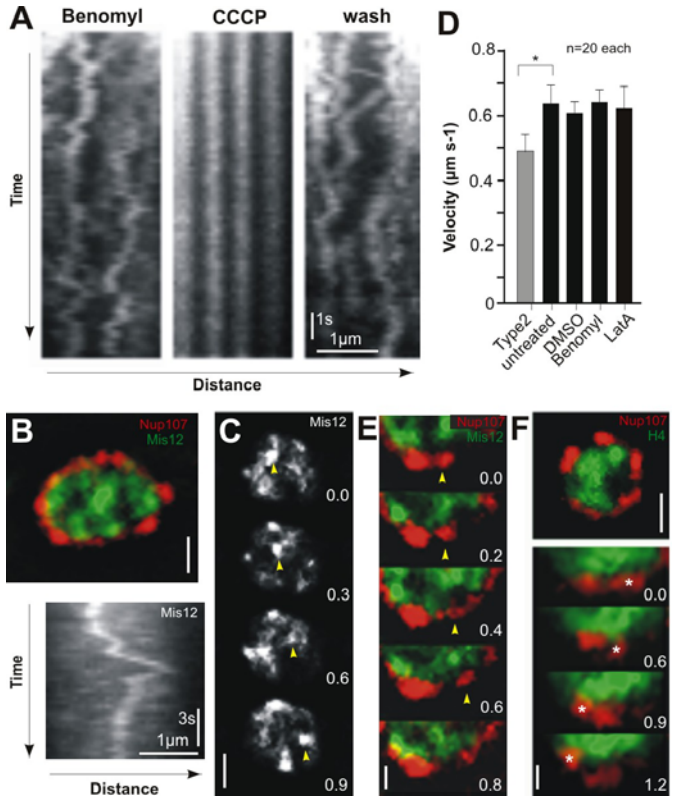

Figure 9. Chromatin movement in interphase is independent of NPC motility. **(A)** Type 2 NPC motility persists in the absence of MTs. However, when cells are depleted of ATP (CCCP 100 µM for 15 min), all NPC motility is abolished. Cells recover from CCCP treatment in 30 min and display full NPC motility. **(B)** Mis12 reveals rapid motility of centromeres in interphase. Bar: 1 µm. **(C)** Centromere displacement can span most of the nucleus. Time in s.ms. Bar: 1 µm. **(D)** Velocities of centromeres under cytoskeleton disrupting drugs show no significant differences. However, centromere velocity is significantly faster than NPC type 2 motility. *, p<0.05. **(E)** Arrowhead points to an example of a moving NPC not adjacent to a Mis12 signal. Time in s.ms. Bar: 0.5 µm. **(F)** Histone 4-GFP was co-expressed with Nup107-RFP to visualize bulk chromatin and adjacent NPC motility. Large image gives an overview of the nucleus, images below are taken from a film, focussed on the lower edge of the nucleus. Asterisk labels a moving NPC which appears to move without adjacent Histone 4, although DNA and NPCs are in close proximity. Time in s.ms. Bar: 0.5 µm.

2.2.5 Transcription participates in Type2 NPC motility

Although chromatin movement appeared to have no direct influence on type 2 NPC motility, processes occurring inside the nucleus could still be involved in NPC movement.

As the Nup84-120 complex in *S. cerevisiae* functions in DNA repair (Loeillet *et al.*, 2005; Therizols *et al.*, 2006), the involvement of repair mechanisms in NPC type 2 motility in

U. maydis was tested. However, initial experiments using chemicals or UV light to inflict different types of DNA damage failed to reveal a reproducible connection between NPC movement and DNA repair (not shown).

DNA replication might also be responsible for NPC short range motility, as it may rely on a functional NE (Spann *et al.*, 1997). A fraction of nuclei in unbudded cells should then exhibit more type 2 NPC motility (Snetselaar and McCann, 1997). However, type 2 motility was found in nuclei of all interphase stages, and preliminary experiments with Hydroxyurea to block S phase in *U. maydis* did not result in a reduction of type 2 NPC motility (not shown), making DNA replication an unlikely candidate to cause most type 2 motility.

Several genetic loci have been shown to shift in nuclear position upon induction of transcription and become located, at least temporarily, at NPCs (Cabal *et al.*, 2006; Taddei *et al.*, 2006). Hence active transcription could have an impact on NPC movement, which was tested by incubating cells first 15 min with 30 µM Benomyl to remove type 1 motility, then adding 5 µg/ml Thiolutin for 30 min. This drug has been demonstrated to efficiently inhibit transcription in budding yeast, presumably by chelating metals and thereby inhibiting all RNA Polymerases (Tipper, 1973; Grigull *et al.*, 2004). A strain expressing GFP from the *crg*-promoter was used as a control for the drug's efficiency in *U. maydis*.

Thiolutin and Benomyl treatment led to a strong reduction of NPC movement of type 2 motility (Figure 10A and 10B). This result could be confirmed by incubating cells in a similar way first with Benomyl, then adding 25 µg/ml Mycophenolate (Figure 10A). Mycophenolate reduces cellular GTP by inhibiting the Inosine Monophophate Dehydrogenase, an enzyme functioning in purine biosynthesis, thereby blocking transcription in *S. cerevisiae* (Shaw and Reines, 2000; Mason and Struhl, 2005). All inhibitor treated cells exhibited NPC motility after the drugs were washed out and cells were allowed to recover in fresh medium for 30 min, demonstrating that the cells had not died during inhibitor treatment, thereby creating artifacts in NPC motility (Figure 10A).

Although treating cells with Thiolutin or Mycophenolate separately efficiently blocked transcription in our assay using strain FB2crgGFPN107R (not shown), the addition of both drugs simultaneously reduced type 2 NPC motility even further (Figure 10B). It is possible that this finding reflects the more efficient block of transcription imposed by the drugs functioning in different pathways. This would then corroborate the involvement of NPCs with active transcription. However, the type 2 NPC motility still was not completely abolished even under both transcription inhibitors, suggesting that other processes not investigated in this study could contribute to NPC movement.

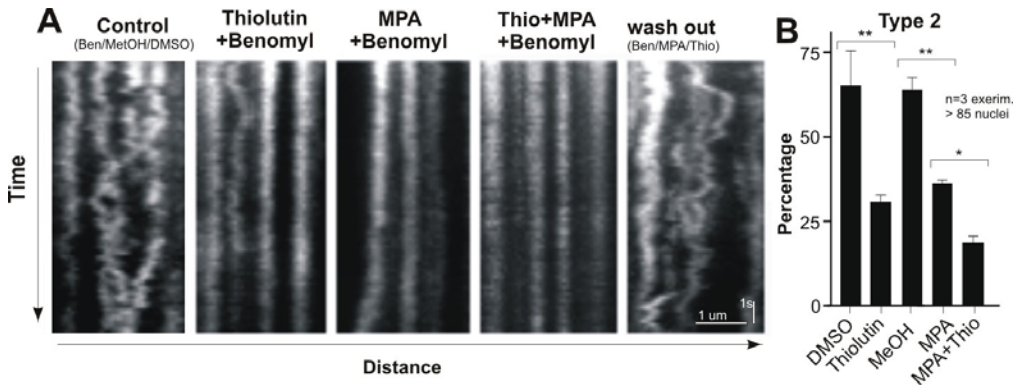

Figure 10. NPC motility type 2 is supported by transcription. **(A)** Benomyl treatment (30 µM for 30 min) abolishes type 1 long range motility, but leaves type 2 short range motility intact. Incubating cells with 30 µM Benomyl and 5 µg/ml Thiolutin or 25 µg/ml Mycophenolate strongly reduces NPC motility, indicating that transcription is involved in moving NPCs in a Type 2 manner. **(B)** Exposing cells to both transcription inhibitors and Benomyl further reduces NPC motility, but does not fully block it. However, Mycophenolate and Thiolutin have an additive effect. *, p<0.05; **, p<0.001

Taken together, NPC motility is largely driven by two mechanisms. The rapid movements rely on the microtubule cytoskeleton with Dynein as MINUS moving motor, and presumably a PLUS-end moving Kinesin. The second, short range motility appears to depend largely on active transcription.

2.2.6 NPC motility ensures equal NPC distribution and efficient protein expression

To investigate the part both types of NPC motility play in distributing NPCs equally, the Benomyl and Thiolutin experiments were repeated in a FRAP (fluorescence recovery after photobleaching) setup. The 405 nm laser was adjusted to bleach an area of about half a nucleus, and signal recovery under drug treatment measured. As Nup107-GFP is thought to be very stably attached to an NPC (in the order of several hours, Rabut *et al.*, 2004a), signal recovery during the total observation time of 6 min should result from NPCs moving into the bleached area rather than exchange of Nup107-GFP from the bleached NPCs against fluorescent Nup107-GFP from the cytoplasmic pool.

In untreated wildtype cells, single NPCs could be seen moving into the darkened area shortly after bleaching, emphasizing that individual NPCs can move directionally (arrowhead in Figure 11A). Most of the bleached area, however, was still dark.

In DMSO treated cells serving as positive control, recovery of the Nup107-GFP signal occurred within ~30 s after bleaching (Figure 11B and 11C). Note that the signal did not reach levels of unbleached nuclei, presumably due to scattering of the bleaching laser which reduced fluorescent levels of NPCs adjacent to the bleached area and a greater spread of the still fluorescent NPCs over the same area. In CCCP exposed cells, no signal recovery

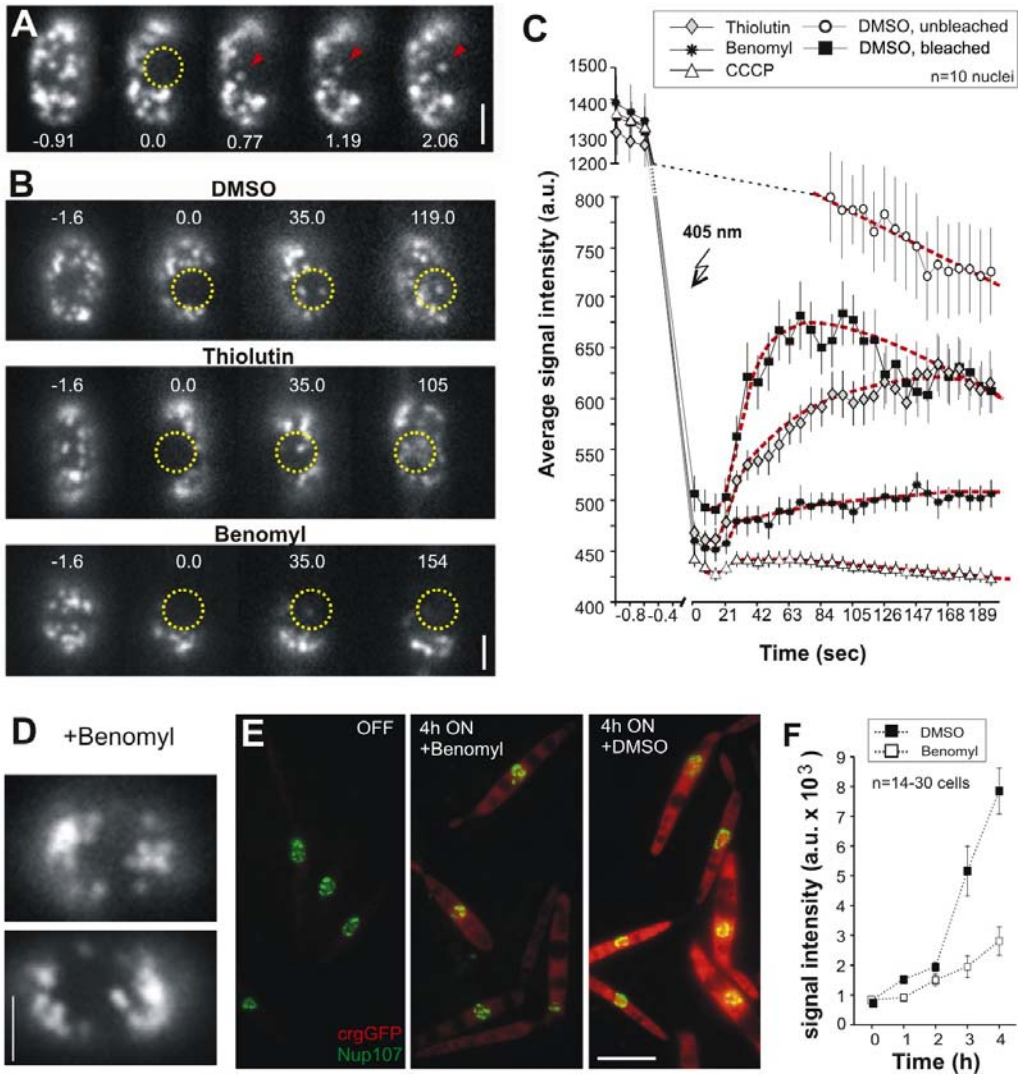

Figure 11. NPC movement is necessary to facilitate efficient protein expression. (A) Shortly after bleaching, an NPC (arrowhead) starts to move into the dark area, demonstrating directed motility. Most of the bleached area remains dark. The laser was adjusted to bleach roughly half the nucleus. Circle indicates bleached area. Time in s.ms. Bar: 1 µm. **(B)** MTs and movement by transcription ensures equal distribution of NPCs in the NE. FRAP experiments on cells treated with different drugs show a delay of recovery of Nup107-GFP signal in the bleached areas. As Nup107 is supposed to be stably attached to the NPCs, recovery of the signal in the bleached area is most likely to originate from NPCs migrating into the bleached area. Circles indicate bleached areas. Time in s.ms. Bar: 1 µm. **(C)** Quantitative analysis of these FRAP experiments confirms the delay in NPC distribution. When type 1 NPC movement is inhibited (Benomyl), the delay is most prominent. But when type 2 NPC movement (Thiolutin) is impaired, signal recovery is also delayed, illustrating that both mechanisms participate in NPC distribution. Fluorescence signal was measured in every plane of a timelapse (7s interval). Bleaching curve is included for reference. Values are mean±SEM. **(D)** Cells exposed to 30 µM Benomyl for 30 min often exhibit clustering of NPCs at opposite poles of the nucleus. Bar: 1 µm. **(E)** Equal NPC distribution aids protein expression. When expression of GFP from the regulatable *crg*-promoter was induced by shift to CM-A, cells were either treated with 30 µM Benomyl or DMSO. After 4 h of treatment, interphase cells of the Benomyl treated cells show weaker GFP signal than control cells. Bar: 10 µm. **(F)** Quantitative measurement of GFP fluorescence in the cytoplasm of cells illustrates delayed protein expression in Benomyl treated cells. Nuclei with equally distributed nuclei in DMSO cells were compared against clustered NPC containing nuclei in Benomyl treated cells.

was observed, consistent with the complete block of NPC motility upon ATP-depletion. Cells incubated in Thiolutin recovered the signal more slowly, but reached equal distribution of NPCs eventually. Therefore type 1 movement, which persists in Thiolutin treated cells, is

sufficient to distribute NPCs over the surface of the nucleus. Benomyl treated cells, however, recovered the signal very slowly, and in the observation time of 6 min only exhibited about half the signal of control cells (Figure 11B and 11C). This suggests that transcription dependent type 2 motility is not able to equally distribute NPCs. The effect was especially pronounced in cells that show NPC clustering at opposite poles of the nucleus upon exposure to Benomyl (Figure 11D).

To investigate the significance of equal NPC distribution, strains that express GFP from the arabinose inducible *crg*-promoter, and Nup107-RFP were exposed to Benomyl upon promoter induction. The strains carried random insertions of the *crg-gfp* construct in their genome, to avoid influences on transcription by the neighbouring chromatin, e.g. heterochromatin silencing. After 4 h, control cells expressed GFP at high levels, whereas Benomyl treated cells showed weaker signal (Figure 11E, note that images were scaled to the same range of brightness). When average GFP intensity in the cytoplasm was measured, the discrepancy of signal intensities in DMSO treated cells with equally distributed NPCs and nuclei with clustered NPCs in the presence of Benomyl became even more pronounced (Figure 11F). These measurements were reproduced in 2 other transformants.

These results suggest that equal NPC distribution depends on type 1 motility and is required for efficient protein expression. Mechanisms to ensure equal distribution might have evolved to aid transcription itself or to efficiently export the transcript, which we cannot distinguish in these assays. To determine the exact mechanism by which NPC distribution supports efficient protein expression, further research is needed.

2.3 Nuclear Pore Behaviour in Mitosis

2.3.1 Peripheral nucleoporins

Nup107-GFP is stably incorporated into NPCs (Rabut *et al.*, 2004a), which made it a good marker to study NPC motility in interphase. To detect NPC disassembly in mitosis, it was necessary to label other nucleoporins in addition to Nup107 and Nup133 from different subcomplexes and localizations at the NPC. The proteins for GFP-tagging were selected from the list of putative nucleoporins in *U. maydis* (Table 1) after their respective homologue's position at the nuclear pore in *S. cerevisiae* and human cells.

Among the FG-repeat containing transport nucleoporins is Nup159 in budding yeast, or Nup214, its homologue in vertebrates. Nup159 and Nup214 are located only on the cytoplasmic face of the nuclear pore in vertebrate cells and budding yeast, where they

participate in anchoring other cytoplasmic face nucleoporins protruding from the central pore, and in nuclear transport (Kraemer *et al.*, 1994; Kraemer *et al.*, 1995). Compared to both Nup159 and Nup214, the *U. maydis* homologue of Nup214 is significantly larger (Figure 12A). Although it is not predicted to possess the N-terminal WD domains, protein identity levels (Table 1) and phylogenetic analysis places it closer to the vertebrate homologue (Figure 12A). The C-terminally tagged Nup214-GFP again was found in the NE, identified by ER-RFP and DAPI staining, and it co-localized with Nup107-RFP in fixed cells (Figure 12B and 12C).

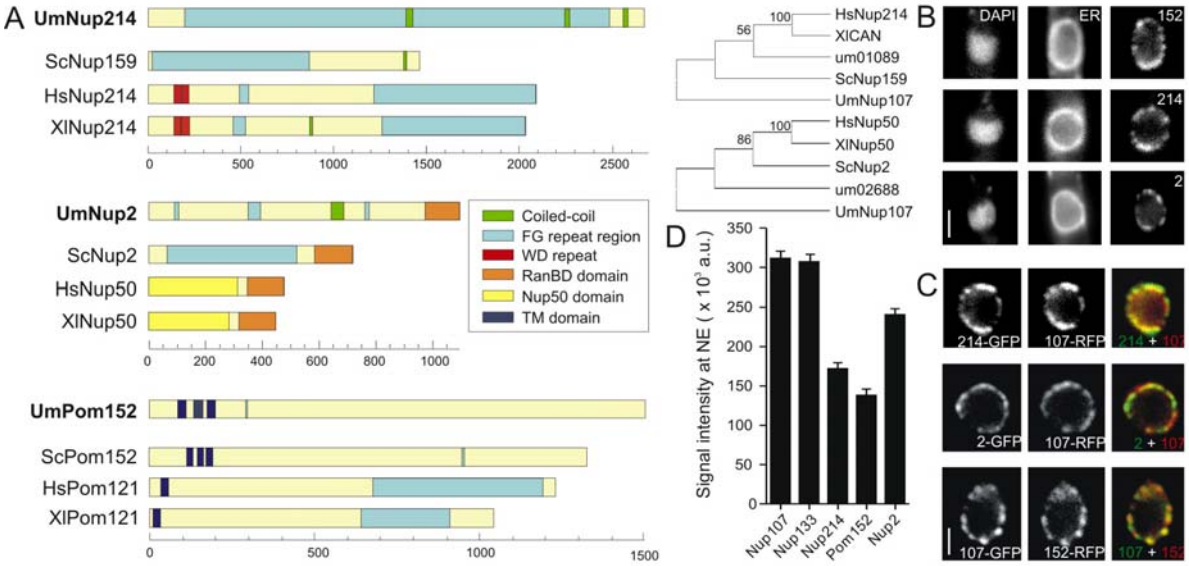

Figure 12. Peripherally attached nucleoporins in *U. maydis*. **(A)** Protein models for all nucleoporins were predicted by the SMART server (Pfam RanBD: P=2.9 e^{-09}). Note that FG repeats are not marked as individual sequences, but as areas of interspersed FG repeats, and are not annotated in areas of overlapping Nup50 domains. Although Pom121 is no orthologue of Pom152, it may execute similar functions and is therefore included for reference. A phylogenetic tree was omitted from the figures, as Pom152 is exclusively found in fungi (Mans *et al.*, 2004). UmNup107 serves as outgroup for the trees of UmNup214 and UmNup2 (minimum evolution, bootstrap values are noted on the graphs). Um, *Ustilago maydis*; Sc, *Saccharomyces cerevisiae*; Hs, *Homo sapiens*; Xl, *Xenopus laevis.* **(B)** When tagged in locus with GFP, the putative nucleoporin-GFP fusion proteins localize at the NE as visualized by co-expression of ER-targeted mRFP. Cells were briefly fixed with formaldehyde or a mixture of formaldehyde and glutaraldehyde and the DNA stained with DAPI. Bar: 2 µm **(C)** Putative peripheral nucleoporins co-localize with Nup107-RFP. Cells of strains FB2N214G_N107R and FB2P152G_N107R were fixed for imaging. FB2N2G_N107R cells were observed in live cells using the dualview imaging technology to allow simultaneous observation on both channels. Bar: 2 µm. **(D)** Stoichiometry of nucleoporins in live cells. The signal intensities of all GFP-tagged nucleoporins in the nuclear envelope were measured. The nuclear envelope was identified by ER-RFP. All values are mean ± standard deviation.

Another nucleoporin involved in traffic through the nuclear pore is Nup2 in budding yeast, Nup50 in vertebrates. It is located at the nuclear face of the pore where it functions in the last steps of nuclear import (Booth *et al.*, 1999; Hood *et al.*, 2000). SMART modelling identified a C-terminal Ran binding domain for the *U. maydis* homologue (P=2.9 e^{-09}), indicative of a possible function in nuclear traffic. Phylogeny places the homologue closer to the fungal sequences than the vertebrate homologue (Figure 12A). Again, the tagged version of Nup2 in *U. maydis* localized to the NE and co-localized with Nup107 (Figure 12B and 12C).

The last nucleoporin investigated in this study, Pom152, represents the transmembrane-domain anchored nucleoporins. Although its function at the nuclear pore is not fully understood, Pom152 in budding yeast appears to play a role in attaching nucleoporins to forming NPCs, in a similar way as has been suggested for Pom121, although the genes are not derived from a common ancestor (Antonin *et al.*, 2005; Madrid *et al.*, 2006). Therefore, the SMART models for Pom121 are included in Figure 12A for reference, but no phylogenetic tree was constructed from them. Once more, the GFP-tagged Pom152 in *U. maydis* was found in the NE and co-localized with Nup107, although the signal from Pom152-GFP appeared to label the NE more diffusely and less concentrated into distinct dots than the other nucleoporins (Figure 12B and 12C).

To gain insights into stoichiometric relations among the selected nucleoporins, fluorescent intensities of all 5 tagged nucleoporins were compared (Figure 12D). Fluorescence signal was measured in the NE and cytoplasmic background was subtracted from these values. Nup107 and Nup133 are present in the same quantities, as expected for proteins directly interacting 1:1 in the Nup107-160 subcomplex in other organisms (Siniossoglou *et al.*, 2000; Boehmer *et al.*, 2008). Compared to these proteins, Nup214 and Pom152 exhibit about half of the fluorescence intensity. As the nuclear pore possesses eight-fold symmetry, a minimum of 8 copies of Nup214 and Pom152 are assumed present in the pore. This would imply a copy number of 16 for Nup107 and Nup133. This result matches data from *S. cerevisiae* (Rout *et al.*, 2000). Nup2, however, does not fall into either class of fluorescence intensity. This could suggest that Nup2 has additional binding sites, or that it does not occupy all possible binding sites at the same time.

2.3.2 NPCs accumulate at the tip of the elongated NE in prophase

Having established these proteins as nucleoporins from different pore locations, they were then used for observations of live cells entering mitosis.

In prophase, the NE appears to be held back in the mother cell, while the spindle pole moves into the daughter cell, thereby stretching the NE (Straube *et al.*, 2005). During the elongation of the NE, Nup107 still retains the punctuate staining of the NE (Figure 13A). However, in ~56% of the cells (N=32) the distribution of the NPCs was slightly uneven, as the cells showed a minor accumulation of NPCs at the tip of the elongated NE where the chromosomes leave the NE (Figure 13A). The accumulation is most prominent in a linescan analysis (Figure 13B). This cluster could result from movement of a few NPCs to the tip of the NE. Directional movement of NPCs was seen when filming Nup107-GFP labelled NPCs in prophase cells (Figure 13C). The question arose whether this NPC movement could be

connected to the migrating chromosomes which are found in close proximity to NPCs at this stage (Figure 13D).

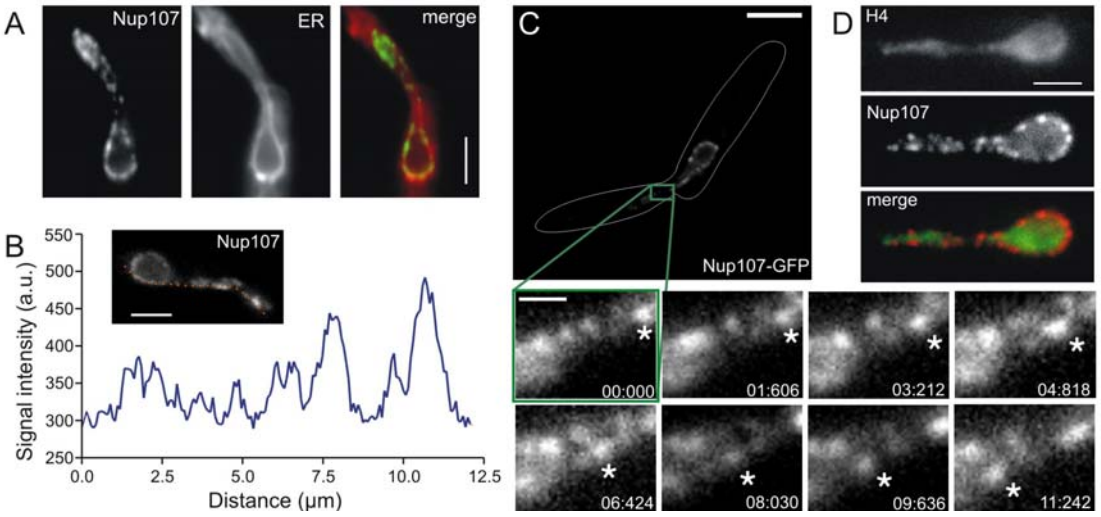

Figure 13. NPCs tend to cluster at the tip of the elongated prophase NE. **(A)** In ~56% of cells, accumulations of NPCs, identified by Nup107-GFP, could be seen at the tip of the prophase NE. Bar: 3 µm. **(B)** Linescan analysis along a side of the NE illustrates a peak of fluorescence at the tip of the NE. Bar: 3 µm. **(C)** NPCs move directionally inside the NE to the tip of the NE. However, in the distal area of the NE, NPCs move bidirectionally. Bar: 5 µm. Inset shows the tip area of the NE. Asterisk marks an NPC entering the magnified area. Bar: 1 µm. Time in s:ms. **(D)** NPCs are adjacent to the migrating chromosomes in stretched prophase envelopes, making connections between NPCs and DNA possible. Bar: 2 µm.

Possible tracks for the movement of the NPCs in prophase could be provided by microtubules or actin. Latrunculin A treatment, which disrupts actin, did not have an effect on NPC movement or distribution (not shown). In prophase, MTs are nucleated from the SPB in the bud neck region and run to the cell ends (Straube *et al.*, 2003). As the SPBs are at the tip of the elongated NE, the MTs need to pass by the nucleus, so that contacts between NPCs and the MTs could occur (Figure 2C). Therefore, movement of NPCs and chromosomes could be linked, and both phenomena driven by the MT cytoskeleton. As disruption of MTs by Benomyl leads to defects in NEBD and chromosome migration (see below; Straube *et al.*, 2005), drug experiments were unsuitable to investigate the involvement of MTs in NPC movement in prophase.

In the NPC clustering mutant P*crg-nup107* most NPCs are trapped in one location at the NE. In prophase cells of strain FB2rN107_N214G_ER, most NPC clusters appeared to be located at the back of the elongated NE (Figure 14A). The cluster retained its position at the elongated NE. Although the majority of NPCs was trapped, the chromosomes were still able to leave the mother cell (Figure 14B), suggesting that chromosome migration is independent of NPC migration. However, a minority of NPCs were still motile in these mutants, probably due to the residual Nup107 (see above). These remaining intact NPCs seemed to accumulate at the tip of the NE over time in prophase. No viability defect due to chromosome

loss, or misplaced spindles were observed (not shown), however, making it unlikely that NPC motility to the tip is necessary to drive chromosome migration.

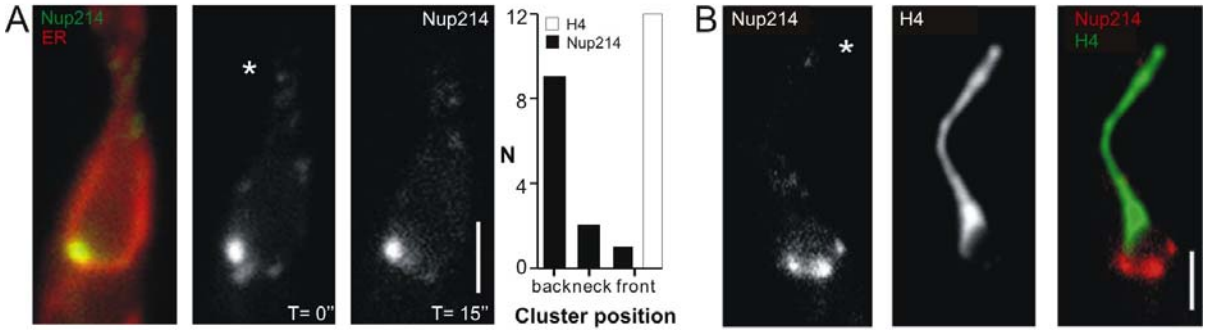

Figure 14. Chromosome movement in prophase occurs independent of NPCs. **(A)** NPCs, labelled by Nup214-GFP, cluster predominantly at the back of the NE in P*crg-nup107* cells grown over night in CM-G. These accumulations retain their position at the NE and do not move from their position. Asterisk indicates the bud-neck. Note that several NPCs can still be seen in this area. Bar: 2 µm. Time in s. **(B)** Chromosomes migrate out of the NE. The accumulation of NPCs can be seen at the back of the NE. Bar: 2 µm.

2.3.3 NPCs disassemble at the end of prophase

Previous results had suggested that the nuclear reporter construct can leak from the nuclear interior before rupture of the elongated prophase nucleus. This implied that the functionality of the NPCs is lost in prophase, presumably due to the release of nucleoporins from the NPCs (Straube *et al.*, 2005).

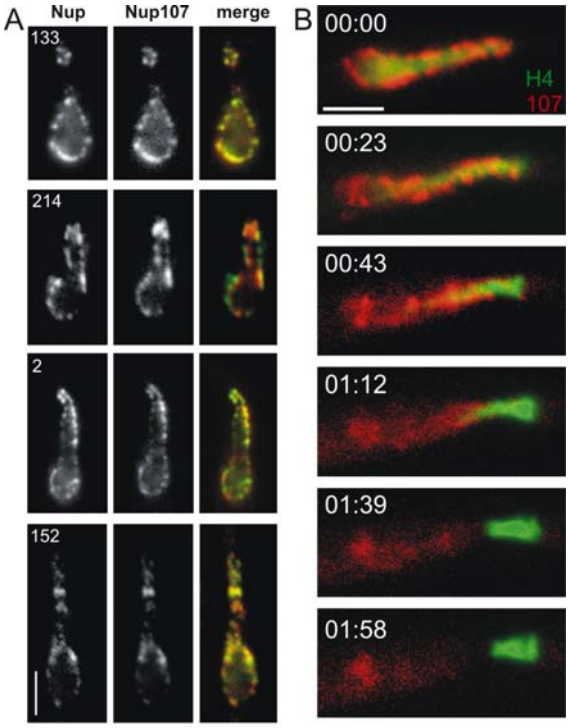

Figure 15. NPCs core structure appears intact in prophase. **(A)** In elongated prophase nuclei, NPCs appear assembled as indicated by co-localization of all tagged components with Nup107 at this stage. Bar: 3 µm. **(B)** As chromosomes exit the NE, the Nup107-RFP signal is lost from the NE. DNA is labelled by Histone 4-GFP. Bar: 3 µm. Time in min:s

In vivo observations of prophase cells however did not reveal major reorganizations of the NPC. All tagged nucleoporins were found at the NE in prophase, and they appeared to co-localize with each other (Figure 15A). As cells progressed into late prophase and the chromosomes left the ruptured NE, Nup107-GFP lost the punctuate position at the NE, suggesting that the NPCs disassembled (Figure 15B). Nup133, Nup214 and Nup2 also left the NE and became dispersed in the cytoplasm (Figure 16A). The increase of cytoplasmic fluorescence after

NEBD supports this observation (Figure 16B). Cytoplasmic signals of the soluble nucleoporins sharply increased at the end of prophase and persisted at these levels throughout mitosis, before they dropped in telophase when new nuclei were established.
The transmembrane domain anchored Pom152 lost the punctuate association with the NE and dispersed in the ER, where it remains until mitosis was completed, although the most prominent signal was usually seen in the membrane stack derived from the collapsed old NE (arrow, Figure 16A).

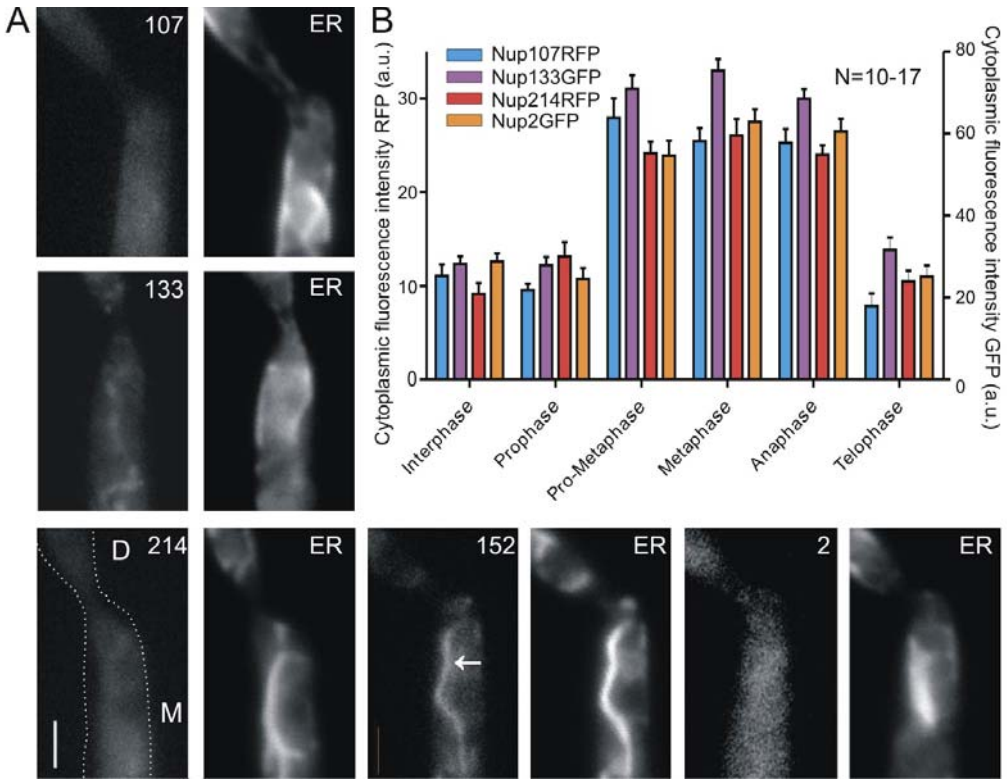

Figure 16. NPCs disassemble at the end of prophase. **(A)** All non-transmembrane-domain containing nucleoporins leave their association with the NE after NEBD and disperse in the cytoplasm. Pom152-GFP also loses its punctuate pattern and disperses in the ER, but the strongest signal can still be seen in the collapsed old NE (arrow). Bar: 2 µm. **(B)** Signal intensity of GFP- or RFP-labelled nucleoporins in the cytoplasm of live cells were measured (N=10-17 cells for each strain and mitotic stage). Mitotic stages were identified by co-expressing Histone 4-GFP or Nup107-RFP. The transmembrane-domain anchored Pom152 was excluded from the analysis.

2.3.4 Scaffold nucleoporins disperse in the cytoplasm and aggregate on the DNA

After complete dispersal of the scaffold nucleoporins Nup107 and Nup133 in the cytoplasm, a fraction of these proteins gathered in a distinct accumulation in the daughter cell (Figure 17A). The position and size of the area suggested a co-localization with the metaphase chromosomes. This assumption was confirmed in a strain co-expressing Nup107-RFP and Histone 4-GFP. Linescan analysis over the Histone 4-GFP signal in late prophase and metaphase cells illustrated that very little Nup107-RFP was associated with DNA in late prophase, but there was a strong signal increase in metaphase (Figure 17B).

While it is possible that traces of Nup107, which were below the detection limit of the microscope, associated with DNA already in late prophase, most of the signal found on chromatin seemed to become recruited to the DNA when the cells progressed through metaphase (Figure 17C).

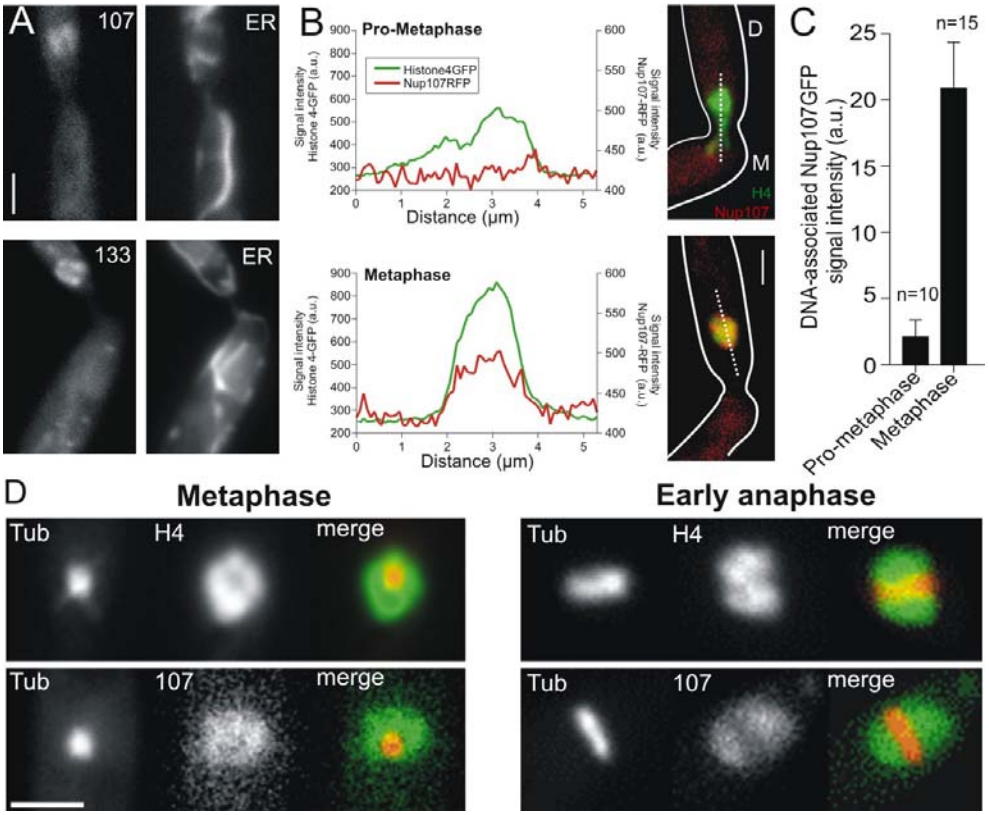

Figure 17. Scaffold nucleoporins associate with DNA in metaphase. **(A)** After NEBD, Nup107 and Nup133 initially evenly disperse in the cytoplasm, before accumulating in a distinct area in the daughter cell. Bar: 2 µm. **(B)** In strains co-expressing Histone 4-GFP and Nup107-RFP, linescans over the Histone 4-GFP signal at the end of prophase and in metaphase show an increase of Nup107-RFP signal that co-localizes with Histone 4-GFP. D, daughter cell, M mother cell. White lines trace the cell's outline. Dotted line indicates the direction of the linescan. Bar: 2 µm. **(C)** Measuring fluorescence of Nup107-RFP co-localizing with DNA over cytoplasmic background supports the notion that Nup107-RFP associates with metaphase chromosomes after a phase of dispersal, rather than increasing signal through concentration into a compacted DNA structure. **(D)** A dot-like or rift-like depression in Nup107-GFP signal bound to DNA indicates metaphase or early anaphase, respectively. Metaphase and early anaphase spindles, labelled by RFP-α-Tubulin, appear to form in these darker areas. Images of metaphase and early anaphase spindles with DNA are included in the top panel for reference. Bar: 2 µm.

In some cells, Nup107-GFP was excluded from the central region of the DNA bound area, resulting in a dot-like or rift-like depression in fluorescence. These darker areas corresponded well with metaphase and early anaphase spindles (Figure 17D). Comparing the signals to the Histone 4-GFP signal underlined that Nup107 appeared to associate with DNA in metaphase and anaphase. Nup107 and Nup133 showed identical localizations in metaphase (Figure 17A). The Nup107-160 subcomplex has been shown to be stably attached in interphase and mitosis in vertebrates (Glavy *et al.*, 2007; Boehmer *et al.*, 2008).

Therefore it appears likely that nucleoporins disassembled into subcomplexes in *U. maydis* rather than dispersed into the cytoplasm and assembled on the DNA as individual proteins.

2.3.5 NEBD is not necessary for Nup107 dispersal and association with DNA

To investigate whether NPC disassembly and DNA association depend on NEBD, the metaphase localization of Nup107-GFP was observed under conditions that inhibit NE removal.

It was previously reported that in *U. maydis* strains deleted for the small GTPase Ras3 (homologue of Tem1 and Spg1 in the MEN/SIN pathways in budding and fission yeast), ~60% of cells exhibit (partly) closed envelopes around spindles forming in the daughter cell (Straube *et al.*, 2005). In Δ*ras3* cells, Nup107 accumulated inside the NE-derived membranes, suggesting that NPC disassembly does not require NE removal (Figure 18A). However, as the NEs in these mutants appeared to be only partly closed, alternative approaches were used to confirm this notion.

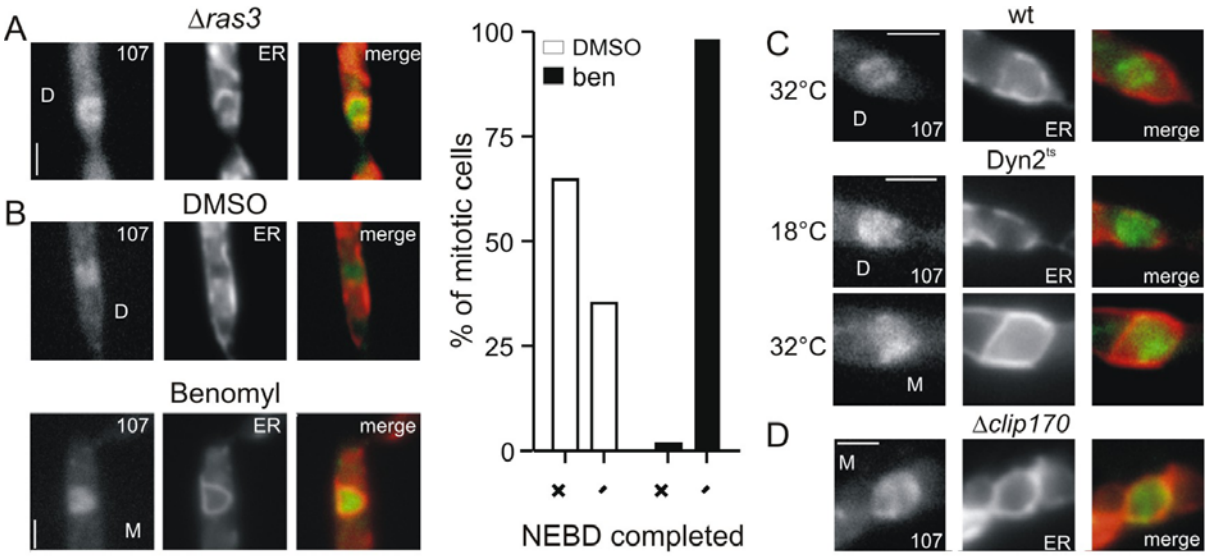

Figure 18. Membrane removal is not necessary for Nup107 to associate with DNA in metaphase. **(A)** Mutants deleted for the SIN signalling network GTPase Ras3 show defects in NEBD, leading to spindles in the daughter cell surrounded by membranes (Straube *et al.*, 2005). This imperfect NEBD nevertheless does not affect NPC disassembly, as suggested by the cytoplasmic dispersal and accumulation of Nup107-GFP. Bar: 2 µm. **(B)** Disruption of MTs by incubation with 20 µM benomyl for 4h leads to misplaced spindles surrounded by membranes (N=55). Although control cells treated with DMSO show a significant proportion of spindles with residual membranes (N=34), neither of these are located in the mother cell. Nup107-GFP is still found inside the membranes around the spindle generated by the absence of MTs, in a structure resembling Nup107 bound to DNA in metaphase. Bar: 2 µm **(C)** Mutants carrying a temperature sensitive allele of Dyn2 exhibit misplaced spindles surrounded by membranes after incubation at 32°C for 2h. Still, Nup107-YFP accumulates inside the membranes. Bars: 2 µm. **(D)** Finally, a deletion mutant of the putative Dynein activator Clip170 show misplaced spindles with membranes around them. Again, Nup107-GFP accumulates inside the membranous compartment. Bar: 2 µm.

It was previously observed that NE removal depends on the MT cytoskeleton and the MINUS end moving motor protein Dynein (Straube *et al.*, 2005). After incubating strains expressing

Nup107-GFP and ER-RFP with 20 µM Benomyl for 4 h, MTs were disassembled (not shown) and ER derived membranes were assembled around misplaced spindles (Figure 18B). In the DMSO treated control cells, all spindles were formed in the daughter cell, but a significant proportion of cells also appeared to be surrounded by membranes (Figure 18B). Again, Nup107 was found inside the NEs in a pattern reminding of DNA association. Similar results were obtained in Dynein temperature sensitive mutants incubated for 2 h at 32°C, or in strains deleted for the homologue of the putative Dynein activating factor Clip170, um06338 (Figure 18C and 18D). Taken together, these results suggest that independent mechanisms and regulatory pathways control NPC disassembly and NE removal, or that NPC disassembly begins before NE removal, and the mutants investigated here affect only the last stages of NEBD and NE removal.

2.3.6 Nup107 does not associate with kinetochores in metaphase

The association of the Nup107-160 subcomplex with DNA in metaphase of *U. maydis* resembles the situation described in vertebrate cells (Belgareh *et al.*, 2001; Loiodice *et al.*, 2004). However, in vertebrate model systems, the subcomplex has been found associated with kinetochores (Belgareh *et al.*, 2001; Loiodice *et al.*, 2004). A copy of the *U. maydis* homologue of Mis12-3xGFP was introduced into a strain carrying Nup107 fused to RFP. In

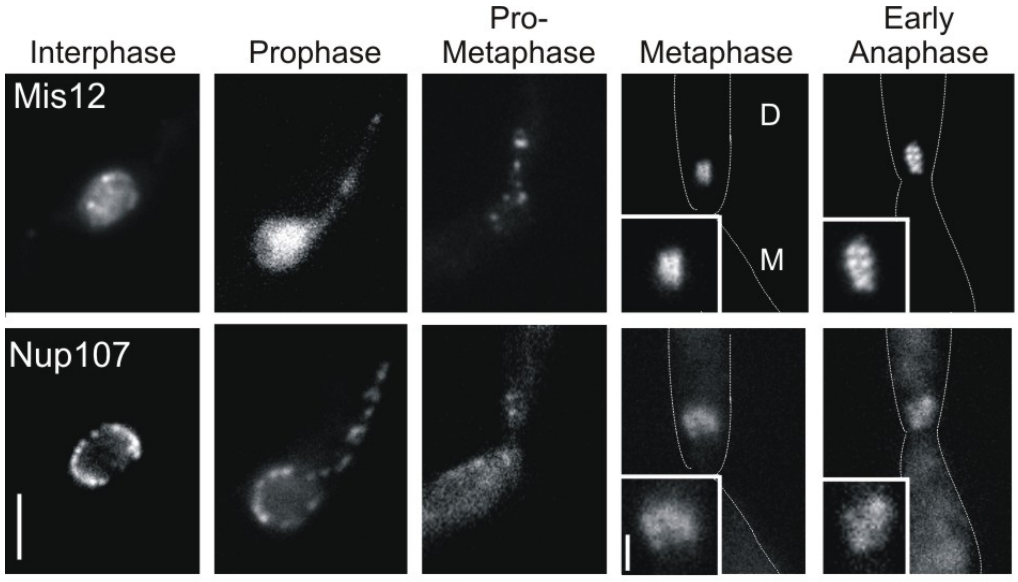

Figure 19. Nup107 does not co-localize with kinetochores in *U. maydis*. Cells expressing Mis12-3xGFP ectopically show dispersed localization of the protein in interphase nuclei. As cells progress into mitosis, the signal becomes concentrated at the tip of the elongated nucleus in prophase. When chromosomes gather in the daughter cell, the signal densely concentrates in a small brightly fluorescent area, which increases as soon as cells enter the first slowly elongating phase of anaphase. Nup107-RFP and Mis12-3xGFP do not co-localize in metaphase and early anaphase. Bar: 3 µm. Insets show the area of Nup107-RFP accumulation in metaphase and early anaphase in the daughter cell. Bar: 1 µm.

interphase and early prophase cells, Mis12-3xGFP appeared in faintly fluorescent spots inside the nucleus, presumably bound to centromers (Figure 19). At the end of prophase, the signal collected into brightly fluorescent dots at the tip of the disassembling NE, which subsequently gathered in the daughter cell around a metaphase spindle. At the onset of anaphase, Mis12-3xGFP could be seen in separating dots in short spindles.

Signals of Mis12-3xGFP and Nup107-RFP did not co-localize in metaphase and early anaphase (Figure 19). It is possible that a co-localisation of the proteins escaped notice due to the low fluorescence of Nup107-RFP. However, the Mis12-3xGFP signal appeared to occupy an area of decreased fluorescence intensity in the Nup107 accumulation in the daughter cell which corresponds to the central area where the spindle forms (Figure 17D). It therefore appears more likely that Nup107 associates with chromatin rather than kinetochores in metaphase cells of *U. maydis*.

2.3.7 Nup2 disperses into the cytoplasm, but accumulates in metaphase

Nup2 left the localization at the NPC in late prophase, like the other nucleoporins. Most of the protein stayed dispersed in the cytoplasm, but a faintly fluorescent “dot” appeared in prometaphase in 72% of cells (N=43). Nup2-Cherry was co-expressed with γ-Tubulin to identify the mitotic stages by the position of the SPBs (Figure 20A). The Nup2-Cherry accumulation in the mother cell occasionally could be seen moving into the daughter cell in metaphase (not shown), where it is found in the vicinity of Nup107 on DNA (Figure 20B). Although faint, the presence of this dot in the majority of cells suggests a function for this structure, but its nature is elusive at present. In early anaphase, when a gap can be discerned in the Nup107 signal, Nup2 faintly labeled the outside of the DNA, but most prominently the outsides of the poles of the spindle (Figure 20B).

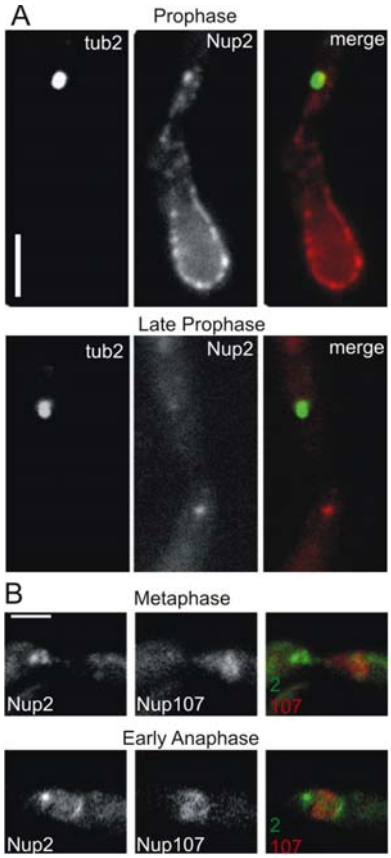

Figure 20. Nup2-Cherry accumulates in a distinct spot in metaphase. **(A)** At the end of prophase, when Nup107-GFP starts to bind to the DNA, about 72% of cells possess a dot-like accumulation of Nup2-Cherry. This accumulation is localized in the mother cell in metaphase. Bar: 3 µm. **(B)** In early anaphase, a faint rim of fluorescence from Nup2-GFP along the outward edges of the DNA can be observed. Bar: 2 µm.

2.3.8 Nup107 rearranges localization in anaphase

Nup107 stayed on the DNA in early anaphase (Figures 17D and 21B). As anaphase progressed and the DNA separated, the localisation of Nup107 shifted to the outward leading edges of the chromosomes (Figure 21B). Next it assembled into dots surrounding the bulk of the DNA even before all chromosomes had separated. Linescan analysis along a spindle of intermediate length illustrates that Nup107 concentrates to the outside of the chromosome fronts, while residues are still found in the centre where the chromosomes are not yet separated (Figure 21C).

During the transition from anaphase A to anaphase B, when kinetochores exchange their centrally focussed metaphase position for the leading edge of the separating chromosomes, Nup107-RFP partially overlaps with Mis12-3xGFP signals (Figure 21D). However, if interaction does occur, it would be transient, as anaphase B progresses rapidly.

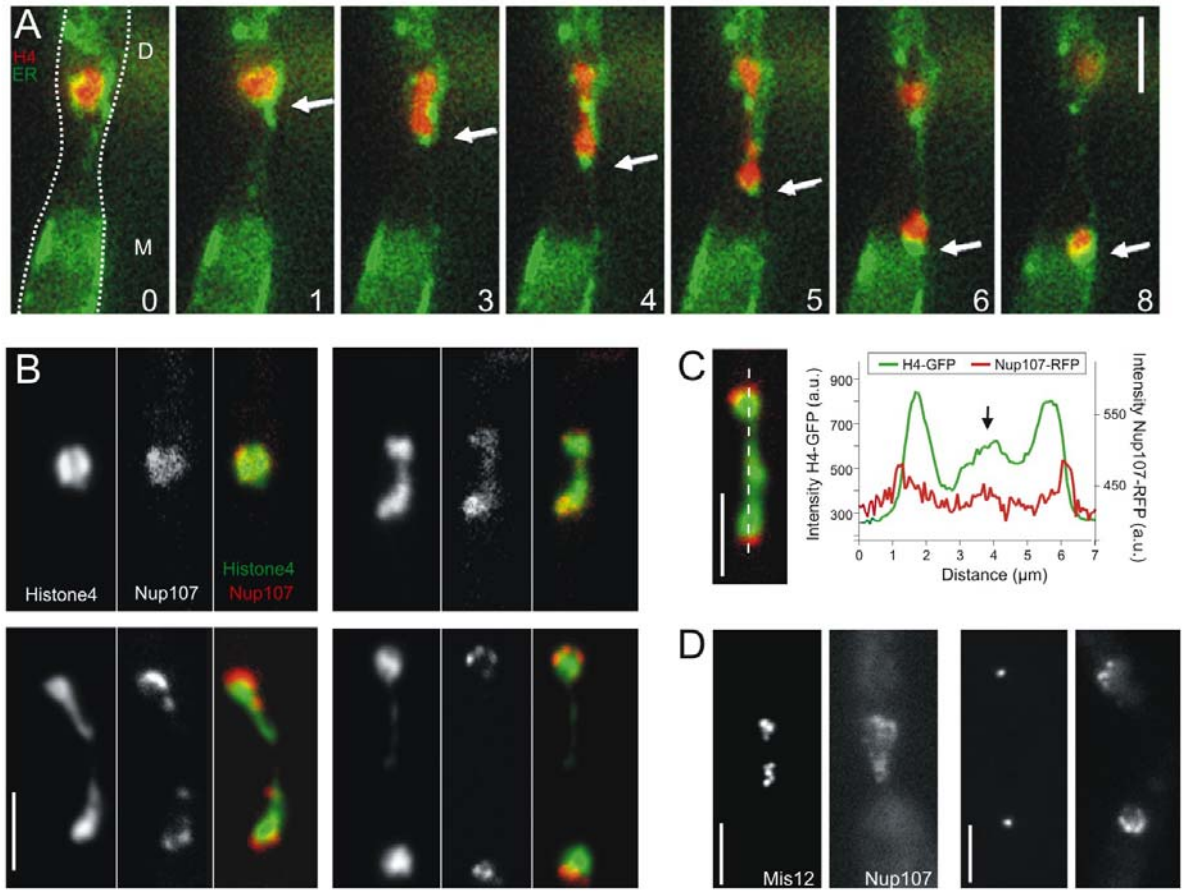

Figure 21. Nup107 rearrangement in anaphase. **(A)** As mitosis progresses through anaphase, the outer rims of the DNA masses (labeled by Histone 4-CFP; H4) are collecting material from the ER (marked by YFP with an ER retention signal). Occasionally, single tubules can be observed to touch the DNA and leave some material behind, which is later incorporated into the newly forming nuclei (arrow). The outline of the cell is indicated by a profile in the first image. D: daughter cell; M: mother cell. Time is given in minutes. Bar: 3 µm. Image series kindly provided by Anne Straube. **(B)** Co-localization of Nup107-RFP and Histone 4-GFP-labelled chromosomes shows that the nucleoporin leaves the diffuse localization on the DNA and appears at the outward edge of the separating chromosome masses during spindle elongation. In late anaphase B, Nup107 concentrates in a punctuate pattern around the DNA. Bar: 3 µm. **(C)** Line-scan analysis of an anaphase B spindle demonstrates that traces of Nup107-RFP are still found on the chromosomes (arrow), while most of the protein concentrates at the poles of the separating DNA. Bar: 3 µm. **(D)** While Nup107-RFP may partially co-localize with Mis12-3xGFP at the onset of anaphase B, a significant overlap of signals is not observed in later stages of anaphase B. Bar: 3 µm.

While Nup107 shifts from the DNA to the outward edges, Nup2-GFP appeared to increase in fluorescence intensity, presumably on the outside of the chromosomes, as the spindle elongated (Figure 22B). From a very faint signal in early anaphase, it brightly stained the newly forming NEs in late anaphase. Nup2-GFP also did not seem to co-localize fully with Nup107 in anaphase (Figure 22B).

Although sometimes ER tubules could be seen that leave material on early anaphase chromosomes (Figure 21A), in most cells, new nuclear membranes were beginning to form from the distal ends of the dividing chromosomes at the end of anaphase, at the sites where Nup107 accumulated into dots (Figure 22A). At this stage when NEs are reforming, but not yet closed, Nup2 and Nup133 were already present in punctuate structures, but Nup214 and Pom152 were still only found in background levels of the cytoplasm and the ER, respectively (Figure 22A). Due to the faint signals at this stage, a clear co-localization of the nucleoporins was difficult to detect (Figure 22C).

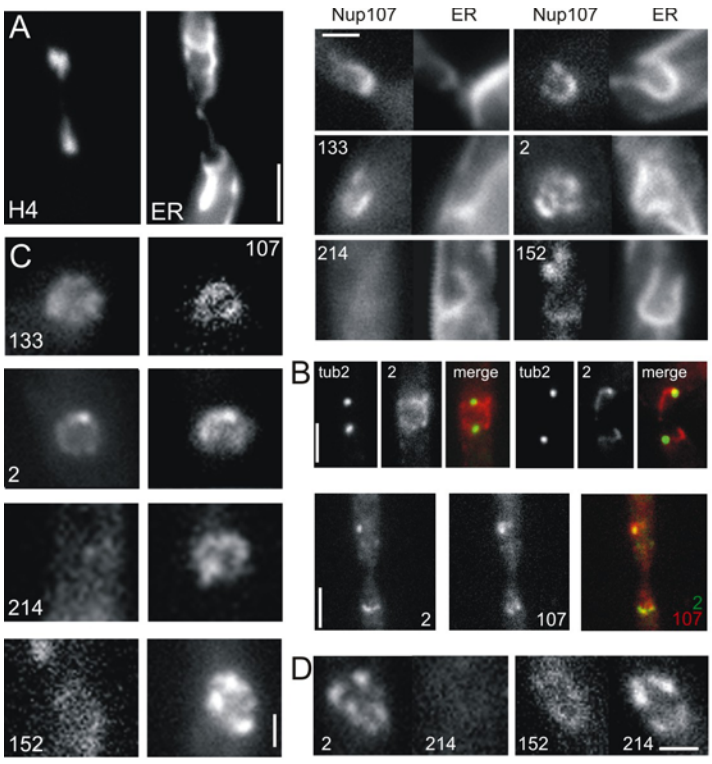

Figure 22. Sequential recruitment of nucleoporins to reforming NPCs. **(A)** In anaphase B, the new envelope is formed from ER membranes that appear at the outward rim of the chromosomes. Bar: 3 µm. While Nup107, Nup133 and Nup2 become incorporated into the newly forming nuclear envelope, Nup214 and Pom152 are not yet present above background levels in the cytoplasm or ER, respectively. Bar: 1.5 µm. **(B)** Nup2-GFP localizes to the outer rims of the separating DNA, as indicated by the crescent-shaped appearance of the signal. However, the signal only partially co-localizes with Nup107-RFP. Bars: 3 µm. **(C)** Nup107 co-localizes with Nup133 and Nup2 in small nuclei, yet not detectably with Nup214 and Pom152. Bar: 1 µm. **(D)** Small nuclei of cells co-expressing Nup2-GFP and Nup214-RFP or Nup214-GFP and Pom152-RFP acquire Nup2 first, followed by Nup214 and finally Pom152. Bar: 1 µm.

These results suggested a step-wise reassembly of NPCs after mitosis, similar to what has been observed in *D. melanogaster* and human cells (Bodoor *et al.*, 1999; Kiseleva *et al.*, 2001; Dultz *et al.*, 2008; Katsani *et al.*, 2008). Nup107 and Nup133 arrive first, presumably together with other members of the Nup107-160 subcomplex. Next, in early anaphase, Nup2 localizes to the dividing chromosomes, but does not fully co-localize with Nup107/Nup133 in anaphase B (Figure 22B). In strains co-expressing Nup2 and Nup214, or Nup214 and Pom152, Nup2 is already present when Nup214 seems to become attached to NEs, shortly

before Pom152 concentrates in dots (Figure 22C and 22D). Therefore, the order in which nucleoporins become attached to forming NPCs in *U. maydis* is Nup107/Nup133 – Nup2 – Nup214 – Pom152.

2.3.9 Nuclear import begins when peripheral components are attached to NPCs

Next the onset of efficient nuclear import, indicative of functional NPCs, was correlated to the presence of nucleoporin-GFP at the NE (Figure 23A). To this end, nuclei with closed

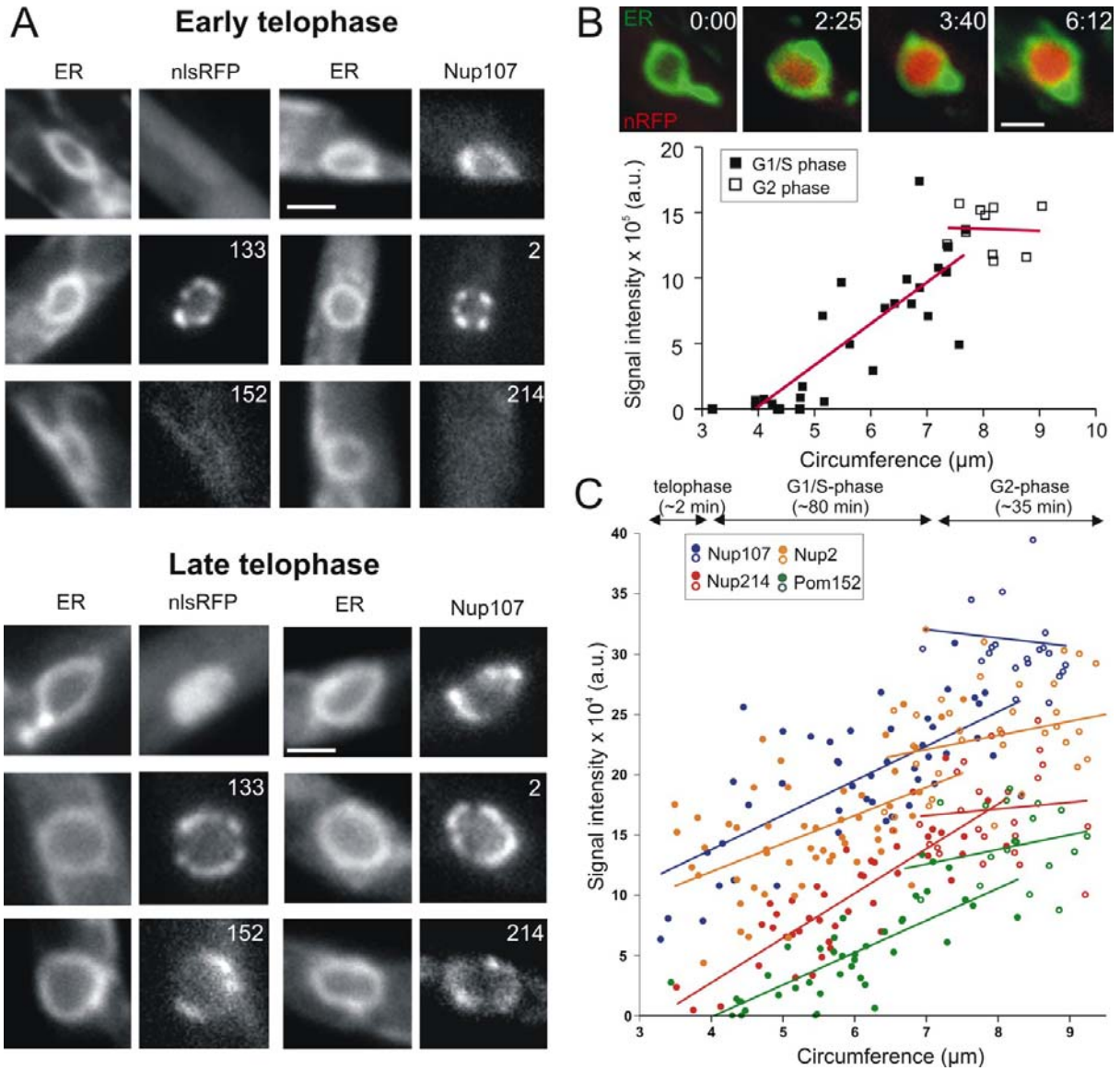

Figure 23. NPCs are continuously inserted in NEs in the cell cycle. **(A)** Although Nup107-GFP, Nup133-GFP and Nup2-GFP are assembled in significant amounts at small nuclei, these nuclei cannot import the reporter construct Nls-3xRFP. As nuclei grow and all nucleoporins investigated in this study are incorporated into NPCs, efficient import begins. Bars: 1.5 µm. **(B)** The top 4 images are taken from a film illustrating the efficient uptake of reporter protein as nuclei grow. Time in min:s. Bar: 1.5 µm. Nuclei continue to acquire reporter protein as they nuclei grow. In G2 phase, however, nuclear import reaches a plateau. For the graph, the RFP intensity of the reporter was measured inside the nucleus, and cytoplasmic background subtracted from these values. Full squares represents G1 and S phase nuclei, open squares G2 phase nuclei, as judged by the cells forming buds (Snetselaar and McCann, 1997). **(C)** Nucleoporins become associated with the NE as nuclei grow, but incorporation slows in G2 phase. The GFP-signal intensity at individual nuclei was measured and plotted on the graph after subtracting cytoplasmic background for the graph. An estimate of the timing and correlation to the cell cycle is presented above the graph.

membranes were selected and fluorescent signal of the reporter construct Nls-3xRFP measured accumulating inside the nuclei over cytoplasmic background (Figure 23B). The circumference of the nuclei served as reference. In small telophase nuclei with nuclear membranes (<4 µm circumference), Nup107, Nup133 and Nup2 were present, and they localized in small dots (Figure 23A). But no protein import is established, probably due to the absence of peripheral nucleoporins, such as Nup214 and Pom152. As the nuclei expand, they start to show signal from Pom152-GFP and Nup214-GFP, and the nuclei begin to import the reporter construct (Figure 23A and 23B).

When fluorescence intensity of nucleoporin-GFP at the NE levels was measured in individual nuclei, Nup214 and Pom152 seem to become attached to nuclei of ~ 4 µm in circumference (Figure 23C) This correlates well with the onset of efficient protein import (Figure 23B). Once functional nuclei are established, all nucleoporins increase at similar rates as nuclei expand in the cell cycle (Figure 23C). NPCs are incorporated throughout the cell cycle, which has been reported in other organisms (Maul *et al.*, 1972; Winey *et al.*, 1997), although the increase slows considerably in G2 phase.

2.3.10 The role of the cytoskeleton in the reassembly of the NE

Occasionally ER material was picked up during anaphase B and later became incorporated into the newly forming NEs (Figure 21A). Therefore, it is possible that the cytoskeleton and spindle elongation is necessary for the delivery of membranous material to the chromatin surface. The role of the cytoskeleton in establishing the new NEs in telophase was investigated in experiments using drugs to disrupt components of the cytoskeleton.

Cells of a logarithmically growing culture were placed on agarose cushions containing either 30 µM Benomyl or 10 µM Latrunculin A, or both, and early anaphase cells were selected for analysis, based on the appearance of the Nup107-GFP signal. After 7 min of exposure, the MTs and actin patches were efficiently disrupted (Figure 24A and 24B). While Latrunculin A treatment did not affect anaphase progression and the assembly of functional NEs, as indicated by the import capability of the nuclei, Benomyl prevented anaphase spindle elongation (Figure 24A and 24B). Cells that showed a dark cleft in the Nup107-GFP fluorescence in the daughter cell, indicative of early anaphase, however formed closed ER membranes with Nup107-GFP appearing in a dot-like pattern, reminding of functional NE (Figure 24C). Next all other tagged nucleoporins were investigated under Benomyl and all of them accumulated into dots in these membranes (Figure 24D). To test whether these structures are functional envelopes, the experiments were repeated with cells expressing Nup107-GFP and the Nls-3xRFP reporter construct. After 7 min of exposure to Benomyl, the cells had accumulated punctuate Nup107-GFP, but nuclear import was absent. Prolonged

exposure led to growth of these structures, which now efficiently imported the reporter (Figure 24E). To test whether the intact part of the cytoskeleton in the above experiments might be able to complement the functions of the other, thereby masking the contribution of

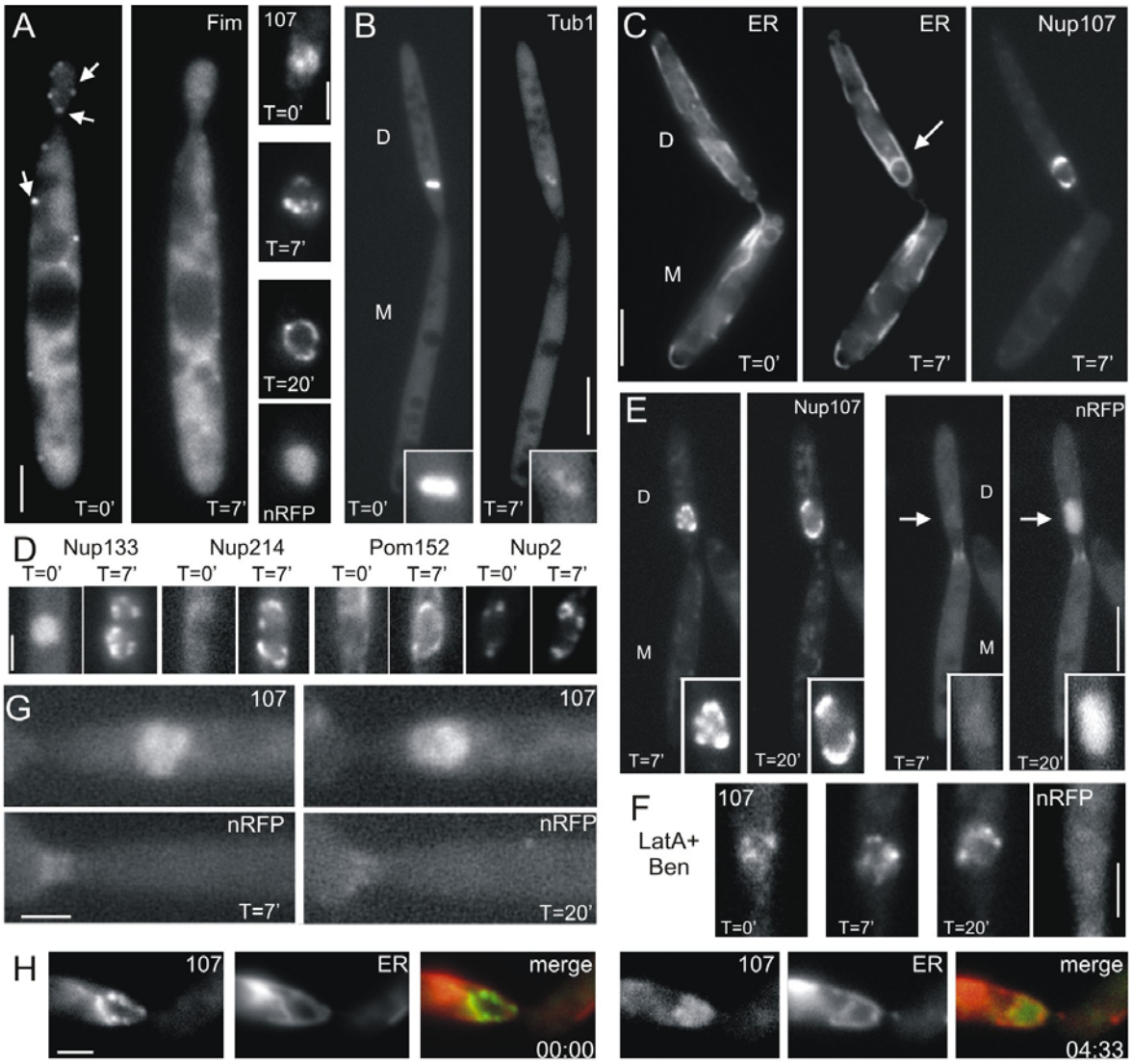

Figure 24. Influence of the cytoskeleton on NE reassembly. **(A)** Disruption of the actin cytoskeleton by 10 µM Latrunculin A in the agarose cushion for 7 min efficiently disperses the Fimbrin-GFP signal in the cytoplasm, but does not inhibit NE reformation. Arrows indicate examples of Fimbrin patches that disappear after 7 min of exposure to Latrunculin A. Bar: 3 µm. Nup107-GFP is present in small nuclei, which show nuclear import compentence after passing through telophase. Bar: 2 µm **(B)** Cells suspended on agarose cushions containing 30 µM Benomyl can no longer undergo anaphase spindle elongation. 7 min after mounting cells on the cushion (T=7'), microtubules of the spindle, labelled by 2xRFP-Tub1 (Tub1), are disrupted (inset). D: daughter cell; M: mother cell. Bar: 5 µm. **(C)** Anaphase cells show formation of closed membranes, marked by ER-RFP (ER), after 7 min of Benomyl exposure (arrow). These ER derived membranes are also decorated with a distinct Nup107-GFP signal. Bar: 5 µm. **(D)** During continued exposure to Benomyl, these membranes accumulate significant amounts of the other nucleoporins investigated (T=7'). Bar: 2 µm. **(E)** Membranes with Nup107-GFP enlarge over time, reminding of nuclear expansion correlated to DNA decondensation in telophase. This growth coincides with efficient import of the NLS-3xRFP reporter construct implying functional NPCs (arrows; insets). Time in minutes. Bar: 5 µm. **(F)** Simultaneous disruption of actin and MTs blocks the formation of NE. Cells accumulate a slightly structured rim of Nup107-GFP on the outside of the DNA, but the Nup107-GFP signal appears fainter and more dispersed after 7 min of exposure. Even after prolonged exposure (t=20 min), the signal had not collected into distinct dots, indicative of NPCs. Correspondingly, no accumulation of the Nls-3xRFP reporter construct was detected (nRFP). Time in min. Bar: 2 µm. **(G)** Metaphase cells arrest in metaphase upon exposure to Benomyl. **(H)** Occasionally, cells can be found that show a faint, but patterned Nup107-GFP distribution around condensed DNA in the daughter cell. Upon removal of Benomyl, these cells lose their patterned Nup107-GFP around the rim. Nup107-GFP reverts to its diffused metaphase appearance (N=9). Time in min:s. Bar: 2 µm.

the cytoskeleton to establishing NEs in telophase, anaphase cells expressing Nup107-GFP and the reporter construct were exposed to both Benomyl and Latrunculin A. After 7 min, the Nup107-GFP signal assumed a patterned distribution on the DNA in the daughter cell, but no import could be detected even after prolonged exposure (Figure 24F). This finding suggests that spindle elongation might not be necessary for NE reassembly, but the cytoskeleton has an important function in NE reassembly. The exact nature of the function of the cytoskeleton in NE re-establishment is currently unknown.

The establishment of functional nuclei in the absence of MTs suggested that this process is controlled by pathways independent of mitotic progression. Cells in metaphase which show uniform Nup107 signal in the daughter cell, arrested in metaphase when placed on the Benomyl containing agarose cushions, probably due to the activation of the spindle assembly checkpoint, and no functional NEs were formed, even after 20 min (Figure 24G). Still, it was possible that NE formation was delayed and the limited observation time was not sufficient to detect NEs around metaphase arrested spindles.

As observations of *U. maydis* cells under the microscope for longer timespans in this setup was not feasible, cells expressing Nup107-GFP and ER-RFP were incubated in liquid culture (CM-G) for 4 h with 20 µM Benomyl at 28°C at 200 rpm, to check for a delay in NE formation. As the cell cycle of *U. maydis* is ~2 h long (Straube *et al.*, 2005), most cells arrested in metaphase. In contrast to the short exposure experiments, many cells had formed small, partly closed membranes in the daughter cells, faintly decorated with punctuate Nup107-GFP (Figure 24H), although smaller than the nuclei formed in early anaphase cells when the MTs were disrupted. When these cells were placed on agarose cushions without Benomyl, and the Benomyl allowed to diffuse out of the cells, Nup107-GFP lost the patterned localization at the membranes, and diffusely labelled the DNA inside the ER membranes in all cells (N=9, Figure 24H). Several cells subsequently entered anaphase (not shown). Taken together, these observations suggest that in metaphase arrested cells, NE formation still proceeds, although it is strongly delayed, and may not lead to the establishment of functional NEs. These results argue in favour of a regulatory mechanism independent of spindle elongation, as the punctuate staining of ER membranes around DNA appears independent of the mitotic stage. However, some influence of the mitotic stage appears to be present, as ER membrane formation is strongly delayed in metaphase arrested cells, and Nup107 quickly reverts to the normal metaphase localization as soon as the cells are released from the mitotic block.

3 Discussion

This work demonstrates that NPCs in *U. maydis* interphase nuclei are motile and investigates the mechanism underlying NPC motility. Initial results also suggest a role for this phenomenon in equal NPC distribution and efficient protein expression.
The second part describes mitotic disassembly and reassembly of NPCs in the open mitosis of *U. maydis*, finding surprising similarities to vertebrate model systems.

3.1 Two types of directed nuclear pore motility exist in interphase nuclei

While NPC behaviour in mitosis closely resembles the situation in vertebrate model systems, NPC movement in interphase nuclei of *U. maydis* is similar to what has been reported in budding yeast (Belgareh and Doye, 1997; Bucci and Wente, 1997). Fungi do not possess a nuclear lamina which holds NPCs in position in higher eukaryotes' nuclear envelopes (Daigle *et al.*, 2001; Mans *et al.*, 2004). NPC movement has been observed in *S. cerevisiae* and *S. pombe*. First reports using heterokaryon fusions and FRAP experiments found that NPCs move in the NE and distribute equally over time in *S. cerevisiae* (Belgareh and Doye, 1997; Bucci and Wente, 1997; Bystricky *et al.*, 2005). It was then concluded that NPCs diffuse by Brownian motion.

3.1.1 NPC type 1 motility in *U. maydis* relies on extranuclear forces

If diffusion were the underlying cause of NPC motility, run length would be shorter and the random displacements would continue under CCCP treatment. However, NPCs in *U. maydis* directionally move in two distinct motility types which are both energy-dependent. These types are distinguished by velocity and run length, but also by their reliance on the cytoskeleton.
The velocity measured for NPCs moving in type 1 fashion matches values determined *in vivo* for Dynein and Kinesins (Presley *et al.*, 1997; King and Schroer, 2000; Lee *et al.*, 2003; Cai *et al.*, 2007). It is likely that NPC type 1 movement in the PLUS direction utilizes a Kinesin. 10 Kinesins have been identified in the *U. maydis* genome (Schuchardt *et al.*, 2005), and experiments are currently carried out to determine the identity of the Kinesin involved. Type 1 movement in the MINUS end direction relies on Dynein, as suggested by the results using temperature-sensitive mutants and co-localisation. A direct interaction of Dynein with NPCs has been suggested in bovine and rhesus monkey pronuclear migration (Payne *et al.*, 2003). A Dynein light chain is associated with NPCs in *S. cerevisiae*, where it is thought to

participate in stabilizing the Nup82-Nsp1-Nup159 complex located at the cytoplasmic side of NPCs (Stelter *et al.*, 2007). The homologous protein is also found a the NE in fission yeast (Miki *et al.*, 2002). These results hint at Dynein interacting with NPCs in these organisms.
Dynein has also been implicated in NE deformation in *U. maydis* (Straube *et al.*, 2001; Straube *et al.*, 2005), and in the course of this study, it appeared as if these deformations are often led by an NPC at the tip. NE deformation in budding yeast has been described in connection with chromosome movement in meiotic prophase (Koszul *et al.*, 2008). Their study concluded that NE deformations arise from chromosome migration. In meiosis of budding yeast and fission yeast, telomeres slide along the nuclear periphery to form a "bouquet" structure, where recombination events between the homologous chromosomes take place (Chikashige *et al.*, 1994; Trelles-Sticken *et al.*, 1999). Chromosome motility can proceed rapidly, with velocities reaching up to 1 µm/s (Conrad *et al.*, 2008; Koszul *et al.*, 2008). In budding yeast meiotic chromosome sliding depends on the polymerizing actin cytoskeleton surrounding the nucleus, whereas Dynein and microtubules provide the driving forces in fission yeast (Yamamoto *et al.*, 1999; Trelles-Sticken *et al.*, 2005; Koszul *et al.*, 2008). These forces are transmitted through telomere binding proteins in budding yeast, or SUN-KASH domain proteins in fission yeast (Miki *et al.*, 2004; Chikashige *et al.*, 2007). Although BLAST searches with SUN- or KASH-domain containing proteins from different organisms did not detect an unambiguous homologue in *U. maydis*, another protein functioning together with SUN-KASH proteins could be found in the *U. maydis* databases (not shown; King *et al.*, 2008). Hence, although NPCs in NE deformation and chromosome velocities suggest a connection between NPCs and underlying chromatin motility, it is possible that NPC type 1 movement and chromatin motility are independent processes in *U. maydis*. This notion is also supported by the finding that type 1 NPC motility relies on MTs, while chromosome velocity was not reduced upon exposure to Benomyl. Also, chromosome motility exists in interphase nuclei of mammalian cells, which have immobile NPCs (Daigle *et al.*, 2001; Chubb *et al.*, 2002; Thomson *et al.*, 2004; Chuang *et al.*, 2006).

3.1.2 NPC type 2 motility depends on intranuclear processes

When MTs were disrupted, type 2 NPC motility still persisted in *U. maydis*. This indicated that processes inside the nucleus could be involved in short-range NPC motion.
Centromeric regions are motile in budding yeast interphase (Marshall *et al.*, 1997; Heun *et al.*, 2001). The velocities of chromosomes are in the range of 0.3 - 0.5 µm/s for Brownian-type motility in meiotic prophase (Conrad *et al.*, 2008; Koszul *et al.*, 2008). The velocity of type 2 NPC motility in *U. maydis* falls within the range of these values. A discrepancy between NPC diffusion velocity and chromatin velocity has also been reported in budding

yeast (Bystricky *et al.*, 2005). This could imply that chromosomes do not move NPCs in a type 2 manner. In addition, co-localization with a centromer marker failed to reveal side-by-side movement of NPCs and chromatin in *U. maydis* for type 2. Co-localization with the chromatin marker Histone 4 neither identified movement of NPCs with DNA, although NPCs and chromatin are in close proximity. These observations suggest that chromatin movement is not directly connected to type 2 NPC motility.

Among the processes occurring inside the nucleus that could influence NPC movements are DNA repair, DNA synthesis or chromatin remodelling and transcription.

The Nup84-120 complex in *S. cerevisiae* has been implicated in mediating double strand break repair (Loeillet *et al.*, 2005; Therizols *et al.*, 2006). However, initial experiments in *U. maydis* failed to reveal a reproducible connection between NPC movement and DNA repair (not shown). DNA replication is another possible candidate for causing NPC movements. Replication in higher eukaryotes needs a functional NE (Spann *et al.*, 1997). Some genetic loci become constrained in S phase of budding yeast cells (Heun *et al.*, 2001). However, if DNA synthesis is significantly contributing to NPC movement, NPC motility is expected to increase in a fraction of nuclei which are in S phase. However, type 2 NPC motility occurs in all interphase nuclei, making DNA replication unlikely as cause of most type 2 motility.

The work presented in this study however links nuclear pore motility to transcription. Type 2 NPC motility is significantly reduced when transcription is inhibited. *In vitro* experiments demonstrated that RNA-Polymerases are able to generate a lot of force (14 pN), even more than Kinesins (e.g. Eg5 7pN; Yin *et al.*, 1995; Valentine *et al.*, 2006). However, NPCs move significantly faster than *in vivo* incorporation rates of e.g. RNA-Pol II in mammalian which can reach maximum velocities of4.3 kb/min or ~ 24 nm/s (Darzacq *et al.*, 2007), so that a simple model, in which RNA-Pol II displaces NPCs while it moves along the DNA does not suffice to explain type 2 NPC motility. It appears more likely that transcription establishes a connection to chromatin which possesses its own motility. This bridge might be very transient which could explain why it was not possible to detect the correlation of NPCs and chromosomes microscopically. The lower velocity of type 2 NPC motility compared to chromosomes in *U. maydis* could then be a result of drag by this enormous protein complex anchored in the double membranes or transcription imposes some restraint which delays NPCs.

This model requires a temporary physical connection between factors participating in transcription, and NPCs. Drubin et al have presented a model how chromosome movements, gene activation and NPC association might be linked (Drubin *et al.*, 2006). In *D. melanogaster*, gene expression increase of the male X chromosome for dosage compensation requires association with NPC components (Mendjan *et al.*, 2006). In yeast and mammalian cells, genes can shift their position upon activation from inside the nucleus

to an association with nuclear pores (Drubin *et al.*, 2006; Taddei *et al.*, 2006; Dundr *et al.*, 2007; Meaburn and Misteli, 2008). After activation, chromosomes in budding yeast slide along the NE, and they have been found to be linked to the NPC through Nup1 (Cabal *et al.*, 2006). Also in budding yeast, promoter-NPC interactions have been found for Nup2 (Ishii *et al.*, 2002; Schmid *et al.*, 2006). Nup145 participates in transcriptional regulation as well (Feuerbach *et al.*, 2002). The Nup84-120 has also been implicated in transcriptional processes (Menon *et al.*, 2005). A tagged locus was shown to stably or transiently associate with NPCs, requiring an mRNA export factor for association (Drubin *et al.*, 2006; Kurshakova *et al.*, 2007), while nascent mRNA appears to link NPCs and DNA in another study (Casolari *et al.*, 2005). All these findings demonstrate a close correlation between DNA, transcription and the nuclear envelope in budding yeast. It is possible that NPCs and DNA are temporarily connected in *U. maydis*, so that the observed NPC type 2 motility could be chromosome motility mediated and modified by transcriptional processes. Preliminary inhibitor experiments, in which cells were exposed to Benomyl and Thiolutin simultaneously, confirmed the loss of NPC motility, but chromatin motility was unaffected (not shown). This supports the idea of active transcription providing the link between chromosome and NPC type 2 motility.

3.1.3 NPC distribution and protein expression are connected in *U. maydis*

The fact that cells invest a lot of energy into motility of NPCs raises the question of the biological significance of the process. While type 2 NPC motility might be a secondary effect of ongoing processes inside the nucleus, NPC type 1 motility relies on external forces generated by Dynein and, presumably, a Kinesin.

When NPC motility type 1 is inhibited by disruption of microtubules, efficient expression of the reporter cytoplasmic GFP from the arabinose promoter is impaired. This deficit is most severe in cells that exhibit NPC clustering arising from the lack of type 1 motility, arguing that type 1 primarily ensures equal NPC distribution. The delay in protein expression can be caused by a number of defects. The distance transcript has to travel inside the nucleus from the chromatin, whose movement is uninfluenced by Benomyl, to an exit from the nucleus is increased in nuclei with clustered NPCs (Kylberg *et al.*, 2008). Another possibility is that clustered NPCs are not as readily available to promoter binding, in cases where promoter-nucleoporin interaction is necessary to efficiently transcribe the gene (Ishii *et al.*, 2002; Taddei *et al.*, 2006). Thirdly, NPCs under Benomyl might be defective in their primary function of RNA export. Further research is needed to elucidate the exact block on the way to protein expression, but also on the biological impact of NPC clustering on protein expression,

especially as NPC accumulations are thought to enhance protein expression in *Chlamydomonas reinhardtii* (Colon-Ramos *et al.*, 2003).

3.2 NPC disassembly in mitosis resembles vertebrate models

While NPC motility in interphase has been reported in organisms without lamina, open mitosis is best characterized in vertebrate model systems. This study found NPC disassembly in *U. maydis*, which together with the already described NEBD (Straube *et al.*, 2005) suggests a more ancient origin for open mitosis than previously assumed.

3.2.1 *U. maydis'* nucleoporins exhibit fungal and vertebrate features

In order to visualize NPC disassembly, it was necessary to establish markers for different NPC subcomplexes that have been shown to disassemble and preferably localize to different cellular compartments in open or partially closed mitosis in other organisms. To this end putative nucleoporins were identified by bioinformatic searches in the genome of *U. maydis*. Using homologues from humans and budding yeast, many candidate proteins with good homologies were discovered. As only this bioinformatic approach was performed, the list of nucleoporins in *U. maydis* presented in Table 1 might not be comprehensive and include all NPC proteins that exist in *U. maydis.* Yet all of the candidates that were chosen from this list co-localized at the NE, confirming their identity as nucleoporins. The nucleoporin markers presumably occupy locations at the cytoplasmic filaments (Nup214), the central scaffold region (Nup107 and Nup133), on the nucleoplasmic side (Nup2) or are membrane-anchored (Pom152). These locations are crucial to be able to also detect partial disassembly of nuclear pores, as is the case in *A. nidulans*, where scaffold and transmembrane-anchored nucleoporins stay associated with the NE in mitosis, while nucleoplasmic and cytoplasmic nucleoporins dissociate (Osmani *et al.*, 2006).

Studies in human cells predict a copy number of 32 for Nup107, 16 for Nup133 and 8 for Nup214 (Cronshaw *et al.*, 2002), while 16 copies of Nup84 and Nup133 and 8 for Nup159 are found in budding yeast (Rout *et al.*, 2000). Nup50, the vertebrate homologue of Nup2, has been demonstrated to be present in 32 copies, but its residence time at the nuclear pore is considerably shorter than that of other nucleoporins (Rabut *et al.*, 2004a). The stoichiometric relation between these nucleoporin homologues in *U. maydis* suggest 8 copies of Nup214 and Pom152, 16 for Nup107 and Nup133, but Nup2 does not fall into either class of copy numbers. This leaves two possible interpretations: Firstly, assuming that Nup2 also possesses 16 binding sites at the nuclear pore, the lower fluorescence level could represent the short residence time of the protein at the pore, maybe not occupying all binding sites at

the pore at the same time. Alternatively, it is possible that the lower level of Nup2 compared to Nup107 indicates that Nup107 and Nup133 are incorporated at the nuclear pore in 32 copies, which would then translate into Pom152 and Nup214 being present in 16 copies, and Nup2 in 24. However, preliminary measurements of single NPCs selected for the weakest Nup2-GFP fluorescence suggested a copy number of 8 (M. Schuster, personal communication), arguing for the idea that Nup2 may not occupy all possible binding sites at the same time at the NPC.

Surprisingly several of the putative nucleoporins showed higher conservation when compared to their mammalian counterparts than to the other fungal sequences. Among these proteins were putative members of the Nup107-160 subcomplex, which has important functions in the reassembly of NPCs after open vertebrate mitoses. When Nup107 is depleted from mammalian cells, nuclear pores are severely impaired (Boehmer *et al.*, 2003; Harel *et al.*, 2003; Walther *et al.*, 2003), whereas the homologues in budding yeast and *A. nidulans* can be deleted (Siniossoglou *et al.*, 1996; Osmani *et al.*, 2006). The essentiality of Nup107 in *U. maydis* might be seen as hinting at a role in *U. maydis* open mitosis similar to vertebrates, however, in *S. pombe*, *nup107* is also essential, although this organism possesses a closed mitosis (Bai *et al.*, 2004).

3.2.2 Mitotic events in *U. maydis* resemble vertebrate model systems

U. maydis' open mitosis shares several features with the process investigated in other model organisms. These include disassembly of the NPCs and membrane removal, although membrane removal in *U. maydis* displays mechanistic differences compared to the membrane disruption described in *H. sapiens*, *D. melanogaster* or starfish oocytes (Paddy *et al.*, 1996; Beaudouin *et al.*, 2002; Lenart *et al.*, 2003). Although nuclear membranes are stripped-off in *U. maydis* rather than torn apart, the process itself is still driven by Dynein (Straube *et al.*, 2005), as is the case in human cells (Salina *et al.*, 2002). Hence NEBD can be seen as an indication of open mitosis having developed in a common ancestor, and of closed mitosis being an adaptation of the ascomycetes.

At the end of prophase in *U. maydis*, NPCs disassemble into separate subcomplexes in vertebrates, dispersing in different locations throughout mitosis (reviewed in Hetzer *et al.*, 2005; Margalit *et al.*, 2005; Antonin *et al.*, 2008). In a previous study it was shown that loss of the nuclear reporter construct begins before the NE ruptures (Straube *et al.*, 2005). Although all tagged nucleoporins investigated in this study still co-localize until the NE breaks, other nucleoporins not included in this study might leave the NPC earlier and this could account for the early release of nuclear reporter. NPC disassembly in prophase has been demonstrated to proceed in a step-wise manner, starting with the phosphorylation of peripheral nucleoporins in other organisms (Favreau *et al.*, 1996; Collas, 1999; De Souza *et al.*, 2004).

After NPC disassembly Nup107 and Nup133 stay associated with each other in the Nup107-160 subcomplex in human cells, and localize partly to chromatin and kinetochores in metaphase (Belgareh *et al.*, 2001; Loiodice *et al.*, 2004). Several studies have found an involvement of the Nup107-106 subcomplex in kinetochore function and spindle assembly (Orjalo *et al.*, 2006; Zuccolo *et al.*, 2007). A similar localization for both Nup107 and Nup133 is observed in *U. maydis*, although no co-localization of Nup107 with kinetochores was detected in metaphase and early anaphase. Any interaction at later stages in mitosis might be transient, and as kinetochores are already fully assembled in anaphase, an involvement of Nup107 and Nup133 in kinetochore assembly, similar to mammalian cells, appears unlikely in *U. maydis*. As the signal intensity of Nup107 in *U. maydis* cells is low, it is possible that a co-localization in metaphase was below the detection limit in the microscopic set-up used in this study. It is also possible that kinetochore association was an invention of vertebrates, as a study in *D. melanogaster* also could not find Nup107 co-localization with a kinetochore marker (Katsani *et al.*, 2008).

In *U. maydis* anaphase, Nup107 changes the localization from dispersed on the DNA to the outward leading edges of the separating chromosomes. In early anaphase, Nup2-GFP traces start to localize to the outer rims of the chromosomes, but the signal strongly increases as anaphase progresses. A similar early arrival of the Nup2 homologue Nup50 followed by a strong increase later has been reported in human cells (Dultz *et al.*, 2008). The stepwise addition of nucleoporins to finally build a functional pore has been determined previously (Bodoor *et al.*, 1999; Antonin *et al.*, 2005). The order in which the nucleoporins in human cells become attached is Nup107-160 subcomplex, Nup2, Pom121, Nup214 and finally gp210. This order can also be observed in *U. maydis*, with the exception of Pom152. Pom152 has no orthologous gene in metazoans, but it has been suggested that Pom121 could perform similar tasks (Mans *et al.*, 2004). In addition to Pom121, vertebrate cells also possess gp210 as transmembrane-domain containing nucleoporin. Fungi are believed to have secondarily lost gp210 (Mans *et al.*, 2004). The role of gp210 in NPC anchoring and insertion is less clear (Eriksson *et al.*, 2004; Antonin *et al.*, 2005), but several authors have argued that gp210 is the functional homologue of Pom152, due to the N-terminal TM domains which leave the bulk of proteins in the lumen of the nuclear membranes (summarized in Tcheperegine *et al.*, 1999; Antonin *et al.*, 2008). The late arrival of Pom152 in *U. maydis* telophase might support this notion.

It has previously been suggested that NPC reassembly can be interrupted by depleting the Nup107-160 subcomplex (Boehmer *et al.*, 2003; Harel *et al.*, 2003; Walther *et al.*, 2003). Although these proteins may not be the initial steps for NPC reassembly after mitosis (Rasala *et al.*, 2006), they appear to be important intermediates for establishing functional pores (D'Angelo *et al.*, 2006). It would be interesting to investigate the role of Nup107 in pore

reassembly in *U. maydis* more closely. A first analysis using the *crg*-promoter mutants did not yield clear results, maybe due to the fact that the promoter is leaky, and the proteins are presumed to be very stably attached (Belgareh *et al.*, 2001; Rabut *et al.*, 2004a), so that the remaining protein helps cells to overcome NPC reassembly blocks imposed by the absence of Nup107. It would also be interesting to see whether Nup2 binds to chromosomes independent of Nup107, as signals in anaphase overlap only partially. This could argue for 2 starting points for reassembly of NPCs, rather than Nup107 providing binding sites for all other subsequent nucleoporins to become attached.

3.2.3 The cytoskeleton is involved in re-establishing NEs in telophase

In this assay, no influence of the cytoskeleton on NPC reassembly was seen when only one part of the cytoskeleton was disrupted. When only MTs were disrupted by Benomyl, cells in anaphase still produced structures around the DNA that were able to import the reporter construct over time. Similarly, when only actin was disrupted, no effect on mitotic progression or NE re-establishment could be observed. This is in contrast to reports that in *X. laevis* actin and nuclear actin play important roles in NE assembly (Krauss *et al.*, 2003). However, this reference also states that the observed defects in NE assembly were only detected when high concentrations of Latrunculin A were used (1mM to 50 µM), but not at low concentrations (10 µM), which were used in this study. This low concentration is sufficient to disrupt F-actin, which has also been reported previously (Fuchs *et al.*, 2005). Therefore, the role of actin in NE reassembly might be underestimated in this study. However, simultaneous disruption of both elements of the cytoskeleton halts NE re-establishment, maybe pointing towards a potential compensatory role of MTs and actin to form functional nuclei.

3.2.4 Model of nuclear pore behaviour in mitosis

Summarizing all results the following model describes NPC disassembly/reassembly in the open mitosis of *U. maydis* (Figure 25). NPCs in prophase tend to accumulate at the tip of the elongated NE. As chromosomes leave the envelope, NPCs disassemble into subcomplexes. The Nup107-160 subcomplex associates with DNA in metaphase. As cells enter anaphase, Nup2 appears at the outward edges of the chromatin masses, and Nup107 is redistributed to the outer edges of chromatin. NPCs are re-established in telophase with nucleoporins becoming incorporated in a step-wise fashion.

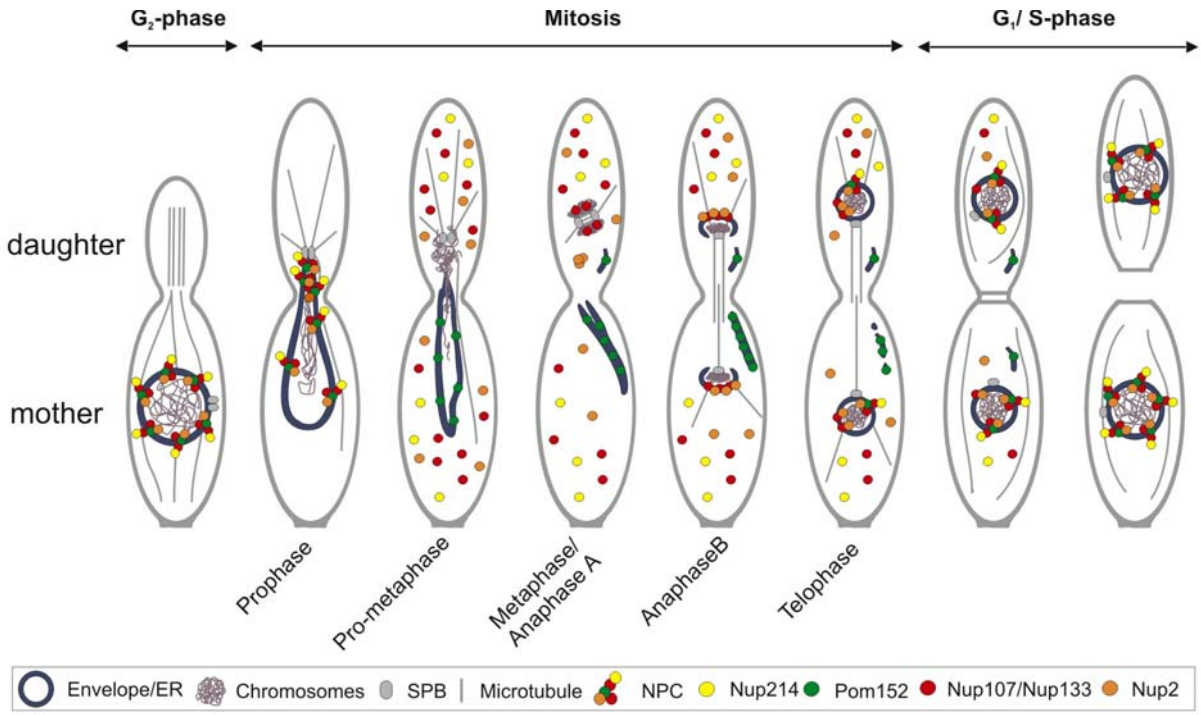

Figure 25. NPCs disassemble in the open mitosis of *U. maydis* and are reconstructed in a step-wise fashion in telophase. In interphase, all nucleoporins co-localize to build a functional nucleus in the mother cell. As the active SPBs nucleate MTs that elongate the NE in prophase, chromosomes start to migrate into the daughter cell. Chromosomes and some of the NPCs concentrate near the tip of this extension, while other NPCs already start to disassemble. At the end of prophase, NPCs completely disassemble into subcomplexes. Soluble nucleoporins equally disperse in the cytoplasm, while the transmembrane-domain anchored Pom152 disperses in the ER. In metaphase, the Nup107 and Nup133 containing subcomplex partially returns to the DNA, while a fraction of Nup2 accumulates initially in the mother cell. In early anaphase, Nup2 faintly associates with the separating DNA. In late anaphase, the separating chromosomes recruit ER membranes and form new envelopes, in which Nup107, Nup133 and Nup2 become concentrated. Nuclear envelopes close in telophase, and protein import starts after Nup214 and Pom152 are recruited. NPC assembly and insertion continue until G2-phase, when cells start to form a bud. Picture modified from Straube *et al.*, 2005

3.3 Summary and Outlook

The work presented here identified mechanisms of NPC movement, and hinted at the biological significance of equal NPC distribution. Mitotic NPC disassembly pointed towards an ancient origin of open mitosis.

The finding that efficient NPC distribution depends on the cytoskeleton, and that this supports protein expression, opens the possibility to gain interesting insights into basic principles underlying the transfer of information from inside the nucleus to the protein level. It will help to better understand the intermediate steps from the production of mRNA to protein expression, and how these steps are optimized to ensure efficient protein expression. The localization of RNA-Polymerases will provide valuable insights into the connection of transcription and NPC movement. Also the impact of NPC clustering on mRNA export should be investigated. The identification of the Kinesin involved in NPC will attribute a novel

function to one of the 10 Kinesins identified in *U. maydis*. The function of many of these is currently unknown.

As the experiments with two transcription inhibitors strongly reduced type 2 NPC motility, but did not completely abolish it, it will be interesting to identify other intranuclear processes involved. These could provide insights into the interplay of different proceses at work inside the nucleus, and how they these are coordinated spatially. In this light, NPC movement might provide valuable results on other mechanisms so far overlooked in other organisms.

Although the findings of open mitosis and NPC disassembly/reassembly suggest that essential mitotic processes mechanistically resemble vertebrate model systems, it still would be interesting to investigate these in more detail. For example, the apparent lack of co-localization of Nup107 with kinetochores in metaphase could hint at differences in the microtubule-kintechore attachment. Also the details of the step-wise NE reassembly in *U. maydis* are currently unknown. An investigation of NE reassembly could also include the role of the Nup107-160 subcomplex, which was not addressed in this study due to technical difficulties with depletion of the protein. A construction of temperature-sensitive mutants could circumvent this problem. Likewise, the regulation of NEBD and NE reassembly has so far not been addressed in *U. maydis*. In particular, the question of an interregulation of NE re-establishment with spindle progression could present interesting results on NE reassembly.

4 Material and Methods

4.1 Material

4.1.1 Chemicals, buffers and solutions

All chemicals used in this study were obtained from Merck (Haar, Germany), Invitrogen (Paisley, UK), Roth (Karlsruhe, Germany), BD Biosciences (Oxford, UK), Biozym Diagnostik (Hessisch Oldendorf, Germany), Acros Organics (Geel, Belgium), Fisher Scientific (Loughborough, UK) and Sigma-Aldrich/Fluka (Hamburg, Germany, and Poole, UK), unless stated otherwise.
Restriction endonucleases and Phusion DNA Polymerase were purchased from New England Biolabs (Frankfurt am Main, Germany) and were used as described in the manufacturer's protocols.

Standard buffers and media were produced following protocols available in lab manuals (Hanahan, 1985; Guthrie and Fink, 1991; Sambrook and Russell, 2001). Solutions needed for specific methods are detailed in the respective chapter of the methods section.

For DNA cleanup and gel extraction, commercially available kits were regularly used. In particular the JetQuick PCR CleanUp kit and DNA Cleanup kit from Genomed (Löhne, Germany), or the Wizard SV Gel and PCR Cleanup from Promega (Southampton, UK) were employed.
PCR products were cloned into vectors by Invitrogen's TOPO TA cloning kit, according to the manufacturer's protocol (Version M).
DIG labelled probes for Southern blot analysis were created using the PCR DIG Labeling Mix (Roche, Mannheim, Germany).

4.1.2 Available plasmids

All plasmids carried an ampicillin resistance marker, with the exception of pmCherry, which carried a Kanamycin resistance cassette. Lotte Søgaard-Andersen (MPI Marburg, Germany) kindly provided the plasmid pmCherry. Commercially available plasmids were purchased from Invitrogen (Paisley, UK), Pharmacia/GE Healthcare (Freiburg, Germany), Takara Bio/ Clontech (Saint-Germain-en-Laye, France).

The following plasmids were available for cloning or expression analysis:

Table 2: Available plasmids

Plasmid	Genotype	Resistance marker	Reference
pCR2.1-TOPO	-		Invitrogen
pCRII-TOPO	-		Invitrogen
pSL1180	-		Pharmacia
pSL-Cbx(+)	P*ip-ip*^{R}-T*ip*	C	(Brachmann, 2001)
pSL-Ble(+)	P*hsp70-ble*-T*trpC*	B	(Brachmann, 2001)
pSL-Nat(+)	P*gap1-nat1*-T*cyc1*	N	(Müller *et al.*, 2003)
pSL-Hyg(-)	P*hsp70-hph*-T*hsp70*	H	(Brachmann *et al.*, 2001)
pmCherry	*mCherry*		Roger Tsien, University of California, San Diego
potef-3xGFP	P*otef-gfp-gfp-gfp*-T*nos*	C	Uta Fuchs, unpublished
pSLmax-GFP_hygR	*chs8-gfp-hyg*-T*chs8*	H	Isabella Weber, unpublished
pPEB1EB1YFP	*eb1-yfp-nat*-T*eb1*	N	Isabel Schuchardt, unpublished
pSLB-Peb1-RFP	*eb1-mrfp-ble*-T*eb1*	B	(Fink and Steinberg, 2006)
pYup1SG2	P*otef-yup1-sgfp*-T*nos*	C	(Wedlich-Söldner *et al.*, 2000)
potefTub2GFP	P*otef-tub2-gfp*-T*nos*	C	(Straube *et al.*, 2003)
pSL-otef-YFP-Hyg(+)	P*otef-yfp*-T*nos*	H	Uta Fuchs, unpublished
pSL1180-crg-ATG#8	P*dyn2-ble*-P*crg-dyn2*	B	Anne Straube, unpublished
pN107Y	*nup107-yfp-ble*-T*nup107*	B	(Theisen *et al.*, 2008)
pH4CFP	P*otef-h4-cfp*-T*nos*	C	(Straube *et al.*, 2005)
pH4GFP	P*otef-h4-gfp*-T*nos*	H	(Straube *et al.*, 2005)
pSLB-Pom152-YFP	*pom152-yfp-ble*-T*pom152*	B	Anne Straube, unpublished
pERRFP	P*otef-cals-mrfp-HDEL*-T*nos*	C	(Theisen *et al.*, 2008)
pERCFP	P*otef-cals-cfp-HDEL*-T*nos*	C	(Adamikova *et al.*, 2004)
pCFPTub1	P*otef-cfp-tub1*-T*tub1*	H	(Wedlich-Söldner *et al.*, 2002b)
pN_RFPTub1	P*otef-2xmrfp-tub1*-T*tub1*	N	(Theisen *et al.*, 2008)
pC_NLS3xRFP	P*otef-gal4*^{S}*-3xmrfp*-T*nos*	C	(Straube *et al.*, 2005)
pH_NLS3xRFP	P*otef-gal4*^{S}*-3xmrfp*-T*nos*	H	(Straube *et al.*, 2005)

Table 2. Resistance marker: C, carboxin; B, phleomycin; H, hygromycin, N, nourseothricin; *ble*-gene of *Streptoalloteichus hindustanus*; *trpC*-terminator of *A. nidulans*; *nat1*-gene of *Streptomyces noursei*; *gap1*-promoter of *U. maydis*; *crg1*-promoter of *U. maydis*; *cyc1*-terminator of *S. cerevisiae*; *hph*-gene of *E. coli*; *hsp70*-promoter and *hsp70*-terminator from *hsp70*-gene of *U. maydis*; *otef*-promoter of *U. maydis*; *gfp* green fluorescent protein; *yfp* yellow fluorescent protein; *mrfp* monomeric red fluorescent protein; *cfp* cyan fluorescent protein; *H4,* Histone 4 of *U. maydis*; *cals,* signalling sequence of calreticulin from rabbit; HDEL, ER retention signal; *tub1*, α-Tubulin gene of *U. maydis*; *gal4*^{S}, nuclear localisation signal of the GAL4 DNA binding domain from pC-ACT1 (Clontech).

4.1.3 Plasmids generated in this study

The following plasmids were constructed for this study. The plasmid numbers refer to the Steinberg lab's plasmid collection. All primers are indicated in 5'-3' orientation, recognition sites for restriction enzymes are underlined. Primers used in the construction of these plasmids were synthesized by Sigma Genosys (Steinheim, Germany), Metabion (Martinsried, Germany) or Eurofins/MWG (Martinsried, Germany). PCR was done on *U. maydis* 521

wildtype strain DNA. All DNA fragments containing parts of an ORF were sequenced by Eurofins/MWG or ADIS (Cologne, Germany).

pP152R_B (#753)

This plasmid is designed to attach mRFP to the C-terminus of the endogenous *pom152* gene. To facilitate integration by homologous recombination, the plasmid contains ~ 500 bp flanks of the 3' end of the gene, and the immediate downstream region containing the putative terminator sequence. The plasmid was created by cutting the vector #2312 with *Nco*I and *BsrG*I, which left the flanks, the phleomycin cassette and the *nos* terminator in a ~7.7 kb vector fragment. The YFP was then replaced by mRFP obtained from #3064 by *Nco*I and *BsrG*I digestion. The resulting plasmid was cut with *Bsiw*I and *Xcm*I for integration into the *U. maydis* genome.

pP152G_B (#754)

This plasmid serves to fuse GFP to the endogenous Pom152 in the same manner as the mRFP construct. It was created from the same vector fragment as described for #753 (see above). The inserted GFP was obtained from #510, also by *Nco*I and *BsrG*I digestion. For genomic integration, the resulting plasmid was cut with *BsiW*I and *Xcm*I.

pP152G_H (#755)

This plasmid is equivalent to #754 (see above), only with hygromycin resistance marker instead of phleomycin for integration in the *pom152* locus. The vector #754 was cut with *Not*I to delete the phleomycin cassette, and exchanged for a hygromycin resistance cassette cut from #19 with *Not*I. Again, the resulting vector was cut with *BsiW*I and *Xcm*I for integration.

pP152R_H (#757)

Analogously, this plasmid contains a *pom152* flank fused to mRFP for integration using the hygromycin marker. The plasmid was created by cutting #753 (see above) with *Not*I to release the phleomycin cassette, which was then replaced by the hygromycin cassette from vector #19, obtained by cutting *Not*I. The resulting plasmid was cut with *BsiW*I and *Xcm*I for integration.

pN107R (#758)

This plasmid carries a ~500 bp flank of the 3' end of *nup107*, fused to *mrfp*, a *nos* terminator, a phleomycin resistance cassette and the downstream region of *nup107* for homologous integration. The plasmid was used to endogenously fuse Nup107 to mRFP at its C-terminus.

The vector #1727 was cut with *Nco*I and *BsrG*I, thereby deleting the previously inserted YFP and leaving a ~7.2 kb fragment with the flanks and the resistance marker. The mRFP was obtained from #3064 by cutting with *Nco*I and *BsrG*I. The resulting plasmid was cut with *Ssp*I for integration.

pN107G (#759)

The plasmid is the equivalent to #758 and was made from the same vector fragment. The inserted GFP was cut from #510 by *Nco*I and *BsrG*I digestion. The plasmid was linearized with *Ssp*I before transformation.

pN107G_H (#760)

In the same way as #759, this plasmid introduces a GFP fusion to the C-terminus of Nup107, but using the hygromycin cassette. Plasmid #759 was cut with *Not*I to delete the phleomycin cassette and ligated to the *Not*I digested hygromycin cassette from #19. The plasmid was cut with *Ssp*I for integration.

pN214G (#762)

This plasmid was used to fuse the endogenous *nup214* C-terminally to GFP. The ORF flank was generated by PCR with primers TU80 (CACACGAGCAAGTCAAAGTTCAGG) and TU83 (CCATGGCGCCGCCGTCCGATTTGTCCACGTTCCTTGC). Primer TU83 introduces a short linker (3 aa) and a *Nco*I site. The downstream *nup214* flank was amplified with primers TU81 (CACATGTCGACACAGCCCAAGC) and TU82 (TTCGCGGCCGCGATCTCATCATCCTTTCTCC), while primer TU82 introduces a *Not*I site. The flanks were cloned into pCRII individually. The vector containing the flank downstream of *nup214* was opened by *Not*I and *Xba*I. Into these sites the ORF flank, cut from the pCRII-nup214 LB vector with *Xba*I and *Nco*I, was inserted, together with the GFP, the *nos* terminator and part of the hygromycin cassette from #510, cut with *Nco*I and *Xho*I, and the remaining part of the hygromycin cassette from #510, cut with *Xho*I and *Not*I.

To achieve homologous recombination, the plasmid was digested with *Pvu*II before transformation of *U. maydis* protoplasts.

prN107 (#790)

This plasmid was used to place *nup107* under the control of the regulatable *crg*-promoter. The primers TU84 (TGACATATGGTCTTCTCGCTCAAACAGC) and TU87 (GCGAGATCTGCATATCACCGAGGTTGTCG) were employed to introduce an *Nde*I site at the start codon of *nup107*, and the ~1.5 kb ORF fragment cloned into pCRII. This plasmid was subsequently opended with *Sac*I and *Nde*I. The putative wild-type promoter of *nup107* was amplified as a

~1.3 kb fragment with primers TU85 (AGAGCGGCCGCAAAAAATGAAAGTGTTGATTCC) and TU86 (CGGTACCCGTAGCATTCAAACC) and cut with *Not*I and *Sac*I. The phleomycin cassette was cut from #862 along with the *crg*-promoter using *Not*I and *Nde*I and the fragments combined by a four-fragment-ligation. The plasmid was cut by *Alw*NI for integration.

pERRFP_H (#810)

This plasmid was used for visualization of the ER. The plasmid is derived from #354. This vector was cut into two fragments with *Alw*NI/*Acc*65I and *Alw*NI/*Afl*II, and the RFP-HDEL, cut with *Acc*65I and *Afl*II from #4085 was used as an insert. Cutting with *Psi*I linearized the resulting plasmid for transformation.

pN214R (#867)

This plasmid is analogous to #762 from which it was created by cutting #762 with *Nco*I/*Xba*I and *Xba*I/*Xma*I. The insert containing the RFP gene was cut with *Nco*I and *Xma*I from plasmid #757. The product was used in co-localization studies with other nucleoporins and Histone 4 in several P*crg-nup107* strains. To integrate into the *U. maydis* genome, the plasmid can be cut by *Sph*I.

pΔnup107 (#872)

This construct targets *nup107* for deletion by homologous recombination. The plasmid #1727 was opened with *Kpn*I and *Not*I to give a vector backbone and the 3´ downstream flank of *nup107*. A PCR product from the primers TU85 (AGAGCGGCCGCAAAAAATGAAAG TGTTGATTCC) and TU86 (CGGTACCCGTAGCATTCAAACC) gave the presumed promoter region of *nup107*. The product was subsequently digested with *Kpn*I and *Not*I and introduced into the vector to give an intermediary construct in which the upstream and downstream regions of *nup107* were joined by a single *Not*I between the fragments. This intermediate plasmid was next linearized by *Not*I and the *nat*-cassette inserted, cut from #15 by *Not*I. The resulting plasmid was cut with *Psi*I before transformation.

pΔnup107_H (#873)

To enhance the chances of obtaining knockout clones of *nup107*, a second construct with the *hyg*-cassette in analogy to #872 was created. The *hyg*-cassette, cut from #19 by *Not*I, was inserted into the *Not*I site of the intermediate plasmid (see above), and the resulting plasmid digested by *Psi*I for transformation.

pH4GFP_C (#892)

Some strains required a Histone 4-GFP with a *cbx*-resistance for co-localization with nucleoporins. To exchange resistance cassettes, the vector #2024 was cut with *EcoR*I and *Nco*I, which left all resistances, the P*otef* and *histone 4*, and exchanged the CFP by introducing GFP, cut from #444 by *EcoR*I and *Nco*I. The plasmid was linearized by *Ssp*I for transformation.

pMis12G (#950)

To create this plasmid, first PCR products with primers TU138 (AGGATCCTTAGAGTCG AAGCTCTCG) and TU139 (AATCCATGGCTCCGCCTCGAGAGCGAGTCGCC) to amplify the promoter region and TU140 (CCGCGGTTGCACCAGATCCGGCTG) and TU141 (CGT CGTGCCTTTCCTGG) for the terminator flank were each TOPO TA cloned into vector pCRII. The latter plasmid containing the putative terminator sequence of *mis12* served as vector for 3 inserts, after opening it with *Hind*III and *Sac*II: The left flank, cut by *Hind*III and *Nco*I from the pCRII-mis12LF clone, a triple GFP, cut from #325 by *Nco*I and *Bgl*II, and the T*nos* and the *nat*-cassette from #246, cut with *Bgl*II and *Sac*II. All fragments were combined in a 4-fragment-ligation, and the resulting plasmid linearized for transformation by *Bam*HI and *Xcm*I. Although the plasmid is designed for homologous recombination, the left flank contains part of the putative promoter and the full ORF of *mis12*. Therefore, obtained transformants were checked by Southern blotting for homologous or ectopic integration.

pTub2G_B (#1012)

To gain insight into the mitotic localization of Nup2,the resistance cassette of the vector #387 was changed by cutting with *EcoR*I and *Hind*III. The *ble* cassette was obtained by cutting #8 with *EcoR*I and *Hind*III. For transformation, the plasmid was digested with *Hind*III and *Spe*I.

pN2G (#1038)

To localize Nup2, this plasmid was constructed for homologous integration of a C-terminally fused GFP. To obtain the flanks for integration, two PCR products were amplified by primer pairs TU173 (GACATCTGCAGCGCCTGC)/ TU174 (TTCCATGGCGCCGCCCGCGGCT GCCTCCTCCAAC) and TU175 (AAGCGGCCGCTGACAAGCATGCA GAGTCG)/ TU176 (GAATTCACGAATTCCTTGCG) and TOPO TA-cloned into pCRII. The plasmid pCRII-Tnup2 with the downstream region of *nup2* was opened by *Not*I and *Xba*I, and the ORF flank, cut from pCRII-Nup2 with *Nco*I and *Spe*I, and the GFP, obtained by *Nco*I and *Not*I from #758, were inserted. The resulting plasmid held the Nup2 ORF flank fused C-terminally to GFP and the downstream flank. This intermediate was cut with *Bsr*GI/*Bsp*HI and *Bsp*HI/*Sph*I and the

fragments ligated with a *hyg*-cassette, cut by *Sph*I and *Bsr*GI from #760. The final plasmid was cut by *Eco*RV and *Spe*I for transformation.

pN133G (#1039)

This plasmid was used for localizing the endogenous Nup133 by introducing a C-terminal fusion to GFP in locus. First, the ORF flank and the downstream region of *nup133* were amplified by primer pairs TU169 (CGGCGTCGACTAAATTGG) and TU170 (TTCCATGGC GCCGCCGCCGGATTCGATCATGCTATCG), and TU171 (AAGCGGCCGCTTATCGAGAGC GACGTTCG) and TU172 (CAGGCATGCTACGCTGCC), respectively. These products were TOPO TA cloned into pCRII. The plasmid holding the putative terminator region was next opened by digestion with *Not*I and *Xba*I. The ORF flank, cut from pCRII-Nup133 by *Spe*I and *Nco*I, and GFP, cut from #758 by *Nco*I and *Not*I, were ligated into this opening to give a vector with the ORF fused to GFP, separated from the downstream region by a single *Not*I site. This intermediate was subsequently linearized at the *Not*I site and the T*nos* and the *nat*-cassette, cut together from #246 by *Not*I, were introduced. The final product was cleaved with *BamH*I and *Pvu*I before transformation.

pmCherry C-terminal (#1063)

This vector was designed as a general cloning tool. The pCRII vector holds an insert of mCherry which was derived from #1047 by PCR using primers IM309 (TAGCCATGGTGAGCAAGG) and TU168 (GGGCGGCCGCTTTACTTGTACAG). The primers introduce an *Nco*I site at the start of the gene, and a *Not*I site behind the stop codon. Therefore, the mCherry from this plasmid can be used in most constructs involving a C-terminal fusion of mCherry.

pNup2Cherry (#1101)

This plasmid was used in co-localization studies with other nucleoporins and Tub2-GFP. It is derived from #1038 (see above). #1038 was cut with *Bsr*GI/*Bgl*II and *Bgl*II/*Nco*I which removed the GFP. In its stead, a mCherry was introduced in two fragments obtained by cutting #1063 with *Nco*I/*Sbf*I and *Sbf*I/*Bsr*GI. All fragments were combined in a 4-fragment-ligation. The resulting plasmid was digested with *Eco*RV and *Spe*I for homologous integration.

pcrgGFP (#1210)

The inducible *crg*-promoter was placed immediately upstream of *gfp* on a plasmid containing a *cbx*-cassette. The plasmid was linearized by *Mfe*I before transformation to increase the probability of random ectopic integration into the genome.

4.1.4 *E. coli* strains

All plasmids were propagated in chemically competent TOP10 cells (Invitrogen, Paisley, UK). These cells have the genotype F- *mcr*A Δ(*mrr-hsd*RMS-*mcr*BC) Φ80*lac*ZΔM15 Δ*lac*X74 *rec*A1 *ara*D139 Δ(*araleu*)7697 *gal*U *gal*K *rps*L (StrR) *end*A1 *nup*G

4.1.5 *U. maydis* strains

Table 3. *U. maydis* strains used in this study

Strain	Genotype	Reference
FB2	a2b2	(Banuett and Herskowitz, 1989)
FBD11	a1b1 a2b2	(Banuett and Herskowitz, 1989)
FB1ERY_H4C	a1b1 /pERYFP /pH4CFP	(Straube *et al.*, 2005)
FB2N107G_ER	a2b2 nup107-gfp, ble^{R} /pERRFP	This study
FB2P152G_ER	a2b2 pom152-gfp, ble^{R} /pERRFP	This study
FB2N214G_ER	a2b2 nup214-gfp, hyg^{R} /pERRFP	This study
FB2N133G_ER	a2b2 nup133-gfp, nat^{R} /pERRFP	This study
FB2N2G_ER	a2b2 nup2-gfp, hyg^{R} /pERRFP	This study
FB2N107R-N214G	a2b2 nup107-rfp, ble^{R} nup214-gfp, hyg^{R}	This study
FB2N107G-P152R	a2b2 nup107-gfp, ble^{R} pom152-rfp, hyg^{R}	This study
FB2P152G_214R	a2b2 nup214-rfp, hyg^{R} pom152-gfp, ble^{R}	This study
FBD11ΔN107	a1b1 a2b2 Δnup107::nat^{R}	This study
FBD11ΔN107_H	a1b1 a2b2 Δnup107::hyg^{R}	This study
FB2N107Y_EC	a2b2 nup107-yfp, ble^{R} /pERCFP	This study
FB2N107Y_H4C	a2b2 nup107-yfp, ble^{R} /pH4CFP	This study
FB2N107R_Mis12G	a2b2 nup107-rfp, ble^{R} /pMis12-3xgfp, nat^{R}	This study
FB2N107R_N133G	a2b2 nup107-rfp, ble^{R} nup133-gfp, nat^{R}	This study
FB2N107R_H4G	a2b2 nup107-rfp, ble^{R} /pH4GFP	This study
FB2N214R_H4G	a2b2 nup214-rfp, hyg^{R} /pH4GFP_C	This study
FB2T2GN2Ch	a2b2 /pTub2GFP nup2-mcherry, hyg^{R}	This study
FB2N2GN107R	a2b2 nup2-gfp, hyg^{R} nup107-mrfp, ble^{R}	This study
FB2N214GN2Ch	a2b2 nup214-gfp, hyg^{R} nup2-mcherry, nat^{R}	This study

Strain	Genotype	Reference
FB2dyn2^{ts}N107Y_ERC	a2b2 dyn2^{ts}, nat^{R} nup107-yfp, ble^{R} /pERCFP	This study
FB1dyn2^{ts}YupG	a1b1 dyn2^{ts},nat^{R} /pYup1SG2	This study
FB2Δ*clip1*NG_ER	a2b2 Δclip1, ble^{R} nup107-gfp, hyg^{R} /pERRFP	This study
FB2Δ*ras3*NG_ER	a2b2 Δras3, nat^{R} nup107-gfp, hyg^{R} /pERRFP	This study
FB2crgGFPN107R	a2b2 nup107-rfp, ble^{R} /pPcrg-GFP	This study
FB23GDyn1_N107R	a2b2 3xgfp-dyn1, hyg^{R} nup107-rfp, ble^{R}	This study
FB2YT1-H4C	a2b2 /pYFPTub1 /pH4CFP	(Straube *et al.*, 2005)
FB2N107Y_CT	a2b2 nup107-yfp, ble^{R} /pCFPTub1	This study
FB2N107G_RT	a2b2 nup107-gfp, ble^{R} /pN_RFPTub1	This study
FB2nRFP_ERG	a2b2 /pC_NLS3xRFP /pN_ERGFP	(Straube *et al.*, 2005)
FB2P152G_nR	a2b2 /pC_NLS3xRFP pom152-gfp, hyg^{R}	This study
FB2N107G_nR	a2b2 nup107-gfp, ble^{R} /pH_NLS3xRFP	This study
FB2N214G_nR	a2b2 /pC_NLS3xRFP nup214-gfp, hyg^{R}	This study
FB2FimG	a2b2 fim-gfp, ble^{R}	This study
FB2rN107G	a2b2 Pcrg-nup107-gfp, ble^{R} hyg^{R}	This study
FB2rN107_N214G_ER	a2b2 Pcrg-nup107, ble^{R}, nup214-gfp,hyg^{R} /pERRFP	This study
FB2rN107_N214G_nR	a2b2 Pcrg-nup107, ble^{R}, nup214-gfp, hyg^{R} /pC_NLS3xRFP	This study

Table 3. Δ, deletion; /, ectopic integration; -, fusion; ::, homologous integration; ble^{R}, phleomycin resistance cassette; cbx^{R}, carboxin resistance cassette; hyg^{R}, hygromycin resistance cassette; nat^{R}, nourseothricin resistance cassette

4.2 Microbiological methods and growth conditions

4.2.1 Cultivation of *E. coli*

All *E. coli* strains were grown in liquid dYT medium or dYT agarose plates (Ausubel *et al.*, 1987; Sambrook and Russell, 2001). Depending on the plasmids used, Ampicillin (100 µg/ml) or Kanamycin (40 µg/ml) was added. X-Gal was supplemented at a concentration of 40 µg/ml to identify clones harbouring pCRII/pCR2.1-derived plasmids. All cultures were incubated at 37°C, liquid cultures shaking at 200 rpm. Glycerol stocks were produced from overnight cultures mixed with dYT containing 87% Glycerol at a 1:1 ratio and stored at -80°C.

4.2.2 Cultivation of *U. maydis*

All *U. maydis* strains, except temperature sensitive and P*crg* mutants, were grown in liquid CM-medium supplemented with 1% glucose (CM-G) at 28°C over night and shaking at 200 rpm, unless indicated otherwise. For light microscopic observation, cultures with an OD_{600} < 1 (see below) were selected.

Among the genetic tools to analyse the function of essential genes in *U. maydis* is the use of regulatable promoters such as the *crg1*-promoter (Bottin *et al.*, 1996). The P*crg1* overexpresses genes under its control in medium containing arabinose as sole carbon source, but it is repressed when glucose is the only carbon source. P*crg-nup107* strains were propagated on CM-plates containing 1% arabinose (CM-A) and grown overnight at 28°C and 200 rpm in CM-G or CM-A as indicated.

Temperature-sensitive $Dyn2^{ts}$ mutants and control strains were grown over night at 18°C. 5 ml of these cultures were transferred to new flasks and incubated at 32°C and 200 rpm for 2 h before analysis. Stop of endosome movement as indication for loss of Dynein function in a control strain was monitored microscopically.

Glycerol stocks were produced from overnight cultures and mixed with NSY medium containing 87% Glycerol at a 1:1 ratio and stored at -80°C.

The following media and additives were used to cultivate *U. maydis*:

$YEPS_{light}$ (modified from (Tsukuda *et al.*, 1988)
10 g Yeast Extract
10 g Pepton
10 g Saccharose
dH_2O added to 1 l

CM Medium (Holliday, 1974)
1 g Yeast Extract
1.5 g NH_4NO_3
2.5 g Casamino Acids
0.5 g DNA (from herring sperm)
62.5 ml Salt Solution (see above)
10 ml Vitamin Solution (see below)
dH_2O added to 980 ml
adjusted to pH 7.0 with 5 M NaOH
autoclave
supplement to 1% with glucose (50% w/v stock)

Salt Solution (Holliday, 1974)
16 g KH_2PO_4
4 g Na_2SO_4
8 g KCl
4 g $MgSO_4 \times 7\ H_2O$
1.32 g $CaCl_2 \times 2\ H_2O$
8 ml trace elements (see below)
dH_2O added to 1 l

Trace Elements (Holliday, 1974)
40 mg $CuSO_4 \times 5\ H_2O$
60 mg H_3BO_3
140 mg $MnCl_2 \times 4\ H_2O$
400 mg $ZnCl_2$
40 mg $NaMoO_4 \times 2\ H_2O$
100 mg $FeCl_3 \times 6\ H_2O$
dH_2O added to 1 l

or 1% arabinose (25% w/v stock)

NSY Glycerol
8 g Bacto Nutrient Broth
1 g Yeast Extract
5 g Sucrose
800 ml 87% Glycerol
dH_2O added to 1 l

Vitamin Solution (Holliday, 1974)
100 mg Thiamine
50 mg Riboflavin
50 mg Pyridoxine
200 mg Calcium Pantothenate
500 mg p-Aminobenoic acid
200 mg Nicotinic acid
200 mg Choline Chloride
1 g *myo*-Inositol
dH_2O added to 1 l

To grow *U. maydis* on solid medium, agarose was added to CM medium to a final concentration of 2% (w/v). Selective CM plates contained carboxine (2 µg/ml), nourseothricin/ClonNAT (150 µg/ml), hygromycin (200 µg/ml) or phleomycin (40 µg/ml).

4.2.3 Determination of optical density

The cell density of liquid *U. maydis* cultures was measured at 600 nm wavelength (OD_{600}) in a Spekol 1500 (Analytik Jena, Germany) photometer against uninoculated medium as reference. If the density of the culture exceeded 1, the culture was diluted to allow accurate measurements. A value of OD_{600} = 1 corresponds to ~ 1-5 $\times 10^7$ cells/ml.

4.3 Molecular Methods

All standard molecular biology methods were performed as described in (Hanahan, 1985; Guthrie and Fink, 1991; Sambrook and Russell, 2001). For transfer and detection of DNA (Southern Blot Analysis) the methods of Southern (Southern, 1975) were followed. DNA probes were labelled using the PCR-DIG labelling mix (Roche Applied Science, Penzberg, Germany).

For ligations, T4-Ligases from Promega (Southampton, UK) and NEB were used according to the manufacturer's instructions. For all transformations, *E. coli* TOP10 cells, available from Invitrogen (Paisley, UK), were used according to the manufacturer's protocol (Version M).

DNA concentration was measured in a Nanodrop instrument (Thermo Fisher Scientific, Wilmington, USA).

4.3.1 Standard PCR reactions

For construction of plasmids and PCR based analysis of knockout strains, Phusion Polymerase was used (NEB). Primer stocks were ordered at 100 µM.
Standard PCR reactions were performed according to the following protocol:

template	1 ul (100 ng)
Primer 1	0.5 µl (f.c. 1 µM)
Primer 2	0.5 µl (f.c. 1 µM)
dNTPs	1 µl (f.c. 20 mM)
DMSO	1.5 µl
5xGC Buffer	10 µl
Phusion	0.5 µl (1 U)
dH_2O	add to total volume of 50 µl

Standard PCR programs were carried out under these conditions:

1. Denaturing	98°C (30 s)
2. Denaturing	98°C (10 s)
3. Annealing	60°C (20 s)
4. Elongation	72°C variable (15-30 s per kb)
5. Elongation	72°C (10 min)

Steps 2. to 5. were repeated 35 times.

4.3.2 Transformation of *U. maydis*

Transformation of *U. maydis* strains was performed as described previously (Schulz *et al.*, 1990). In brief, *U. maydis* cells were grown overnight in $YEPS_{light}$ medium at 28°C (or 22°C for temperature sensitive strains) to a cell density of OD_{600} 0.6 – 0.8. Cells were collected by centrifugation (10 min, 3000 rpm, RT) and washed in 25 ml SCS before resuspension in 2 ml SCS containing 3.5 mg/ml Novozyme. Cells were incubated at RT for 10-15 min. After the incubation, the removal of the cell wall was monitored by microscopic assessment of cell morphology. When most cells showed at least rounding tips of the normally cigar-shaped cells, cells were washed tree times with pre-chilled (4°C) SCS, centrifuging at 2400 rpm for 10 min at 4°C each time. The cells were then washed once in pre-chilled STC buffer before

resuspending them in 0.5 ml STC. The cell suspension was aliquotted into 50 µl samples which were used immediately in a transformation, or stored at - 80°C.
For transformation, 5 µg of linearised DNA and 1 µl Heparin were mixed with the protoplasts and incubated for 10 min on ice. Next, 500 µl STC/PEG were added and the transformation attempt was incubated for another 15 min on ice. The cells were then plated on Regeneration-Agar supplemented with the antibiotic at their respective concentration (see above). Strains harbouring *nup107* under the control of the inducible *crg*-promoter were placed on CM-Regenerationagar containing 1% arabinose and the antibiotic. Plates were then incubated at 28°C or 22°C for temperature-sensitive mutants. Colonies appeared after 4-7 days and were singled-out on CM-agar plates containing the appropriate antibiotic and sugar. Single colonies were picked and saved on CM-plates. Obtained clones were evaluated in the microscope and homologous integration verified by Southern Blot analysis.

SCS
20 mM Na-Citrate, pH 5.8
1 M Sorbitol
in ddH_2O, filter sterilized

STC
10 mM Tris-HCl, pH 7.5
100 mM $CaCl_2$
1 M Sorbitol
in ddH_2O, filter sterilised

CM-Regeneration-Agar
a) Top-agar
1.5% (w/v) Bacto Agar
1 M Sorbitol
in CM medium, supplemented with 1% glucose or arabinose
b) Bottom Agar:
same as a) plus double concentrated antibiotic.
For plates, use 10 ml of each.

Regeneration-Agar
a) Top-agar
1.5% (w/v) Bacto Agar
1 M Sorbitol
in YEPS medium
b) Bottom Agar:
same as a) plus double concentrated antibiotic.
For plates, use 10 ml of each.

STC/PEG
15 ml STC
10 g PEG 4000
Add ddH_2O to 25 ml

4.3.3 DNA isolation from *U. maydis*

The following protocol was adapted from Hoffman and Winston, 1987. 2 ml of an overnight culture, grown in $YEPS_{light,}$ were pelleted in 2 ml Eppendorf tubes by centrifugation (1 min,

13000 rpm). The supernatant was discarded and 0.3 g glass beads, 400 µl Ustilago lysis buffer and 500 µl of Phenol-Chloroform (1:1) were added. The samples were incubated for ~ 10 min on a Vibrax-VXR shaker (IKA, Staufen, Germany) at full speed. After phase separation by centrifugation for 15 min at 13000 rpm, 400 µl of the top phase of the supernatant were transferred to a 1.5 µl Eppendorf tube and mixed with 1 ml of ethanol. The samples were subsequently centrifuged for 2 min at 13000 rpm and the pellet was resuspended in 50 µl TE/RNase A at 55°C and stored at –20°C for further analyses. 10-20 µl of DNA was used for Southern Blotting, 0.5 µl of a 1:4 dilution in standard PCR reaction.

Ustilago lysis buffer
50 mM Tris-Cl, pH 7.5
50 mM Na_2-EDTA
1% (w/v) SDS

4.3.4 Protein isolation and Western Blotting

To analyze protein content in Nup107 downregulated cells, whole cell extracts were prepared from overnight cultures of strains FB2N107G_ER and FB2rN107G that were grown to an OD_{600} ~ 0.5 in CM-G or CM-A. The cells were harvested by centrifugation at 3000 rpm for 10 min. After one wash in extraction buffer (100 mM PIPES, pH 6.9, 5 mM $MgSO_4$, 1 mM EDTA, 1 mM EGTA), cells were resuspended in extraction buffer supplemented with complete protease inhibitor (1 tablet/ 10 ml buffer; Roche Applied Sciences, Penzberg, Germany). The cell suspension was then frozen by liquid nitrogen and disrupted in a mixer mill MM200 (Retsch, Haan, Germany), 2x5 min at full speed. After thawing, the solution was centrifuged for 30 min at 24,000 rpm to clear the supernatant of cellular debris and large organelles. Protein content of the supernatant was then analyzed using the Bradford test. A reference graph was constructed with known concentrations of BSA, against which the samples were analyzed. Equal amounts of proteins from the different samples were subsequently loaded onto a gel for a Western Blot.
Protein samples were denatured by adding loading dye (300 mM Tris-HCl, pH 8.0, 30% glycerol, 20% SDS, 0.5 mg/ml Bromphenolblue, 15% β-Mercaptoethanol) and incubating samples for 5 min at 95°C. Proteins were separated on an 8% Polyacrylamide gel and transferred onto a nitrocellulose memberane for 60 min at 400 mA in a wet blot chamber (Hoefer Scientific Instruments, San Francisco, CA, USA). Nup107-GFP was identified by an antibody against the C-terminal GFP tag (from mouse, used at a concentration of 1:5000; Roche Applied Sciences, Penzberg, Germany), while an antibody against α–Tubulin served as internal loading control (also from mouse, used at a concentration of 1:5000, Sigma). The

secondary antibody against mouse IgG (Promega, Madison, USA) was coupled to horseradish peroxidase. The ECL system was used to detect the protein, and film processing was done in a Kodak Film Developer machine.

4.3.5 Plant infections and teliospore isolation

To test whether *nup107* is an essential gene, a diploid strains was created in which one copy of the gene was replaced with the nourseothricin-resistance cassette or the hygromycin-resistance cassette. Maize plants were infected with an overnight culture of strain FB2Δnup107 (*nat*-resistance, Table 3) supplemented with 0.5% Tween 20 before injection following a standard protocol (Fuchs *et al.*, 2006). Plants were grown for 25 days at 28°C before harvesting tumors.

4.3.6 Spore germination and analysis

Spores from these tumors were isolated as described in Fuchs *et al.*, 2006. Spores were germinated on CM-G agar plates at 22°C. Fifty-seven spores were selected from these plates and placed on CM-G agar plates containing 150 µg/ml nourseothricin. DNA was extracted from the thirty-six colonies that grew in the presence of the antibiotic and analyzed to ORF-specific PCR and Southern blot analysis.

4.4 Bioinformatic analyses

Protein sequences of *U. maydis* were obtained from the MIPS and the Broad Institute's databases (http://mips.gsf.de/genre/proj/ustilago/ and http://www.broad.mit.edu/annotation/genome/ustilago_maydis/Home.html). Protein sequences from all other organisms were found in the PubMed database (http://www.ncbi.nlm.nih.gov/sites/entrez?db=PubMed). These proteins were used in BLAST searches on the MIPS and Broad Institute's website. Protein domains were modelled according to SMART evaluation of the protein sequences (http://smart.embl-heidelberg.de/). Predictions of transmembrane domains were based on results from SMART and TMHMM (http://www.cbs.dtu.dk/services/TMHMM-2.0). The program Lalign (http://www.ch.embnet.org/ software/LALIGN_form.html) calculated identity values of two proteins.

Putative homologues were aligned by ClustalX software (Thompson *et al.*, 1997), and phylogenetic trees were constructed in MEGA (version 2.1) using the minimum evolution method with bootstrap values (Kumar *et al.*, 2001). The initial tree was created by neighbour-joining and gaps pair-wise deleted. Bootstraps values were based on 1000 replications.

4.5 Cell biological methods and imaging

4.5.1 Fixation and staining

For co-localization studies of nucleoporins, cells from strains expressing Nup214-GFP were fixed with 0.4% formaldehyde and 0.1% glutaraldehyde (Polysciences, Eppelheim, Germany) for 5 min incubation at RT, whereas cells from strains expressing Nup107-GFP or Pom152-GFP were fixed in 0.5% formaldehyde for 10 min at RT. Cells expressing Nup133-GFP or Nup2-GFP were fixed with 1% formaldehyde for 15 min at RT.
These fixations were also applied before mounting the cells on Poly-L-Lysin (Sigma-Aldrich, Steinheim, Germany) coated coverslips for 3 min before adding DAPI (Sigma) at a final concentration of 0.5 µg/ml and incubating for 15 min at 37°C. The samples were washed several times in PBS before microscopy.
To obtain Z-stacks of NPC accumulations in interphase, cells from strain FB2N107G_ER were fixed with 0.5% formaldehyde for 10 min at room temperature (Polysciences) and imaged every 0.5 µm.

4.5.2 Microcopy, image processing and analysis

For live cell imaging, cells were grown over night in CM-G or CM-A at 28°C at 200 rpm, unless otherwise indicated. 1 µl of a growing culture was placed on a 2% agarose cushion, supplemented with inhibitors when applicable, and immediately observed in the microscope.
Two microscopic systems were employed:

a) Epifluorescence on mitotic events was mostly done on the Zeiss Axioplan II microscope (Jena, Germany). Filter sets for fluorescein isothiocyanate (FITC) (BP470/20, FT510, and BP515-565; Carl Zeiss), DsRed (BP565/30, FT585, and BP620/60; Carl Zeiss), YFP (BP500/20, FT515, and BP535/30; Carl Zeiss), and CFP (BP436, FT455, and BP480-500; Carl Zeiss) or for GFP (HC470/40, T495LP, and HC525/50; AHF, Tübingen, Germany) and Texas-Red (HC562/40, BS 593, and HC624/40; AHF) were used with an HBO lamp for illumination. Z-Stacks of fixed cells were obtained at 0.5 µm intervals.
b) NPC movement was observed in the IX81 inverted microscope (Olympus, Hamburg, Germany). Excitation of fluorescent proteins was achieved by solid state lasers (488nm/50mW and 561nm/50mW) under the control of a VS-AOTF100 System (Visitron System, Munich, Germany). YFP-labelled proteins were imaged using a U-RFL-T lamp (Olympus, Hamburg, Germany) and the respective filter set from Chroma

(HC 542/27, BS 520, HC 500/24; Rockingham, USA). Co-localization of proteins in GFP/RFP was observed using a Dual-View Microimager (Optical Insights, Tucson, USA) equipped with specific filter sets adjusted for laser excitation (Chroma, Rockingham, USA; Semrock, Rochester, USA). To obtain Z-streams from strain FB2N107GRT, cells were photographed every 0.4 µm using a Piezo device (Piezosystem Jena, Germany).

For FRAP experiments, the intensity of a 405 nm laser was adjusted to bleach an area roughly corresponding to half the surface area of a nucleus. After bleaching, NPC movement was monitored in timelapse, taking one image every 7 s for 6 min.

All images were captured using a Charged-Coupled Device camera (Photometric CoolSNAP HQ2, Roper Scientific, Germany). Both microscopes were controlled by MetaMorph (Molecular Devices, Downingtown, USA).

All fluorescence intensity measurements and kymograph analyses were carried out in MetaMorph. Statistical analysis was performed in Prism 5 (GraphPad Software, San Diego, USA). Images were processed with MetaMorph and Photoshop (Adobe, San Jose, CA, USA). Z-streams of nuclei were processed by 10 to 100 iterations of 3-D deconvolution; maximum projections and 3D reconstructions of the resulting images were created in AutoQuantX software (AutoQuant Imaging, Troy, N.Y., USA).

To determine the amount of nucleoporin-GFP fusion proteins, the integrated intensity of fluorescence signal in the nuclear envelope was measured and the cytoplasmic background fluorescence was subtracted. The same method was used for determining NLS-3xRFP and NPC reassembly in telophase. The fluorescence signal in the cytoplasm during mitosis was determined by average intensity measurements. The Nup107-GFP signal on the DNA in metaphase was measured against the fluorescence intensity of the cytoplasmic background.

Kymographs to evaluate NPC motility were generated from streams focussed on an area of ~ 1 μm^2 of the top or bottom of a nucleus (80 planes, 150ms each). The 488 nm laser was set to 50% intensity at the beginning of the film, which was gradually increased as imaging continued to compensate for bleaching of the NPCs. All run length and velocities were determined from these kymographs.

NPC motility was classified according to run length and velocity. Type 1 comprises long-range, fast directed motility, type 2 short-range, slow directed motility, and diffusion random displacements of low velocity. Diffusion was not further investigated in this study. Nuclei exhibiting at least one single motility event were counted as type 1 or type 2. These categories were mutually exclusive, and nuclei exhibiting both motility types were included only in the type 1 category.

Chromosome motility was assessed in films processed by 2D deconvolution (Metamorph Software).
For protein expression analysis, images of cells were taken at 1 h, 2 h, 3 h and 4 h after promoter induction. Nuclei with clustered NPCs were selected from the Benomyl treated sample, while nuclei with distributed NPCs were chosen in the DMSO treated culture.
Statistical analysis by two-tailed *t* test at α = 0.05, 0.001 and 0.0001 used Prism 5 software (GraphPad Software, San Diego, CA). All values are given as means ± standard unless otherwise indicated. Prism software was also used to generate regression lines.

4.5.3 Inhibitor studies

For experiments investigating the role of the cytoskeleton in NE reassembly, Benomyl-induced depolymerization of microtubules was monitored by placing 1 µl of logarithmically growing cells on a 2% agarose cushion containing 30 µM Benomyl (Sigma, Taufkirchen, Germany) as described previously (Fink and Steinberg, 2006). Analogously, depolymerization of the actin cytoskeleton was achieved by adding 10 µM Latrunculin A (kindly provided by P. Crews, University of California, Santa Cruz, Santa Cruz, CA) to the agarose cushion. Cells in anaphase were identified under the microscope by the diffuse appearance with a dark rift of Nup107-GFP/Nup133-GFP in the daughter cell or completed nuclear envelope breakdown in the case of strains expressing Nup2-GFP, Nup214-GFP or Pom152-GFP, and the first image pair taken. The second image pair was obtained 7 min after exposure of cells to the inhibitor. A third image pair was taken at 20 min of inhibitor treatment to observe effects of inhibitor treatment on NPC functionality.
Inhibitor experiments to analyze NPC movement in interphase were carried out under the following conditions: 1 ml of a growing over night culture was supplemented with 30 µM Benomyl, 10 µM Latrunculin A, 100 µM CCCP (Sigma-Aldrich, Poole, UK), 5 µg/ml Thiolutin (Sigma-Aldrich, Poole, UK) or 25 µg/ml Mycophenolate (Sigma-Aldrich, Poole, UK). Cells were incubated for 30 min at room temperature, with the exception of CCCP, which was incubated for 15 min at room temperature. Cells that were treated with a combination of drugs were incubated simultaneously with Benomyl and Latrunculin A for 30 min, or 15 min pre-incubated with Benomyl before adding Thiolutin or Mycophenolate for 30 min. Control strains were treated similarly, supplemented with DMSO or methanol. For recovery experiments, cells were centrifuged at 5000 rpm for 3 min after inhibitor treatment and washed twice in CM-G. Finally, cells were resuspended in 1 ml CM-G and incubated at room temperature for 30 min.
All experiments were performed in triplicates, and the functionality of the inhibitors monitored in the appropriate control strains (FB2GT, FB2FimGFP, FB23GDyn1, FB2crgGFPN107R).

1 ml of a growing over night culture (CM-G) of strain FB2crgGFPN107R was harvested at 5000 rpm for 3 min. After discarding the supernatant, DMSO, Benomyl (30 µM), Thiolutin (5 µg/ml) or Mycophenolate (25 µg/ml) was added and cells resuspended in 1 ml of CM-A. Images were taken at the indicated time intervals to monitor protein expression, or after 3.5 h for control of transcription inhibition.

5 Bibliography

Adamikova, L., Straube, A., Schulz, I., and Steinberg, G. (2004). Calcium signaling is involved in dynein-dependent microtubule organization. Mol Biol Cell *15*, 1969-1980.

Akhtar, A., and Gasser, S.M. (2007). The nuclear envelope and transcriptional control. Nat Rev Genet *8*, 507-517.

Alber, F., Dokudovskaya, S., Veenhoff, L.M., Zhang, W., Kipper, J., Devos, D., Suprapto, A., Karni-Schmidt, O., Williams, R., Chait, B.T., Sali, A., and Rout, M.P. (2007). The molecular architecture of the nuclear pore complex. Nature *450*, 695-701.

Antonin, W., Ellenberg, J., and Dultz, E. (2008). Nuclear pore complex assembly through the cell cycle: regulation and membrane organization. FEBS Lett *582*, 2004-2016.

Antonin, W., Franz, C., Haselmann, U., Antony, C., and Mattaj, I.W. (2005). The integral membrane nucleoporin pom121 functionally links nuclear pore complex assembly and nuclear envelope formation. Mol Cell *17*, 83-92.

Ausubel, F.M., Brenz, R., Kingston, R.E., Moor, D.D., Seidmann, J.G., Smith, J.A., and Strukl, K. (1987). Current Protocols in Molecular Biology. John Wiley & Sons.

Bai, S.W., Rouquette, J., Umeda, M., Faigle, W., Loew, D., Sazer, S., and Doye, V. (2004). The fission yeast Nup107-120 complex functionally interacts with the small GTPase Ran/Spi1 and is required for mRNA export, nuclear pore distribution, and proper cell division. Mol Cell Biol *24*, 6379-6392.

Banuett, F., and Herskowitz, I. (1989). Different a alleles of *Ustilago maydis* are necessary for maintenance of filamentous growth but not for meiosis. Proc Natl Acad Sci U S A *86*, 5878-5882.

Beaudouin, J., Gerlich, D., Daigle, N., Eils, R., and Ellenberg, J. (2002). Nuclear envelope breakdown proceeds by microtubule-induced tearing of the lamina. Cell *108*, 83-96.

Beck, M., Lucic, V., Forster, F., Baumeister, W., and Medalia, O. (2007). Snapshots of nuclear pore complexes in action captured by cryo-electron tomography. Nature *449*, 611-615.

Belgareh, N., and Doye, V. (1997). Dynamics of nuclear pore distribution in nucleoporin mutant yeast cells. J Cell Biol *136*, 747-759.

Belgareh, N., Rabut, G., Bai, S.W., van Overbeek, M., Beaudouin, J., Daigle, N., Zatsepina, O.V., Pasteau, F., Labas, V., Fromont-Racine, M., Ellenberg, J., and Doye, V. (2001). An evolutionarily conserved NPC subcomplex, which redistributes in part to kinetochores in mammalian cells. J Cell Biol *154*, 1147-1160.

Berke, I.C., Boehmer, T., Blobel, G., and Schwartz, T.U. (2004). Structural and functional analysis of Nup133 domains reveals modular building blocks of the nuclear pore complex. J Cell Biol *167*, 591-597.

Bodoor, K., Shaikh, S., Salina, D., Raharjo, W.H., Bastos, R., Lohka, M., and Burke, B. (1999). Sequential recruitment of NPC proteins to the nuclear periphery at the end of mitosis. J Cell Sci *112 (Pt 13)*, 2253-2264.

Boehmer, T., Enninga, J., Dales, S., Blobel, G., and Zhong, H. (2003). Depletion of a single nucleoporin, Nup107, prevents the assembly of a subset of nucleoporins into the nuclear pore complex. Proc Natl Acad Sci U S A *100*, 981-985.

Boehmer, T., Jeudy, S., Berke, I.C., and Schwartz, T.U. (2008). Structural and functional studies of Nup107/Nup133 interaction and its implications for the architecture of the nuclear pore complex. Mol Cell *30*, 721-731.

Booth, J.W., Belanger, K.D., Sannella, M.I., and Davis, L.I. (1999). The yeast nucleoporin Nup2p is involved in nuclear export of importin alpha/Srp1p. J Biol Chem *274*, 32360-32367.

Bottin, A., Kamper, J., and Kahmann, R. (1996). Isolation of a carbon source-regulated gene from *Ustilago maydis*. Mol Gen Genet *253*, 342-352.

Brachmann, A. (2001). Die frühe Infektionsphase von *Ustilago maydis*: Genregulation durch das bW/bE- Heterodimer. PhD thesis (LMU Munich, Germany).

Brachmann, A., Weinzierl, G., Kämper, J., and Kahmann, R. (2001). Identification of genes in the bW/bE regulatory cascade in *Ustilago maydis*. Mol Microbiol *42*, 1047-1063.

Bucci, M., and Wente, S.R. (1997). *In vivo* dynamics of nuclear pore complexes in yeast. J Cell Biol *136*, 1185-1199.

Byers, B. (1981). Cytology of the yeast cell cycle. The Molecular Biology of the Yeast Saccharomyces: Life Cycle and Inheritance *Strathern, J.N., Jones E. W. Broach, JR (eds)*, 59-96.

Bystricky, K., Laroche, T., van Houwe, G., Blaszczyk, M., and Gasser, S.M. (2005). Chromosome looping in yeast: telomere pairing and coordinated movement reflect anchoring efficiency and territorial organization. J Cell Biol *168*, 375-387.

Cabal, G.G., Genovesio, A., Rodriguez-Navarro, S., Zimmer, C., Gadal, O., Lesne, A., Buc, H., Feuerbach-Fournier, F., Olivo-Marin, J.C., Hurt, E.C., and Nehrbass, U. (2006). SAGA interacting factors confine sub-diffusion of transcribed genes to the nuclear envelope. Nature *441*, 770-773.

Cai, D., Verhey, K.J., and Meyhofer, E. (2007). Tracking single Kinesin molecules in the cytoplasm of mammalian cells. Biophys J *92*, 4137-4144.

Casolari, J.M., Brown, C.R., Drubin, D.A., Rando, O.J., and Silver, P.A. (2005). Developmentally induced changes in transcriptional program alter spatial organization across chromosomes. Genes Dev *19*, 1188-1198.

Casolari, J.M., Brown, C.R., Komili, S., West, J., Hieronymus, H., and Silver, P.A. (2004). Genome-wide localization of the nuclear transport machinery couples transcriptional status and nuclear organization. Cell *117*, 427-439.

Chaudhary, N., and Courvalin, J.C. (1993). Stepwise reassembly of the nuclear envelope at the end of mitosis. J Cell Biol *122*, 295-306.

Chikashige, Y., Ding, D.Q., Funabiki, H., Haraguchi, T., Mashiko, S., Yanagida, M., and Hiraoka, Y. (1994). Telomere-led premeiotic chromosome movement in fission yeast. Science *264*, 270-273.

Chikashige, Y., Haraguchi, T., and Hiraoka, Y. (2007). Another way to move chromosomes. Chromosoma *116*, 497-505.

Chuang, C.H., Carpenter, A.E., Fuchsova, B., Johnson, T., de Lanerolle, P., and Belmont, A.S. (2006). Long-range directional movement of an interphase chromosome site. Curr Biol *16*, 825-831.

Chubb, J.R., Boyle, S., Perry, P., and Bickmore, W.A. (2002). Chromatin motion is constrained by association with nuclear compartments in human cells. Curr Biol *12*, 439-445.

Collas, P. (1999). Sequential PKC- and Cdc2-mediated phosphorylation events elicit zebrafish nuclear envelope disassembly. J Cell Sci *112*, 977-987.

Colon-Ramos, D.A., Salisbury, J.L., Sanders, M.A., Shenoy, S.M., Singer, R.H., and Garcia-Blanco, M.A. (2003). Asymmetric distribution of nuclear pore complexes and the cytoplasmic localization of beta2-tubulin mRNA in *Chlamydomonas reinhardtii*. Dev Cell *4*, 941-952.

Conrad, M.N., Lee, C.Y., Chao, G., Shinohara, M., Kosaka, H., Shinohara, A., Conchello, J.A., and Dresser, M.E. (2008). Rapid telomere movement in meiotic prophase is promoted by NDJ1, MPS3, and CSM4 and is modulated by recombination. Cell *133*, 1175-1187.

Coué, M., Brenner, S.L., Spector, I., and Korn, E.D. (1987). Inhibition of actin polymerization by latrunculin A. FEBS Lett *213*, 316-318.

Cronshaw, J.M., Krutchinsky, A.N., Zhang, W., Chait, B.T., and Matunis, M.J. (2002). Proteomic analysis of the mammalian nuclear pore complex. J Cell Biol *158*, 915-927.

D'Angelo, M.A., Anderson, D.J., Richard, E., and Hetzer, M.W. (2006). Nuclear pores form *de novo* from both sides of the nuclear envelope. Science *312*, 440-443.

D'Angelo, M.A., and Hetzer, M.W. (2006). The role of the nuclear envelope in cellular organization. Cell Mol Life Sci *63*, 316-332.

Daigle, N., Beaudouin, J., Hartnell, L., Imreh, G., Hallberg, E., Lippincott-Schwartz, J., and Ellenberg, J. (2001). Nuclear pore complexes form immobile networks and have a very low turnover in live mammalian cells. J Cell Biol *154*, 71-84.

Darzacq, X., Shav-Tal, Y., de Turris, V., Brody, Y., Shenoy, S.M., Phair, R.D., and Singer, R.H. (2007). *In vivo* dynamics of RNA polymerase II transcription. Nat Struct Mol Biol *14*, 796-806.

De Boni, U., and Mintz, A.H. (1986). Curvilinear, three-dimensional motion of chromatin domains and nucleoli in neuronal interphase nuclei. Science *234*, 863-866.

De Souza, C.P., Horn, K.P., Masker, K., and Osmani, S.A. (2003). The SONB(NUP98) nucleoporin interacts with the NIMA kinase in *Aspergillus nidulans*. Genetics *165*, 1071-1081.

De Souza, C.P., Osmani, A.H., Hashmi, S.B., and Osmani, S.A. (2004). Partial nuclear pore complex disassembly during closed mitosis in *Aspergillus nidulans*. Curr Biol *14*, 1973-1984.

De Souza, C.P., and Osmani, S.A. (2007). Mitosis, not just open or closed. Eukaryot Cell *6*, 1521-1527.

Denning, D.P., Patel, S.S., Uversky, V., Fink, A.L., and Rexach, M. (2003). Disorder in the nuclear pore complex: the FG repeat regions of nucleoporins are natively unfolded. Proc Natl Acad Sci U S A *100*, 2450-2455.

Denning, D.P., and Rexach, M.F. (2007). Rapid evolution exposes the boundaries of domain structure and function in natively unfolded FG nucleoporins. Mol Cell Proteomics *6*, 272-282.

Devos, D., Dokudovskaya, S., Williams, R., Alber, F., Eswar, N., Chait, B.T., Rout, M.P., and Sali, A. (2006). Simple fold composition and modular architecture of the nuclear pore complex. Proc Natl Acad Sci U S A *103*, 2172-2177.

Dillon, N. (2008). The impact of gene location in the nucleus on transcriptional regulation. Dev Cell *15*, 182-186.

Ding, R., McDonald, K.L., and McIntosh, J.R. (1993). Three-dimensional reconstruction and analysis of mitotic spindles from the yeast, *Schizosaccharomyces pombe*. J Cell Biol *120*, 141-151.

Drubin, D.A., Garakani, A.M., and Silver, P.A. (2006). Motion as a phenotype: the use of live-cell imaging and machine visual screening to characterize transcription-dependent chromosome dynamics. BMC Cell Biol *7*, 19.

Dultz, E., Zanin, E., Wurzenberger, C., Braun, M., Rabut, G., Sironi, L., and Ellenberg, J. (2008). Systematic kinetic analysis of mitotic dis- and reassembly of the nuclear pore in living cells. J Cell Biol *180*, 857-865.

Dundr, M., Ospina, J.K., Sung, M.H., John, S., Upender, M., Ried, T., Hager, G.L., and Matera, A.G. (2007). Actin-dependent intranuclear repositioning of an active gene locus *in vivo*. J Cell Biol *179*, 1095-1103.

Ellenberg, J., Siggia, E.D., Moreira, J.E., Smith, C.L., Presley, J.F., Worman, H.J., and Lippincott-Schwartz, J. (1997). Nuclear membrane dynamics and reassembly in living cells: targeting of an inner nuclear membrane protein in interphase and mitosis. J Cell Biol *138*, 1193-1206.

Eriksson, C., Rustum, C., Hallberg, E., Cohen, M., Feinstein, N., Wilson, K.L., and Gruenbaum, Y. (2004). Dynamic properties of nuclear pore complex proteins in gp210 deficient cells. FEBS Lett *572*, 261-265.

Fabre, E., and Hurt, E. (1997). Yeast genetics to dissect the nuclear pore complex and nucleocytoplasmic trafficking. Annu Rev Genet *31*, 277-313.

Favreau, C., Worman, H.J., Wozniak, R.W., Frappier, T., and Courvalin, J.C. (1996). Cell cycle-dependent phosphorylation of nucleoporins and nuclear pore membrane protein Gp210. Biochemistry *35*, 8035-8044.

Feuerbach, F., Galy, V., Trelles-Sticken, E., Fromont-Racine, M., Jacquier, A., Gilson, E., Olivo-Marin, J.C., Scherthan, H., and Nehrbass, U. (2002). Nuclear architecture and spatial positioning help establish transcriptional states of telomeres in yeast. Nat Cell Biol *4*, 214-221.

Fink, G., Schuchardt, I., Colombelli, J., Stelzer, E., and Steinberg, G. (2006). Dynein-mediated pulling forces drive rapid mitotic spindle elongation in *Ustilago maydis*. Embo J *25*, 4897-4908.

Fink, G., and Steinberg, G. (2006). Dynein-dependent motility of microtubules and nucleation sites supports polarization of the tubulin array in the fungus *Ustilago maydis*. Mol Biol Cell *17*, 3242-3253.

Fitzpatrick, D.A., Logue, M.E., Stajich, J.E., and Butler, G. (2006). A fungal phylogeny based on 42 complete genomes derived from supertree and combined gene analysis. BMC Evol Biol *6*, 99.

Fuchs, U., Hause, G., Schuchardt, I., and Steinberg, G. (2006). Endocytosis is essential for pathogenic developement in the corn smut fungus *Ustilago maydis*. Plant Cell *18*, 2066-2081.

Fuchs, U., Manns, I., and Steinberg, G. (2005). Microtubules are dispensable for the initial pathogenic development but required for long-distance hyphal growth in the corn smut fungus *Ustilago maydis*. Mol Biol Cell *16*, 2746-2758.

Galy, V., Olivo-Marin, J.C., Scherthan, H., Doye, V., Rascalou, N., and Nehrbass, U. (2000). Nuclear pore complexes in the organization of silent telomeric chromatin. Nature *403*, 108-112.

Glavy, J.S., Krutchinsky, A.N., Cristea, I.M., Berke, I.C., Boehmer, T., Blobel, G., and Chait, B.T. (2007). Cell-cycle-dependent phosphorylation of the nuclear pore Nup107-160 subcomplex. Proc Natl Acad Sci U S A *104*, 3811-3816.

Gorsch, L.C., Dockendorff, T.C., and Cole, C.N. (1995). A conditional allele of the novel repeat-containing yeast nucleoporin RAT7/NUP159 causes both rapid cessation of mRNA export and reversible clustering of nuclear pore complexes. J Cell Biol *129*, 939-955.

Goshima, G., Kiyomitsu, T., Yoda, K., and Yanagida, M. (2003). Human centromere chromatin protein hMis12, essential for equal segregation, is independent of CENP-A loading pathway. J Cell Biol *160*, 25-39.

Grigull, J., Mnaimneh, S., Pootoolal, J., Robinson, M.D., and Hughes, T.R. (2004). Genome-wide analysis of mRNA stability using transcription inhibitors and microarrays reveals posttranscriptional control of ribosome biogenesis factors. Mol Biol Cell *24*, 5534-5547.

Gruenbaum, Y., Margalit, A., Goldman, R.D., Shumaker, D.K., and Wilson, K.L. (2005). The nuclear lamina comes of age. Nat Rev Mol Cell Biol *6*, 21-31.

Guan, T., Kehlenbach, R.H., Schirmer, E.C., Kehlenbach, A., Fan, F., Clurman, B.E., Arnheim, N., and Gerace, L. (2000). Nup50, a nucleoplasmically oriented nucleoporin with a role in nuclear protein export. Mol Cell Biol *20*, 5619-5630.

Guthrie, C., and Fink, G.R. (1991). Guide to Yeast Genetics and Molecular Biology. Academic Press.

Hanahan, D. (1985). Techniques of Transformation of *E. coli*. In DNA cloning, a practical approach *Rickwood D., Hames B.D. (eds)*, 109-135.

Harel, A., Orjalo, A.V., Vincent, T., Lachish-Zalait, A., Vasu, S., Shah, S., Zimmerman, E., Elbaum, M., and Forbes, D.J. (2003). Removal of a single pore subcomplex results in vertebrate nuclei devoid of nuclear pores. Mol Cell *11*, 853-864.

Heath, I.B. (1980). Variant mitosis in lower eukaryotes: indicators of the evolution of mitosis? Int Rev Cytol *64*, 1-80.

Hemmerich, P., Weidtkamp-Peters, S., Hoischen, C., Schmiedeberg, L., Erliandri, I., and Diekmann, S. (2008). Dynamics of inner kinetochore assembly and maintenance in living cells. J Cell Biol *180*, 1101-1114.

Hetzer, M., Walther, T.C., and Mattaj, I.W. (2005). Pushing the Envelope: Structure, Function, and Dynamics of the Nuclear Periphery. Annu Rev Cell Dev Biol.

Heun, P., Laroche, T., Shimada, K., Furrer, P., and Gasser, S.M. (2001). Chromosome dynamics in the yeast interphase nucleus. Science *294*, 2181-2186.

Hoffman, C.S., and Winston, F. (1987). A ten-minute DNA preparation from yeast efficiently releases autonomous plasmids for transformation of *Escherichia coli*. Gene *57*, 267-272.

Holliday, R. (1974). *Ustilago maydis*. The Handbook of Genetics. Plenum Press.

Hood, J.K., Casolari, J.M., and Silver, P.A. (2000). Nup2p is located on the nuclear side of the nuclear pore complex and coordinates Srp1p/importin-alpha export. J Cell Sci *113 (Pt 8)*, 1471-1480.

Hutten, S., and Kehlenbach, R.H. (2006). Nup214 is required for CRM1-dependent nuclear protein export *in vivo*. Mol Cell Biol *26*, 6772-6785.

Ishii, K., Arib, G., Lin, C., Van Houwe, G., and Laemmli, U.K. (2002). Chromatin boundaries in budding yeast: the nuclear pore connection. Cell *109*, 551-562.

Katsani, K.R., Karess, R.E., Dostatni, N., and Doye, V. (2008). *In Vivo* Dynamics of Drosophila Nuclear Envelope Components. Mol Biol Cell *19*, 3652-3666.

King, M.C., Drivas, T.G., and Blobel, G. (2008). A network of nuclear envelope membrane proteins linking centromeres to microtubules. Cell *134*, 427-438.

King, S.J., and Schroer, T.A. (2000). Dynactin increases the processivity of the cytoplasmic dynein motor. Nat Cell Biol *2*, 20-24.

Kiseleva, E., Allen, T.D., Rutherford, S., Bucci, M., Wente, S.R., and Goldberg, M.W. (2004). Yeast nuclear pore complexes have a cytoplasmic ring and internal filaments. J Struct Biol *145*, 272-288.

Kiseleva, E., Rutherford, S., Cotter, L.M., Allen, T.D., and Goldberg, M.W. (2001). Steps of nuclear pore complex disassembly and reassembly during mitosis in early *Drosophila* embryos. J Cell Sci *114*, 3607-3618.

Koszul, R., Kim, K.P., Prentiss, M., Kleckner, N., and Kameoka, S. (2008). Meiotic chromosomes move by linkage to dynamic actin cables with transduction of force through the nuclear envelope. Cell *133*, 1188-1201.

Kraemer, D., Wozniak, R.W., Blobel, G., and Radu, A. (1994). The human CAN protein, a putative oncogene product associated with myeloid leukemogenesis, is a nuclear pore complex protein that faces the cytoplasm. Proc Natl Acad Sci U S A *91*, 1519-1523.

Kraemer, D.M., Strambio-de-Castillia, C., Blobel, G., and Rout, M.P. (1995). The essential yeast nucleoporin NUP159 is located on the cytoplasmic side of the nuclear pore complex and serves in karyopherin-mediated binding of transport substrate. J Biol Chem *270*, 19017-19021.

Krauss, S.W., Chen, C., Penman, S., and Heald, R. (2003). Nuclear actin and protein 4.1: essential interactions during nuclear assembly *in vitro*. Proc Natl Acad Sci U S A *100*, 10752-10757.

Kumar, S., Tamura, K., Jakobsen, I.B., and Nei, M. (2001). MEGA2: molecular evolutionary genetics analysis software. Bioinformatics *17*, 1244-1245.

Kurshakova, M.M., Krasnov, A.N., Kopytova, D.V., Shidlovskii, Y.V., Nikolenko, J.V., Nabirochkina, E.N., Spehner, D., Schultz, P., Tora, L., and Georgieva, S.G. (2007). SAGA and a novel *Drosophila* export complex anchor efficient transcription and mRNA export to NPC. Embo J *26*, 4956-4965.

Kylberg, K., Björkroth, B., Ivarsson, B., Fomproix, N., and Daneholt, B. (2008). Close coupling between transcription and exit of mRNP from the cell nucleus. Exp Cell Res *314*, 1708-1720.

Lee, J.R., Shin, H., Ko, J., Choi, J., Lee, H., and Kim, E. (2003). Characterization of the movement of the kinesin motor KIF1A in living cultured neurons. J Biol Chem *278*, 2624-2629.

Lee, K.K., Gruenbaum, Y., Spann, P., Liu, J., and Wilson, K.L. (2000). *C. elegans* nuclear envelope proteins emerin, MAN1, lamin, and nucleoporins reveal unique timing of nuclear envelope breakdown during mitosis. Mol Biol Cell *11*, 3089-3099.

Lenart, P., Rabut, G., Daigle, N., Hand, A.R., Terasaki, M., and Ellenberg, J. (2003). Nuclear envelope breakdown in starfish oocytes proceeds by partial NPC disassembly followed by a rapidly spreading fenestration of nuclear membranes. J Cell Biol *160*, 1055-1068.

Levy, J.R., and Holzbaur, E.L. (2008). Dynein drives nuclear rotation during forward progression of motile fibroblasts. J Cell Sci *121*, 3187-3195.

Loeillet, S., Palancade, B., Cartron, M., Thierry, A., Richard, G.F., Dujon, B., Doye, V., and Nicolas, A. (2005). Genetic network interactions among replication, repair and nuclear pore deficiencies in yeast. DNA Repair (Amst) *4*, 459-468.

Loiodice, I., Alves, A., Rabut, G., Van Overbeek, M., Ellenberg, J., Sibarita, J.B., and Doye, V. (2004). The entire Nup107-160 complex, including three new members, is targeted as one entity to kinetochores in mitosis. Mol Biol Cell *15*, 3333-3344.

Lutzmann, M., Kunze, R., Buerer, A., Aebi, U., and Hurt, E. (2002). Modular self-assembly of a Y-shaped multiprotein complex from seven nucleoporins. Embo J *21*, 387-397.

Madrid, A.S., Mancuso, J., Cande, W.Z., and Weis, K. (2006). The role of the integral membrane nucleoporins Ndc1p and Pom152p in nuclear pore complex assembly and function. J Cell Biol *173*, 361-371.

Makhnevych, T., Lusk, C.P., Anderson, A.M., Aitchison, J.D., and Wozniak, R.W. (2003). Cell cycle regulated transport controlled by alterations in the nuclear pore complex. Cell *115*, 813-823.

Mans, B.J., Anantharaman, V., Aravind, L., and Koonin, E.V. (2004). Comparative genomics, evolution and origins of the nuclear envelope and nuclear pore complex. Cell Cycle *3*, 1612-1637.

Mansfeld, J., Guttinger, S., Hawryluk-Gara, L.A., Pante, N., Mall, M., Galy, V., Haselmann, U., Muhlhausser, P., Wozniak, R.W., Mattaj, I.W., Kutay, U., and Antonin, W. (2006). The

Conserved Transmembrane Nucleoporin NDC1 Is Required for Nuclear Pore Complex Assembly in Vertebrate Cells. Mol Cell *22*, 93-103.

Margalit, A., Vlcek, S., Gruenbaum, Y., and Foisner, R. (2005). Breaking and making of the nuclear envelope. J Cell Biochem *95*, 454-465.

Marshall, W.F., Straight, A., Marko, J.F., Swedlow, J., Dernburg, A., Belmont, A., Murray, A.W., Agard, D.A., and Sedat, J.W. (1997). Interphase chromosomes undergo constrained diffusional motion in living cells. Curr Biol *7*, 930-939.

Mason, P.B., and Struhl, K. (2005). Distinction and relationship between elongation rate and processivity of RNA polymerase II *in vivo*. Mol Cell *17*, 831-840.

Maul, G.G., Maul, H.M., Scogna, J.E., Lieberman, M.W., Stein, G.S., Hsu, B.Y., and Borun, T.W. (1972). Time sequence of nuclear pore formation in phytohemagglutinin-stimulated lymphocytes and in HeLa cells during the cell cycle. J Cell Biol *55*, 433-447.

Meaburn, K.J., and Misteli, T. (2008). Locus-specific and activity-independent gene repositioning during early tumorigenesis. J Cell Biol *180*, 39-50.

Mendjan, S., Taipale, M., Kind, J., Holz, H., Gebhardt, P., Schelder, M., Vermeulen, M., Buscaino, A., Duncan, K., Mueller, J., Wilm, M., Stunnenberg, H.G., Saumweber, H., and Akhtar, A. (2006). Nuclear pore components are involved in the transcriptional regulation of dosage compensation in *Drosophila*. Mol Cell *21*, 811-823.

Menon, B.B., Sarma, N.J., Pasula, S., Deminoff, S.J., Willis, K.A., Barbara, K.E., Andrews, B., and Santangelo, G.M. (2005). Reverse recruitment: the Nup84 nuclear pore subcomplex mediates Rap1/Gcr1/Gcr2 transcriptional activation. Proc Natl Acad Sci U S A *102*, 5749-5754.

Miki, F., Kurabayashi, A., Tange, Y., Okazaki, K., Shimanuki, M., and Niwa, O. (2004). Two-hybrid search for proteins that interact with Sad1 and Kms1, two membrane-bound components of the spindle pole body in fission yeast. Mol Genet Genomics *270*, 449-461.

Miki, F., Okazaki, K., Shimanuki, M., Yamamoto, A., Hiraoka, Y., and Niwa, O. (2002). The 14-kDa dynein light chain-family protien Dlc1 is required for regular oscillatory nuclear movement and efficient recombination during meiotic prophase in fission yeast. Mol Biol Cell *13*, 930-946.

Muhlhausser, P., and Kutay, U. (2007). An *in vitro* nuclear disassembly system reveals a role for the RanGTPase system and microtubule-dependent steps in nuclear envelope breakdown. J Cell Biol *178*, 595-610.

Müller, P., Weinzierl, G., Brachmann, A., Feldbrügge, M., and Kahmann, R. (2003). Mating and pathogenic development of the smut fungus *Ustilago maydis* are regulated by one mitogen-activated protein kinase cascade. Eukaryot Cell *2*, 1187-1199.

Orjalo, A.V., Arnaoutov, A., Shen, Z., Boyarchuk, Y., Zeitlin, S.G., Fontoura, B., Briggs, S., Dasso, M., and Forbes, D.J. (2006). The Nup107-160 Nucleoporin Complex Is Required for Correct Bipolar Spindle Assembly. Mol Biol Cell.

Osmani, A.H., Davies, J., Liu, H.L., and Osmani, S.A. (2006). Systematic Deletion and Mitotic Localization of the Nuclear Pore Complex Proteins of *Aspergillus nidulans*. Mol Biol Cell.

Paddy, M.R., Saumweber, H., Agard, D.A., and Sedat, J.W. (1996). Time-resolved, in vivo studies of mitotic spindle formation and nuclear lamina breakdown in *Drosophila* early embryos. J Cell Sci *109 (Pt 3)*, 591-607.

Patel, S.S., Belmont, B.J., Sante, J.M., and Rexach, M.F. (2007). Natively unfolded nucleoporins gate protein diffusion across the nuclear pore complex. Cell *129*, 83-96.

Payne, C., Rawe, V., Ramalho-Santos, J., Simerly, C., and Schatten, G. (2003). Preferentially localized dynein and perinuclear dynactin associate with nuclear pore complex proteins to mediate genomic union during mammalian fertilization. J Cell Sci *2003*, Pt 23.

Presley, J.F., Cole, N.B., Schroer, T.A., Hirschberg, K., Zaal, K.J., and Lippincott-Schwartz, J. (1997). ER-to-Golgi transport visualized in living cells. Nature *389*, 81-85.

Prunuske, A.J., and Ullman, K.S. (2006). The nuclear envelope: form and reformation. Curr Opin Cell Biol *18*, 108-116.

Rabut, G., Doye, V., and Ellenberg, J. (2004a). Mapping the dynamic organization of the nuclear pore complex inside single living cells. Nat Cell Biol *6*, 1114-1121.

Rabut, G., Lenart, P., and Ellenberg, J. (2004b). Dynamics of nuclear pore complex organization through the cell cycle. Curr Opin Cell Biol *16*, 314-321.

Rasala, B.A., Orjalo, A.V., Shen, Z., Briggs, S., and Forbes, D.J. (2006). ELYS is a dual nucleoporin/kinetochore protein required for nuclear pore assembly and proper cell division. Proc Natl Acad Sci U S A *103*, 17801-17806.

Rout, M.P., Aitchison, J.D., Suprapto, A., Hjertaas, K., Zhao, Y., and Chait, B.T. (2000). The yeast nuclear pore complex: composition, architecture, and transport mechanism. J Cell Biol *148*, 635-651.

Salina, D., Bodoor, K., Eckley, D.M., Schroer, T.A., Rattner, J.B., and Burke, B. (2002). Cytoplasmic dynein as a facilitator of nuclear envelope breakdown. Cell *108*, 97-107.

Sambrook, J., and Russell, D. (2001). Molecular Cloning: A Laboratory Manual (3rd edit). Cold Spring Harbor Laboratory Press.

Scherthan, H., Wang, H., Adelfalk, C., White, E.J., Cowan, C., Cande, W.Z., and Kaback, D.B. (2007). Chromosome mobility during meiotic prophase in *Saccharomyces cerevisiae*. Proc Natl Acad Sci U S A *104*, 16934-16939.

Schirmer, E.C., and Gerace, L. (2005). The nuclear membrane proteome: extending the envelope. Trends Biochem Sci *30*, 551-558.

Schmid, M., Arib, G., Laemmli, C., Nishikawa, J., Durussel, T., and Laemmli, U.K. (2006). Nup-PI: the nucleopore-promoter interaction of genes in yeast. Mol Cell *21*, 379-391.

Schneider, R., and Grosschedl, R. (2007). Dynamics and interplay of nuclear architecture, genome organization, and gene expression. Genes Dev *21*, 3027-3043.

Schuchardt, I., Assmann, D., Thines, E., Schuberth, C., and Steinberg, G. (2005). Myosin-V, Kinesin-1, and Kinesin-3 cooperate in hyphal growth of the fungus *Ustilago maydis*. Mol Biol Cell *16*, 5191-5201.

Schulz, B., Banuett, F., Dahl, M., Schlesinger, R., Schafer, W., Martin, T., Herskowitz, I., and Kahmann, R. (1990). The b alleles of *U. maydis*, whose combinations program pathogenic

development, code for polypeptides containing a homeodomain-related motif. Cell *60*, 295-306.

Shaw, R.J., and Reines, D. (2000). *Saccharomyces cerevisiae* transcription elongation mutants are defective in PUR5 induction in response to nucleotide depletion. Mol Biol Cell *20*, 7427-7437.

Shulga, N., Mosammaparast, N., Wozniak, R., and Goldfarb, D.S. (2000). Yeast nucleoporins involved in passive nuclear envelope permeability. J Cell Biol *149*, 1027-1038.

Siniossoglou, S., Lutzmann, M., Santos-Rosa, H., Leonard, K., Mueller, S., Aebi, U., and Hurt, E. (2000). Structure and assembly of the Nup84p complex. J Cell Biol *149*, 41-54.

Siniossoglou, S., Wimmer, C., Rieger, M., Doye, V., Tekotte, H., Weise, C., Emig, S., Segref, A., and Hurt, E.C. (1996). A novel complex of nucleoporins, which includes Sec13p and a Sec13p homolog, is essential for normal nuclear pores. Cell *84*, 265-275.

Snetselaar, K.M., and McCann, M.P. (1997). Using microdensitometry to correlate cell morphology with the nuclear cycle in *Ustilago maydis*. Mycologia *89*, 689-697.

Southern, E.M. (1975). Detection of specific sequences among DNA fragments separated by gel electrophoresis. J Mol Biol *98*, 503-517.

Spann, T.P., Moir, R.D., Goldman, A.E., Stick, R., and Goldman, R.D. (1997). Disruption of nuclear lamin organization alters the distribution of replication factors and inhibits DNA synthesis. J Cell Biol *136*, 1201-1212.

Stafstrom, J.P., and Staehelin, L.A. (1984). Dynamics of the nuclear envelope and of nuclear pore complexes during mitosis in the *Drosophila* embryo. Eur J Cell Biol *34*, 179-189.

Stavru, F., Hulsmann, B.B., Spang, A., Hartmann, E., Cordes, V.C., and Gorlich, D. (2006). NDC1: a crucial membrane-integral nucleoporin of metazoan nuclear pore complexes. J Cell Biol *173*, 509-519.

Steinberg, G., Wedlich-Soldner, R., Brill, M., and Schulz, I. (2001). Microtubules in the fungal pathogen *Ustilago maydis* are highly dynamic and determine cell polarity. J Cell Sci *114*, 609-622.

Stelter, P., Kunze, R., Flemming, D., Hopfner, D., Diepholz, M., Philippsen, P., Bottcher, B., and Hurt, E. (2007). Molecular basis for the functional interaction of dynein light chain with the nuclear-pore complex. Nat Cell Biol *9*, 788-796.

Stewart, M. (2007). Molecular mechanism of the nuclear protein import cycle. Nat Rev Mol Cell Biol *8*, 195-208.

Straube, A., Brill, M., Oakley, B.R., Horio, T., and Steinberg, G. (2003). Microtubule organization requires cell cycle-dependent nucleation at dispersed cytoplasmic sites: polar and perinuclear microtubule organizing centers in the plant pathogen *Ustilago maydis*. Mol Biol Cell *14*, 642-657.

Straube, A., Enard, W., Berner, A., Wedlich-Soldner, R., Kahmann, R., and Steinberg, G. (2001). A split motor domain in a cytoplasmic dynein. Embo J *20*, 5091-5100.

Straube, A., Weber, I., and Steinberg, G. (2005). A novel mechanism of nuclear envelope break-down in a fungus: nuclear migration strips off the envelope. Embo J *24*, 1674-1685.

Strawn, L.A., Shen, T., Shulga, N., Goldfarb, D.S., and Wente, S.R. (2004). Minimal nuclear pore complexes define FG repeat domains essential for transport. Nat Cell Biol *6*, 197-206.

Taddei, A., Van Houwe, G., Hediger, F., Kalck, V., Cubizolles, F., Schober, H., and Gasser, S.M. (2006). Nuclear pore association confers optimal expression levels for an inducible yeast gene. Nature *441*, 774-778.

Tcheperegine, S.E., Marelli, M., and Wozniak, R.W. (1999). Topology and functional domains of the yeast pore membrane protein Pom152p. J Biol Chem *274*, 5252-5258.

Theisen, U., Straube, A., and Steinberg, G. (2008). Dynamic Rearrangement of Nucleoporins during Fungal "Open" Mitosis. Mol Biol Cell *19*, 1230-1240.

Therizols, P., Fairhead, C., Cabal, G.G., Genovesio, A., Olivo-Marin, J.C., Dujon, B., and Fabre, E. (2006). Telomere tethering at the nuclear periphery is essential for efficient DNA double strand break repair in subtelomeric region. J Cell Biol *172*, 189-199.

Thompson, J.D., Gibson, T.J., Plewniak, F., Jeanmougin, F., and Higgins, D.G. (1997). The CLUSTAL_X windows interface: flexible strategies for multiple sequence alignment aided by quality analysis tools. Nucleic Acids Res *25*, 4876-4882.

Thomson, I., Gilchrist, S., Bickmore, W.A., and Chubb, J.R. (2004). The radial positioning of chromatin is not inherited through mitosis but is established *de novo* in early G1. Curr Biol *14*, 166-172.

Tipper, D.J. (1973). Inhibition of yeast ribonucleic acid polymerase by thiolutin. J Bacteriol *116*, 245-256.

Tran, E.J., and Wente, S.R. (2006). Dynamic nuclear pore complexes: life on the edge. Cell *125*, 1041-1053.

Trelles-Sticken, E., Adelfalk, C., Loidl, J., and Scherthan, H. (2005). Meiotic telomere clustering requires actin for its formation and cohesin for its resolution. J Cell Biol *170*, 213-223.

Trelles-Sticken, E., Loidl, J., and Scherthan, H. (1999). Bouquet formation in budding yeast: initiation of recombination is not required for meiotic telomere clustering. J Cell Sci *112 (Pt 5)*, 651-658.

Tsukuda, T., Carleton, S., Fotheringham, S., and Holloman, W.K. (1988). Isolation and characterization of an autonomously replicating sequence from *Ustilago maydis*. Mol Cell Biol *8*, 3703-3709.

Tzur, Y.B., Wilson, K.L., and Gruenbaum, Y. (2006). SUN-domain proteins: 'Velcro' that links the nucleoskeleton to the cytoskeleton. Nat Rev Mol Cell Biol *7*, 782-788.

Valentine, M.T., Fordyce, P.M., Krzysiak, T.C., Gilbert, S.P., and Block, S.M. (2006). Individual dimers of the mitotic kinesin motor Eg5 step processively and support substantial loads *in vitro*. Nat Cell Biol *8*, 470-476.

Vasu, S., Shah, S., Orjalo, A., Park, M., Fischer, W.H., and Forbes, D.J. (2001). Novel vertebrate nucleoporins Nup133 and Nup160 play a role in mRNA export. J Cell Biol *155*, 339-354.

Walther, T.C., Alves, A., Pickersgill, H., Loiodice, I., Hetzer, M., Galy, V., Hulsmann, B.B., Kocher, T., Wilm, M., Allen, T., Mattaj, I.W., and Doye, V. (2003). The conserved Nup107-160 complex is critical for nuclear pore complex assembly. Cell *113*, 195-206.

Walther, T.C., Pickersgill, H.S., Cordes, V.C., Goldberg, M.W., Allen, T.D., Mattaj, I.W., and Fornerod, M. (2002). The cytoplasmic filaments of the nuclear pore complex are dispensible for selective nuclear protein import. J Cell Biol *158*, 63-77.

Wedlich-Söldner, R., Bölker, M., Kahmann, R., and Steinberg, G. (2000). A putative endosomal t-SNARE links exo- and endocytosis in the pythopathogenic fungus *Ustilago maydis*. Embo J *19*, 1974-1986.

Wedlich-Söldner, R., Schulz, I., Straube, A., and Steinberg, G. (2002a). Dynein supports motility of endoplasmic reticulum in the fungus *Ustilago maydis*. Mol Biol Cell *13*, 965-977.

Wedlich-Söldner, R., Straube, A., Friedrich, M.W., and Steinberg, G. (2002b). A balance of KIF1A-like kinesin and dynein organizes early endosomes in the fungus *Ustilago maydis*. Embo J *21*, 2946-2957.

Wilhelmsen, K., Ketema, M., Truong, H., and Sonnenberg, A. (2006). KASH-domain proteins in nuclear migration, anchorage and other processes. J Cell Sci *119*, 5021-5029.

Winey, M., Yarar, D., Giddings, T.H., Jr., and Mastronarde, D.N. (1997). Nuclear pore complex number and distribution throughout the *Saccharomyces cerevisiae* cell cycle by three-dimensional reconstruction from electron micrographs of nuclear envelopes. Mol Biol Cell *8*, 2119-2132.

Yamamoto, A., West, R.R., McIntosh, J.R., and Hiraoka, Y. (1999). A cytoplasmic dynein heavy chain is required for oscillatory nuclear movement of meiotic prophase and efficient meiotic recombination in fission yeast. J Cell Biol *145*, 1233-1249.

Yang, L., Guan, T., and Gerace, L. (1997). Integral membrane proteins of the nuclear envelope are dispersed throughout the endoplasmic reticulum during mitosis. J Cell Biol *137*, 1199-1210.

Yang, Q., Rout, M.P., and Akey, C.W. (1998). Three-dimensional architecture of the isolated yeast nuclear pore complex: functional and evolutionary implications. Mol Cell *1*, 223-234.

Yin, H., Wang, M.D., Svoboda, K., Landick, R., Block, S.M., and Gelles, J. (1995). Transcription against an applied force. Science *270*, 1653-1657.

Zuccolo, M., Alves, A., Galy, V., Bolhy, S., Formstecher, E., Racine, V., Sibarita, J.B., Fukagawa, T., Shiekhattar, R., Yen, T., and Doye, V. (2007). The human Nup107-160 nuclear pore subcomplex contributes to proper kinetochore functions. Embo J *26*, 1853-1864.

Danksagung

Zum Schluss möchte ich mich bei allen bedanken, die direkt und indirekt zum Entstehen dieser Arbeit beigetragen haben.

Besonderer Dank gilt Gero Steinberg für die Betreuung der Arbeit, die Diskussionen und das Abenteuer Exeter. Ich habe in den vier Jahren viel von ihm gelernt. Insbesondere aber danke ich ihm für den praktischen Beistand im letzten Jahr.

Für die Unterstützung insbesondere während der ersten drei Jahre der Doktorarbeit danke ich Uwe Maier, Michael Bölker, dem MPI Marburg und der Studienstiftung des deutschen Volkes. Für die Unterstützung in meinem letzten Jahr der Doktorarbeit der Universität Exeter. Für die Teilnahme an meinem Kommitee Frau Renkawitz-Pohl.

Besonderer Dank für technische, aber auch intellektuelle und moralische Hilfe geht an die aktiven und ehemaligen Kollegen aus dem C-Labor. Von den „Ehemaligen“ insbesondere Gero II, Uta und Isabel, die bis zum Schluss an den Diskussionen teil hatten, und sich auch die Zeit zum Lesen der Doktorarbeit genommen haben, obwohl sie schon länger anderen Aufgaben nachgehen. Dani und Petra haben mich technisch unterstützt, aber vor allem habe ich ihre Gesellschaft geschätzt. Unter den C-lab Mitgliedern, die mein letztes Jahr in Exeter miterlebt haben, möchte ich insbesondere Christoph danken, für technische Unterstützung beim Klonieren als die Zeit knapp wurde, aber auch für die nette Gesellschaft. Gleiches gilt für Sam und Martin.

Daneben sollen auch die Menschen nicht unerwähnt bleiben, die durch ihre Anteilnahme und geduldigem Zuhören dazu beigetragen haben, dass diese Arbeit entstanden ist. Neben meiner Familie und Freunden von früher gehören dazu aus dem beruflichen Umfeld vor allem Silke, Julia, Melanie und Nils.

Keep on rocking.

Curriculum Vitae

Personal data	Ulrike Theisen born January 20th, 1979 in Munich, Germany
Education	1985 – 1989 Grundschule an der Senftenauerstr., Munich 1989 – 1995 Ludwigsgymnasium, Munich 1995 – 1998 Theresia-Gerhardinger Gymnasium am Anger, Munich 06/1998 Abitur
University	1998 – 2004 Regensburg University, Germany 07/2004 – 09/2004 Osaka University, Japan 2001/ 2002 University of Colorado, Boulder, CO, USA 06/2004 Diploma in Biology (Prof. Hans-Jörg Linde, University Clinic of Regensburg)
Dissertation	2004 – 2008 MPI Marburg, Germany, and Exeter University, UK „Nuclear Pore Behaviour in Interphase and the “Open” Mitosis of *Ustilago maydis*“ Supervisor: Gero Steinberg